

Syracuse University

SURFACE

Dissertations - ALL

SURFACE

May 2016

Developing iodine proxies for oceanic oxygenation conditions during greenhouse episodes

Xiaoli Zhou
Syracuse University

Follow this and additional works at: <https://surface.syr.edu/etd>



Part of the [Physical Sciences and Mathematics Commons](#)

Recommended Citation

Zhou, Xiaoli, "Developing iodine proxies for oceanic oxygenation conditions during greenhouse episodes" (2016). *Dissertations - ALL*. 466.

<https://surface.syr.edu/etd/466>

This Dissertation is brought to you for free and open access by the SURFACE at SURFACE. It has been accepted for inclusion in Dissertations - ALL by an authorized administrator of SURFACE. For more information, please contact surface@syr.edu.

Abstract

Anthropogenic global warming affects marine ecosystems in complex ways, and declining ocean oxygenation is a growing concern. Forecasting the geographical and bathymetric extent, rate, and intensity of future deoxygenation and its ecological effects, however, remains highly challenging because of the complex feedbacks in the climate-ocean-biota system. Global warming lowers the solubility of oxygen in the ocean and drives an enhanced hydrological cycle with increased nutrient delivery to the oceans, leading to increases in organic production, the degradation of which causes a further decrease in dissolved oxygen. In extreme cases in the geological past, this trajectory has led to strong marine oxygen depletion during the so-called oceanic anoxic events (OAEs). How the water column oscillated between generally oxic conditions and local/global anoxia remains a challenging question, exacerbated by a lack of sensitive redox proxies, especially at the interface between oxic and anoxic conditions. To address this problem, I use I/Ca in bulk carbonate and I/TOC in black shale to reconstruct redox changes in the upper and deep waters in multiple ocean basins through the Cretaceous OAE 2 at the Cenomanian-Turonian boundary (94 Ma). The iodine proxy records are interpreted in the context of a wide range of other geochemical data and Earth system biogeochemical model simulations.

Iodate and iodide are the most thermodynamically stable iodine ions in seawater. The speciation of iodine depends on the redox condition of the ambient seawater. Iodate is abundant in oxic water, and iodide dominates in anoxic water. Iodate is the only iodine ion that can precipitate with carbonate, and carbonate associated iodine increases with iodate concentration in the matrix solution. Therefore, I/Ca values in carbonate can be used as a redox proxy of seawater.

In general, I/Ca ratios were relatively low preceding and during the OAE interval, indicating deep suboxic or anoxic waters exchanging directly with near-surface waters. However, individual sites display a wide range of initial values and variability in I/Ca through the OAE interval, reflecting the importance of local controls and potentially suggesting a high spatial variability in redox state. Both I/Ca and cGENIE model suggest that the northeast proto-Atlantic had notably higher oxygen levels in the upper water column than the rest of the North Atlantic, highlighting important regional differences in redox conditions during OAE 2. A lack of correlation with calcium, lithium, and carbon isotope records suggests that neither enhanced global weathering nor carbon burial was a dominant control on the I/Ca proxy during OAE 2.

I/TOC and I_{org} records were generated from six sections in proto-North Atlantic and southern Indian Ocean. I/TOC in modern surface and subsurface sediment decreases with decreasing bottom-water oxygen, a feature potentially useful for reconstructing seafloor paleo-redox. I/TOC decreases into OAE 2, suggesting more reducing bottom-water conditions. Higher I/TOC values (more oxic conditions) are recorded in two high-latitude and possibly in one low-latitude site, where higher oxygen levels are also indicated by other redox indicators and Earth System Modeling by cGENIE. I/TOC and I/Ca records at a near-equatorial coastal site in Morocco (Tarfaya) decreased during OAE 2, likely suggesting reducing water throughout the water column due to strong vertical mixing and shallow paleo-depth, consistent with a wide range of other proxies. These observations indicate that coeval carbonate and shale iodine records may be able to depict oxygenation changes in different parts of the water column, and reflect the change in marine iodine reservoir.

Another rapid global warming event, the Paleocene-Eocene Thermal Maximum (PETM, ~55.5 Ma), may represent a better analog for present and future global warming. I apply the

iodine to calcium ratio (I/Ca) in bulk coarse fraction sediment and planktonic foraminiferal tests from pelagic sites in different oceans, and compared the reconstruction with modeled oxygen levels. The reconstructed iodate gradients indicate that deoxygenation occurred in the upper water column in the Atlantic, Indian Oceans, and possibly the Pacific Ocean, as well during the PETM, due to vertical and potentially lateral expansion of OMZs.

Overall, this thesis further establishes the use of iodine as a proxy for ocean oxygen levels in the geological history.

Developing iodine proxies for oceanic oxygenation conditions during greenhouse episodes

By

Xiaoli Zhou

B.S. Geochemistry University of Science and Technology of China, 2011

DISSERTATION

Submitted in partial fulfillment of the requirements for the degree of
Doctor of Philosophy in Earth Sciences

Syracuse University

May 2016

Copyright © Xiaoli Zhou 2016

All rights reserved

Acknowledgements

I would like to thank everyone I have met during my stay in Syracuse, somehow you all have contributed to this work. I would not be able to finish my PhD program without all of you. I specially thank my PhD advisor Dr. Zunli Lu for your guidance and impact on my study and beyond my academic life, your trust on my teaching and research abilities, and your financial support for my stay in this program. I have learned all sorts of skills from you, from lab experiments to publishing papers, and I also acquired your active and collaborative attitudes imperceptibly. My dissertation committee members have provided valuable comments on my dissertation and assisted me in my seeking for academic career. I appreciate your help and value all the advice you have given me.

I am grateful to NSF for supporting the projects I have been working on. The Department of Earth Sciences at Syracuse University also granted me funding for short-term research. I am most grateful to the department for providing me this opportunity to pursue a PhD degree at Syracuse University. I thank all the colleagues at this department for contributing all sorts of ideas and stimulating discussions. The secretaries have always been helpful.

Special thanks go to my friends in Syracuse, I would not have survived the long journey without your company. I also thank my lab mates, Sunshyne, Kristy and Wanyi, for your help in sample preparations and chemical experiments and your comments on my presentations and manuscripts. I remember all the days we have spent together. I owe a lot of my accomplishments to my parents. You have always been respecting and supporting my decisions. You are the best and will always be my love.

Table of Contents

Abstract	i
Title Page	iii
Acknowledgments	v
List of Tables	x
List of Figures	xi
Chapter 1: Upper ocean oxygenation dynamics from I/Ca ratios during the Cenomanian-Turonian OAE	1
Abstract	2
1. Introduction	3
1.1. Marine Environmental Changes During Oceanic Anoxic Events	3
1.2. I/Ca as a Paleoredox Proxy	5
1.3. Multiproxy Comparisons	8
2. Study Sites	9
3. Analytical Methods	10
3.1. Sample Preparation and Measurements	10
3.2. Earth System Modeling	10
4. Results and Discussions	11
4.1. Influence of Diagenesis and Organically Bound Iodine	11
4.2. Shallow-Water Sites	12
4.3. Low-Latitude Pelagic Sites	14
4.4. Mid-latitude Pelagic Sites	16
4.5. Data Model Comparisons	18

4.6. Tempo of Local Redox Changes	20
4.7. Marine Iodine Budget	21
5. Conclusions	22
Acknowledgments	23
References	24
Tables	38
Figures	39
Chapter 2: Records of organically bound iodine during the Cenomanian–Turonian OAE 2: implications for bottom water condition and iodine cycling	48
Abstract	49
1. Introduction	50
1.1. OAE 2 and redox proxies	50
1.2. Organically bound iodine in recent sediments	51
2. Study Sites	52
3. Methods	55
4. Results and discussion	56
4.1. Method development	56
4.2. I/TOC as a qualitative bottom water oxygenation proxy	57
4.3. Oceanographic patterns of I/TOC during pre- and post-OAE 2 intervals	59
4.4. I/TOC vs. modeled seafloor oxygen	62
4.5. Temporal changes in I/TOC across the OAE 2	63
4.6. Seawater iodine inventory	63
5. Conclusions	65

Acknowledgments	65
References	66
Tables	78
Figures	79
Chapter 3: I/Ca evidence for upper ocean deoxygenation during the PETM	85
Abstract	86
1. Introduction	87
2. Iodine in Seawater and Foraminifera	89
2.1. Marine Chemistry of Iodine	90
2.2. Water Column Depth Gradient in Planktonic Foraminiferal I/Ca	91
3. Methods	91
3.1. Samples, Sites, and Age Models.....	92
3.2. Cleaning Procedures	92
3.3. Inductively Coupled Plasma Mass Spectrometry Measurements	93
3.4. Partial Dissolution, Mn Oxide Coatings, and Temperature	93
4. Results	94
5. Discussion	96
5.1. Pre-PETM Productivity Versus I/Ca	96
5.2. Productivity Changes During the PETM	97
5.3. PETM Open Ocean Deoxygenation	97
5.4. Iodate Gradients and OMZs	99
5.5. Shell Recrystallization	102
5.6. Depth Habitat	103

5.7. Symbiont Bearing Planktonic Foraminifera	103
5.8. Whole-Ocean Change in Iodine	104
6. Conclusions	104
Acknowledgments	105
References	106
Figures	119
Biographical Data	123

List of Tables

Chapter 1

Table 1. OAE 2 Sections Used for I/Ca Measurements and Multiproxy Comparison.

Chapter 2

Table 1. Evidence of anoxia at each site except for the evidence for oxygenation in seawater at Site South Ferriby as indicated.

List of Figures

Chapter 1

Figure 1. Global paleogeographic map of OAE 2 sections	39
Figure 2. Chemostratigraphic plot for OAE 2 at Raia del Pedale	40
Figure 3. Preliminary I/Ca data from the Aristocrat Angus core in the Western Interior Seaway, plotted with wt % TOC, wt % CaCO ₃ , and $\delta^{13}\text{C}_{\text{org}}$	41
Figure 4. Geochemical and stable isotope data for OAE 2 at Tarfaya (core S57)	42
Figure 5. I/Ca for ODP Site 1258 on Demerara Rise, compared with $\delta^{13}\text{C}_{\text{org}}$, wt % TOC, and wt % CaCO ₃	43
Figure 6. I/Ca data from South Ferriby, compared with $\delta^{13}\text{C}_{\text{carb}}$, $\delta^{34}\text{C}_{\text{CAS}}$, Ca, and Li isotopes ..	44
Figure 7. I/Ca record of Site U1407, IODP X342 on Newfoundland Drifts	44
Figure 8. Geochemical and isotope data for Eastbourne	45
Figure 9. Modeled upper water column-dissolved oxygen distributions (a–c) before and (d–f) during OAE 2	46
Figure 10. I/Ca records correlated by $\delta^{13}\text{C}$ showing distinct local surface water redox evolution	47
Figure 11. I/Ca and $\delta^7\text{Li}$ plotted against $\delta^{13}\text{C}$ during the rising limb of the CIE for Eastbourne and Raia del Pedale	47

Chapter 2

Figure 1. I/TOC of modern marine sediments plotted with bottom-water oxygen concentration immediately overlying the sea floor	79
Figure 2. Paleogeographic map for the Late Cretaceous	80
Figure 3. Iodine extraction results of the test run of two OAE 2 samples	81

Figure 4. Stratigraphic records of $\delta^{13}\text{C}$, I/TOC, I_{org} , and TOC at the six study sites	82
Figure 5. Pre-CIE average I/TOC values plotted against modeled bottom-water oxygen for the Late Cretaceous with a deeper Panama	83
Figure 6. Organically bound iodine concentration in bulk sediment (I_{org}) plotted against corresponded TOC content for samples during OAE 2	84
Chapter 3	
Figure 1. (a–c) Schematic seawater iodate and oxygen concentration profiles	119
Figure 2. Studied sites plotted on a paleomap of the modeled export productivity during the late Paleocene	119
Figure 3. Coarse fraction and single genus I/Ca for open ocean sites	120
Figure 4. Differences in I/Ca between the deep (D) and mixed-layer (M) calcifiers for each site	121
Figure 5. I/Ca values in different size fractions of bulk coarse fraction in samples from Sites 1262 and 865	121
Figure 6. Average values and standard deviations of I/Ca in late Paleocene mixed-layer and deep- dwelling calcifiers, correlated with the modeled productivity in Winguth et al. (2012) .	122
Figure 7. O_2 profiles simulated in CCSM3 model under $4\times\text{CO}_2$ conditions	122

**Chapter 1: Upper ocean oxygenation dynamics from I/Ca ratios
during the Cenomanian-Turonian OAE**

Published As:

Zhou, X., Jenkyns, H.C., Owens, J.D., Junium, C.K., Zheng, X., Sageman, B.B., Hardisty, D.S., Lyons, T.W., Ridgwell, A., and Lu, Z., 2015, Upper ocean oxygenation dynamics from I/Ca ratios during the Cenomanian-Turonian OAE 2: *Paleoceanography*, v. 30, p. 510–526. doi:10.1002/2014PA002741.

Abstract

Global warming lowers the solubility of gases in the ocean and drives an enhanced hydrological cycle with increased nutrient loads delivered to the oceans, leading to increases in organic production, the degradation of which causes a further decrease in dissolved oxygen. In extreme cases in the geological past, this trajectory has led to catastrophic marine oxygen depletion during the so-called oceanic anoxic events (OAEs). How the water column oscillated between generally oxic conditions and local/global anoxia remains a challenging question, exacerbated by a lack of sensitive redox proxies, especially for the suboxic window. To address this problem, we use bulk carbonate I/Ca to reconstruct subtle redox changes in the upper ocean water column at seven sites recording the Cretaceous OAE 2. In general, I/Ca ratios were relatively low preceding and during the OAE interval, indicating deep suboxic or anoxic waters exchanging directly with near-surface waters. However, individual sites display a wide range of initial values and excursions in I/Ca through the OAE interval, reflecting the importance of local controls and suggesting a high spatial variability in redox state. Both I/Ca and an Earth System Model suggest that the northeast proto-Atlantic had notably higher oxygen levels in the upper water column than the rest of the North Atlantic, indicating that noxia was not global during OAE 2 and that important regional differences in redox conditions existed. A lack of correlation with calcium, lithium, and carbon isotope records suggests that neither enhanced global weathering nor carbon burial was a dominant control on the I/Ca proxy during OAE 2.

1. Introduction

1.1. Marine Environmental Changes During Oceanic Anoxic Events

The concept of oceanic anoxic events (OAEs) was introduced upon the discovery of globally deposited coeval marine organic-rich sediments (black shales) of Cretaceous age, a phenomenon associated directly and indirectly with profound environmental and chemical changes (Schlanger and Jenkyns, 1976; Schlanger et al., 1987; Arthur et al., 1990; Jenkyns, 2003, 2010). Globally recorded OAEs are recognized as the early Toarcian or T-OAE (~182 Ma) from the Jurassic Period and OAE 1a in the early Aptian (~125 Ma) and OAE 2 (~94 Ma) at the Cenomanian-Turonian boundary from the Cretaceous Period (Ogg and Hinnov, 2012a, 2012b).

During OAE 2, positive carbon isotope excursions (CIEs) in both inorganic and organic carbons are found in different environmental settings (Jarvis et al., 2011). Because organic carbon has strongly negative $\delta^{13}\text{C}$ values, ranging from -25 to -60‰, enhanced rates of organic carbon burial left residual seawater with relatively high carbon isotope values in dissolved inorganic carbon, producing carbonates and organic matter with elevated $\delta^{13}\text{C}$. These positive CIEs, together with macrofossil, microfossil, and nannofossil biostratigraphy, allow correlation of stratigraphic columns from different OAE 2 sections (Tsikos et al., 2004).

Before the CIE started, different proxies suggest that $p\text{CO}_2$ was unusually high (Jarvis et al., 2011), likely introduced by volcanic and hydrothermal activities (Jones and Jenkyns, 2001; Kuroda et al., 2007) related to the formation of the Caribbean and other Large Igneous Provinces (Wignall, 2001; Erba, 2004; Turgeon and Creaser, 2008; Zheng et al., 2013; Du Vivier et al., 2014). Addition of CO_2 to the atmosphere would have increased global temperature, which enhanced the hydrological cycle and delivered more nutrients to the ocean. In turn, enhanced nutrient availability would have stimulated planktonic productivity, increasing the oxygen

demand in the water column as well as fostering burial of more organic carbon in marine sediments (Weissert, 1989; Jenkyns, 2003; Adams et al., 2010). A positive excursion of sulfur isotopes in bulk carbonates of Cenomanian-Turonian age indicates that sulfate reduction and enhanced rates of pyrite burial became more significant globally as bottom water euxinia expanded during OAE 2 (Ohkouchi et al., 1999; Owens et al., 2013). Consistent with this observation, there is considerable biomarker evidence indicating episodic but widespread photic zone sulfide accumulation (euxinia) in the North and South Atlantic regions, the proto-Indian Ocean, and in the Tethys (Sinninghe Damsté and Koster, 1998; Kuypers et al., 2002; Pancost et al., 2004; Forster et al., 2008; van Bentum et al., 2009).

Beyond the sulfur, carbonate, and organic matter isotope records, the inorganic elemental proxies applied to OAE 2 are mostly restricted to concentrations and elemental ratios of redox-sensitive metals in shales (e.g., Mn, Mo, V, Fe, U, Co, Ce, and Cd), although metal isotopes are being increasingly used. Trace metals precipitate as sulfides under anoxic and euxinic conditions, some with valence changes (e.g., Mo and V) and some without, such as Zn (Hetzl et al., 2009). During OAE 2, some trace metals, such as As, Bi, Cd, Co, Cr, Cu, Mo, Ni, Sb, Tl, V, and U, were concentrated in organic matter or precipitated with sulfide, suggesting euxinia in the sediments and/or in the water column (Arthur et al., 1990; Kuypers et al., 2002; Jenkyns, 2010), as documented for the proto-Atlantic (Kuypers et al., 2002; Kolonic et al., 2005; Brumsack, 2006; Forster et al., 2008; Hetzel et al., 2009; Tribovillard et al., 2012; van Helmond et al., 2014; Little et al., 2015) and for southern Europe (Scopelliti et al., 2006, 2008; Turgeon and Brumsack, 2006). Molybdenum isotope data (Westermann et al., 2014) and uranium isotope data (Montoya-Pino et al., 2010) also indicate expanded bottom water euxinia during the OAE 2. Although these geochemical species are interpreted as paleoredox tracers, they may also have responded to

changes in hydrothermal flux that may have further contributed to metal enrichments during OAE 2 (Orth et al., 1993; Snow et al., 2005; Elrick et al., 2009; Jenkyns, 2010; Eldrett et al., 2014).

The details of how the global ocean evolved from relatively widespread oxidizing conditions, with only localized anoxia in restricted marine settings and areas of particularly high primary production, to globally extensive anoxia (Pancost et al., 2004; Hetzel et al., 2009; Montoya-Pino et al., 2010; Owens et al., 2013) remain unclear for OAE 2 and OAEs more generally. Newly developed geochemical techniques utilizing the biophilic element iodine in carbonates help to bridge this gap and shed novel light on the geographic patterns and controls on the development of anoxia.

1.2. I/Ca as a Paleoredox Proxy

Although iodine can exist in several oxidation states, iodide (I^-) and iodate (IO_3^-) are the thermodynamically stable inorganic forms in seawater. The standard reduction potential of IO_3^-/I^- is very close to that of O_2/H_2O (Rue et al., 1997; Harris, 2006), making iodine one of the first elements to respond to oceanic deoxygenation. Most of the iodine in the modern well-oxygenated ocean occurs as iodate (Wong, 1995; Farrenkopf et al., 1997; Campos et al., 1999; Waite et al., 2006). Because only iodate precipitates with carbonate, the simple presence of carbonate-associated iodine requires locally oxic conditions in the water column. Iodate is, however, almost completely reduced to iodide in all investigated modern anoxic basins and oxygen minimum zones where dissolved O_2 is less than $3 \mu M$ (Wong and Brewer, 1977; Wong et al., 1985; Luther and Campbell, 1991; Farrenkopf et al., 1997; Rue et al., 1997; Farrenkopf

and Luther, 2002). Consequently, a drop in iodate concentration to ~0 indicates strong deoxygenation within the local water column.

I/Ca ratios in calcite increase linearly with iodate concentrations in the precipitating medium, but iodide does not incorporate into carbonate (Lu et al., 2010). The mechanism of iodate incorporation is unclear but may involve substitution for the carbonate ion and/or the presence of lattice defects, perhaps analogous to the mechanism proposed for sulfate incorporation into carbonate (Staudt and Schoonen, 1995). The lack of iodide incorporation is likely due to the large ionic radius of iodide relative to iodate.

Most pelagic carbonate is produced within the upper levels of the water column as coccolith and planktonic foraminiferal calcite, which in recent environments falls to the seafloor roughly in the proportion of 1:1 (Broecker and Clark, 2009). Hence, a bulk carbonate chemical signal should reflect conditions in near-surface waters. Although the percentage of biogenic carbonate produced at the seafloor is generally very small, the influence of benthic calcifiers cannot be ruled out. For these reasons, the bulk carbonate I/Ca ratio in this work is taken as an indicator for the integrated conditions in the upper ocean water column.

Once oxic conditions are established, iodine speciation at a given location is secondarily influenced by regional mixing. The kinetics of iodide oxidation are not well constrained (Luther et al., 1995) but are currently estimated to be slow, with the lifetime of iodide in oxygenated waters ranging from months to several decades (Chance et al., 2014). Since iodide is not oxidized instantaneously, upwelling of anoxic (iodide-rich) waters from anoxic basins or oxygen minimum zones (OMZs) to well-oxygenated surface waters results in lower iodate concentrations compared to those in the open ocean, promoting accumulation of bulk carbonate with relatively low I/Ca ratios. Such a decrease in bulk I/Ca does not necessarily represent lower

dissolved oxygen levels in the mixed layer but instead reflects redox conditions in the underlying water masses that are in direct exchange with near-surface waters.

From a global perspective, local I/Ca ratios are also expected to reflect potential significant shifts in the size of the marine iodine reservoir. The contemporary marine iodine budget is not accurately constrained. However, the iodine fluxes (e.g., river and mantle inputs, output of organic matter burial) in and out of seawater are estimated to be 1 to 2 orders of magnitude lower than the amount of iodine associated with biological production (Lu et al., 2010, and references therein). The biological pump results in some iodate loss from mixed-layer waters in high-productivity regions. Such surface depletions have been observed at stations off Hawaii, Bermuda (Campos et al., 1996), the Weddell Sea (Bluhm et al., 2011; Campos et al., 1999), Mediterranean Sea (Tian et al., 1996), Arabian Sea (Farrenkopf and Luther, 2002), and an Antarctic coastal site (Chance et al., 2010). Most of this iodine is released back into the seawater during the decomposition of organic matter in an oxic water column (Lu et al., 2010, and references therein), but organic carbon burial results in a large flux of iodine to the sediments. Consequently, enhanced primary production should export more organic iodine out of the mixed layer, lowering total iodine concentration and hence lowering I/Ca in bulk carbonate. If the burial of organic carbon can lead to global iodine drawdown, it is anticipated that I/Ca decreases will generally correlate with increases in $\delta^{13}\text{C}$.

Bulk carbonate I/Ca signals may be affected by other factors in addition to the local upper ocean redox conditions. Mixing with diagenetic carbonate or recrystallization of primary carbonate in anoxic pore waters should lower the I/Ca values, since iodide, the only inorganic iodine species in anoxic marine or pore waters (Wong and Brewer, 1977; Wong et al., 1985; Kennedy and Elderfield, 1987a, 1987b; Luther and Campbell, 1991; Farrenkopf et al., 1997; Rue

et al., 1997; Farrenkopf and Luther, 2002), cannot be incorporated into carbonate (Lu et al., 2010). Therefore, carbonates with obvious diagenetic features should be avoided for measurements of I/Ca.

1.3. Multiproxy Comparisons

New I/Ca data presented and discussed in this study represent several end-member locations recording OAE 2, covering different paleowater depths, paleolatitudes, organic carbon contents, and accumulation rates (Figure 1 and Table 1). Sulfur isotope data (Adams et al., 2010; Owens et al., 2013) are compared with our I/Ca records to further constrain the global redox conditions. Relatively low I/Ca values found at multiple sections recording the OAE may indicate widespread oxygen-depleted conditions. For example, during the early Toarcian OAE, a section of shallow-water carbonates recorded an I/Ca decrease of $\sim 4 \mu\text{mol/mol}$ in phase with the onset of positive carbon isotope excursion (CIE) and coincided tightly with the beginning of a large shift in the sulfur isotope composition of carbonate-associated sulfate (Lu et al., 2010; Gill et al., 2011).

The $\delta^{34}\text{S}_{\text{CAS}}$ can provide useful information about changes in paleoredox, but it could be affected by multiple environmental changes, such as changes in the input from continental weathering, volcanism, and hydrothermal activity; pyrite and evaporite deposition; and the availability of sulfate, iron, and organic matter (e.g., Paytan et al., 2004). However, recording a positive $\delta^{34}\text{S}_{\text{CAS}}$ excursion in multiple ocean basins over a short event is nearly impossible without the burial of isotopically light sulfur, most plausibly from a global increase in pyrite burial. Importantly, although I/Ca and $\delta^{34}\text{S}$ are expected to show general similarities in their behavior during major oxygenation changes, they will not necessarily covary precisely, due to

their distinct biogeochemical behaviors (Hardisty et al., 2014). In the modern ocean, the residence time for sulfate is 10–15 Myr (Walker, 1986), which is much longer than the ~300 kyr estimated for iodine (Broecker and Peng, 1982), although this residence time is likely to have been different during the OAE 2 since oceanic sulfate concentrations perhaps were ~1/4 of the modern value (7 mM versus 28 mM) (Paytan et al., 2004; Owens et al., 2013). Generally, however, $\delta^{34}\text{S}_{\text{CAS}}$ should illustrate dominantly a global signal and I/Ca a local one.

Calcium and lithium isotopes are important markers for crustal weathering rates during OAE 2 (Blättler et al., 2011; Pogge von Strandmann et al., 2013). These isotopic records are also examined to illuminate any potential influence of weathering on the marine iodine budget and I/Ca signals. Finally, the oceanographic I/Ca pattern is linked to the oxygenation conditions modeled in the Grid Enabled Integrated Earth System Model (GENIE) (Monteiro et al., 2012).

2. Study Sites

New I/Ca data are reported from seven sections and compared with the previously published data from Eastbourne, UK (Table 1) (Lu et al., 2010; Tsikos et al., 2004). The sections are mostly located either within or peripheral to the proto-Atlantic Ocean (Figure 1). This sample set covers a variety of paleowater depths and lithologies from shallow-water platform carbonates to pelagic chalks and shales. Material from Raia del Pedale, Italy; Eastbourne, UK; South Ferriby, UK; and Newfoundland Drifts, northwestern Atlantic are mostly organic-lean carbonates, although the latter two sites contain thin (centimeter-scale) black organic-rich shales. The Aristocrat Angus core in the U.S. Western Interior Seaway (WIS) and at Demerara Rise, offshore Suriname and the Tarfaya (Morocco) site, have relatively elevated total organic carbon (TOC) in marls and shales (commonly >5%) throughout the studied interval.

3. Analytical Methods

3.1. Sample Preparation and Measurements

Powdered samples (3–5 mg) from different lithological settings were weighed out on a microgram balance and then rinsed with deionized water to remove dissolvable iodine salt potentially attached to the surface of the samples. Next, a volume of nitric acid (3%) was calculated according to sample weight, and the acid was added to each sample in a sonicating bath to allow complete dissolution of the carbonate. Residual noncarbonate impurities were removed by centrifuging. The final solutions for the inductively coupled plasma–mass spectrometry (ICP-MS) measurements contain approximately 50 ppm Ca and 0.5% tertiary amine to help stabilize iodate (Schnetger and Muramatsu, 1996) and internal standards. For each batch of measurements, pure potassium iodate was dissolved and diluted as a calibration standard. I/Ca was measured on a quadrupole ICP-MS (Bruker M90) at Syracuse University. The sensitivity of I-127 is tuned to about 80–100 kcps for a 1 ppb standard. The precision of ^{127}I is typically better than 1% and is not reported individually for each sample. The long-term accuracy is guaranteed by repeated measurements of the reference material JCp-1 (Lu et al., 2010). The detection limit of I/Ca is usually below 0.1 $\mu\text{mol/mol}$. I/Ca values generated in this process are specific to carbonate, with minor influence from clay, silicate, and organic matter. The liberation of iodine attached to noncarbonate phases during chemical analysis can artificially increase the I/Ca values. This process is particularly important when dealing with sediments relatively high in TOC, because marine organic matter is enriched in iodine.

3.2. Earth System Modeling

As an aid to the interpretation of our I/Ca records, we make use of a pair of simulations carried out in a 3-D ocean circulation-based Earth System Model (“cGENIE”) (Ridgwell et al., 2007). For this paper, the climatology and continental arrangements are configured for the Cenomanian-Turonian as described in Monteiro et al. (2012). Carbon and other biogeochemical cycles in the ocean include PO_4^{3-} , NO_3^- , and NH_4^+ as nutrients controlling biological export production, plus O_2 , NO_3^- , and SO_4^{2-} as potential oxidants (Ridgwell et al., 2007; Monteiro et al., 2012). We ran two experiments: one representing potential pre-OAE 2 redox conditions and assuming a modern ocean PO_4^{3-} inventory and $\times 2$ preindustrial CO_2 in the atmosphere and another assuming syn-OAE 2 conditions, with $\times 2$ PO_4^{3-} and $\times 4$ CO_2 . These combinations of oceanic PO_4^{3-} and atmospheric CO_2 determined by Monteiro et al. (2012) yield the best possible fit to available indicators of ocean floor anoxia and photic zone euxinia. We ran both experiments for 20 kyr to achieve full steady state with respect to patterns of ocean oxygenation and nitrogen cycling. The model code and experimental configurations are identical to those described in Monteiro et al. (2012) and can be replicated via the instructions given in the supporting information.

4. Results and Discussions

4.1. Influence of Diagenesis and Organically Bound Iodine

Bulk carbonate I/Ca signals may be affected by secondary factors in addition to the local upper ocean redox conditions. Mixing with diagenetic carbonate or recrystallization of primary carbonate in anoxic pore waters should lower the I/Ca values, since iodide in anoxic waters cannot be incorporated in carbonate. It is possible that all of the I/Ca values are influenced by diagenesis to some extent. However, the consistency demonstrated by multiproxy and data-

model comparisons across different depositional settings suggests that bulk carbonate I/Ca can still serve as a reasonably reliable redox proxy for the suboxic window. Site 1258 on Demerara Rise is the only locality where diagenetic carbonate is common (Erbacher et al., 2004). The CIE is not very well expressed in the carbonates at the Tarfaya section, indicating possible diagenesis, but the carbonate record in Eastbourne appears largely unaffected by diagenesis and has proved an invaluable geochemical archive (Tsikos et al., 2004). Minor dolomite is present in the basal part of the Raia del Pedale section but below the CIE interval. As demonstrated below, Tarfaya and the Western Interior Seaway (WIS) sites both have relatively high TOC contents, but the corresponding I/Ca values are much lower than those at sites dominated by low-TOC chalk, suggesting that organic iodine does not always significantly affect I/Ca. Furthermore, the lowest I/Ca values at Tarfaya and in the WIS correlate with high TOC during the OAE. These observations strongly argue against organic matter being an important contaminant of the carbonate I/Ca signal, particularly since our method employs brief exposure to only dilute acid.

4.2. Shallow-Water Sites

At all seven sections, the OAE is defined by the positive CIE and ensuing recovery. Raia del Pedale, Italy, is an organic-lean, carbonate-platform section comprising gray lime mudstones containing benthic foraminifera and thick-shelled fossils such as rudists, likely deposited in waters only a few meters deep (Parente et al., 2008) (Figure 1). Although the pre-OAE interval is not exposed in outcrop, the OAE and post-OAE intervals were sampled in detail (Figure 2). During the pre-CIE and CIE, I/Ca values are consistently low at $\sim 1 \mu\text{mol/mol}$, indicating that the local near-surface waters had relatively low iodate concentrations and were likely proximal to and were mixing with low-oxygen iodide-rich waters brought onto the platform. These

conditions were stable locally before and during OAE 2, as indicated by the small variability in I/Ca. Immediately above the level of the CIE, I/Ca briefly increases to above 4 $\mu\text{mol/mol}$ and then returns to low values similar to those of the OAE, but with scattering between ~ 0.5 and 2.5 $\mu\text{mol/mol}$. I/Ca values average at 1.2 $\mu\text{mol/mol}$, which are lower than those at pelagic shelf sea sites such as Eastbourne (Lu et al., 2010).

The $\delta^{34}\text{S}_{\text{CAS}}$ plot for Raia del Pedale shows a gradual increase of up to 6‰ during and slightly post-CIE and then declines further up section. The timing of the reversal of $\delta^{34}\text{S}_{\text{CAS}}$ trend coincides precisely with the rapid recovery in I/Ca at the end of the CIE (Figure 2), suggesting that a more oxygenated water mass developed post-OAE at this site, conforming to global trends of lower pyrite burial rates. There is no notable relationship between I/Ca ratios and Li isotope profiles (Pogge von Strandmann et al., 2013), suggesting that weathering rates do not control the iodine trend at this locality.

The Aristocrat Angus core in Western Interior Seaway (WIS) records the well-established positive global carbon isotope excursion during the OAE 2 (Sageman et al., 2006; Joo and Sageman, 2014). Sulfur isotope records have been generated from the Portland core (Adams et al., 2010); wt % TOC does not covary systematically with these isotopic records (Sageman et al., 1998; Meyers et al., 2005). The WIS represents a unique depositional environment among the studied sites. It was a relatively restricted shallow-water seaway (100 to 200m water depth (Kauffman and Caldwell, 1993)), where local iodine concentration and speciation should have been very sensitive to organic matter burial and redox conditions. I/Ca ratios from the Aristocrat Angus core (Joo and Sageman, 2014), WIS, are all relatively low (<1.2 $\mu\text{mol/mol}$; Figure 3). The I/Ca ratios peak at the early stage of the CIE at levels marked by relatively low TOC content. This observation may indicate a short period characterized by better

oxygenated local waters, known as the Plenus Cold Event/Benthic Oxidic Event. This event has been linked to climatic cooling and the presence of more oxygenated waters in other regions during the same time interval and was characterized by a temporary influx of benthic foraminifera in successions otherwise generally barren of benthic fauna (Gale and Christensen, 1996; Keller and Pardo, 2004; Forster et al., 2007; Jarvis et al., 2011; Alegret and Thomas, 2013; Eldrett et al., 2014). Lower I/Ca and higher TOC following the Plenus Cold Event suggest a return to local more poorly oxygenated conditions during the latter part of the global OAE.

4.3. Low-Latitude Pelagic Sites

The tropical proto-Atlantic, particularly the northern South Atlantic, is thought to have hosted the most reducing water masses during OAE 2, based on the relative abundance of biomarkers for phototrophic sulfide oxidizers (Sinninghe Damsté and Koster, 1998; Kuypers et al., 2002). Our study centered on two locations: Demerara Rise and Tarfaya, Morocco, which are characterized by high TOC levels and serve as tropical peri-equatorial end-member sites (Figure 1). Both sites are within the modeled upwelling region (Topper et al., 2011) dominated by deepwater euxinia and episodic photic-zone euxinia (Kuypers et al., 2002; van Bentum et al., 2009). Shallow euxinic conditions or upwelling of euxinic deep water should have limited the iodate concentrations in surface waters significantly and set up a steep gradient of iodate concentration between the sea surface and the base of the photic zone.

The I/Ca ratios at Tarfaya are between 0.14 and 1.6 $\mu\text{mol/mol}$ (Figure 4), which are significantly lower than the range at Eastbourne ($\sim 2\text{--}5 \mu\text{mol/mol}$). The I/Ca profile generally changes in the opposite direction to that of carbon isotopes at the same time. During the peak CIE, I/Ca ratios are relatively low, and $\delta^{15}\text{N}$ values illustrate a broad positive excursion, which

may indicate regional upwelling of anoxic waters that promoted both iodate reduction and denitrification and/or anammox processes (Jenkyns et al., 2007).

Site 1258 on Demerara Rise is currently located at a water depth of over 3 km below modern sea level, although the exact depth of this submarine feature during the mid-Cretaceous remains unresolved. The majority of I/Ca ratios at Site 1258 are below 0.6 $\mu\text{mol/mol}$, with the lowest average ratio among all the sections (Figure 1). The stratigraphic trend for I/Ca is broadly the inverse of the trend for carbonate content (Figure 5), which is likely a result of authigenic carbonate diluting/dominating the bulk rock I/Ca signal. Sediments with lighter colors in the studied interval reflect higher carbonate content, identified as layers of significant diagenetic calcite growth (Erbacher et al., 2004). The high $\text{CaCO}_3\%$ and near-zero I/Ca values at core depths of 421 and 428m also coincide with peaks of bulk sediment Mn concentration, interpreted to reflect formation of authigenic Mn-rich carbonate (Hetzl et al., 2009). Diagenetic carbonate that precipitated in anoxic pore waters does not incorporate iodine, because iodide is the only iodine species in reducing pore water (Kennedy and Elderfield, 1987a, 1987b), and as discussed above, the calcite structure does not accommodate this ion (Lu et al., 2010). Hence, a significant quantity of diagenetic calcite has likely compromised the primary I/Ca record of this particular locality.

However, other proxies suggest that euxinic water masses were present at this site (Hetzl et al., 2009), which may indicate that low I/Ca ratios, if not solely due to diagenesis, also represent anoxic conditions near the surface, either by reduction in the local area or by mixing with underlying or laterally adjacent anoxic water masses. Euxinic conditions, below the surface waters, are suggested at Site 1258 by the Fe, S, and Mo data (Hetzl et al., 2009), and $\delta^{15}\text{N}$ values suggest upwelling of reduced nitrogen species that fueled planktonic productivity

(Higgins et al., 2012). Consistent with these indicators, the interval analyzed in our study consists of finely laminated black shales with locally developed phosphatic limestone nodules (Erbacher et al., 2005).

4.4. Midlatitude Pelagic Sites

New I/Ca data have been generated from a northeast European shelf sea pelagic sequence (South Ferriby in the UK) and from a lithologically similar sequence in the Newfoundland Drifts in the northwest Atlantic (Expedition 342 Scientists, 2012). The South Ferriby section contains mostly organic-lean chalk, except for an interval of ~10 cm thick black shale, where TOC rises to 8% (Jenkyns et al., 2007). The onset and main part of the CIE are missing at South Ferriby due to a hiatus (Figure 6). The baseline of I/Ca ratios shows a slight decrease starting below the CIE and a gradual increase above the CIE. The preevent baseline varies between 2 and ~4 $\mu\text{mol/mol}$, which is very similar to the range at Eastbourne, indicating an oxygenated water mass. Notably, much higher I/Ca spikes are observed immediately below three clayrich layers in this section (Figure 6). The spikes became increasingly muted during the recovery from the peak CIE. The highest I/Ca value (7.4 $\mu\text{mol/mol}$) found here is the highest among all OAE 2 carbonates. These spikes may be related to local invasion of well-oxygenated water masses with high iodate concentrations.

The $\delta^{34}\text{S}_{\text{CAS}}$ increases during the CIE and then starts to decrease at ~140 cm, postdating the CIE, where the I/Ca spikes disappear and the baseline rises. Both Ca and Li isotopes indicate enhanced global weathering (Blätler et al., 2011; Pogge von Strandmann et al., 2013), which may have increased river input of iodine into the ocean and generated higher I/Ca values. These negative Ca and Li isotope trends, however, broadly correspond to the interval of low I/Ca

values in most sections, with the exception of a few spikes at South Ferriby. These oscillations in I/Ca are more likely the result of local episodic oceanographic changes rather than changes in the global iodine budget. Unlike the WIS and Eastbourne sites, the Plenus Cold Event is not recorded from the South Ferriby site. The South Ferriby section is, however, condensed by a factor of ~20 compared to Eastbourne (Gale et al., 1993), and a hiatus is present near the level of onset of the CIE in this section, making it likely that the Plenus Cold Event was lost from the sedimentary sequence (e.g., Hart and Leary, 1989).

The lithostratigraphy at Site U1407, Newfoundland Drifts, comprises a thick sequence of nannofossil chalk, varying from white to dark gray in color, above and below the black shale (~0.4 m near the depth of 232 m). A hiatus appears within the CIE interval at ~231–232 m. Unpublished carbon isotope data (C. Junium) indicate that the CIE bracketing the black shale outlines the OAE 2 interval between 229 and 233m (Figure 7). I/Ca ratios mostly fluctuate at 2–4 $\mu\text{mol/mol}$ before the CIE, with lower values occasionally observed coinciding with dark chalk. The I/Ca ratios decrease right at the onset level of the CIE, coincident with the base of the black shale. The recovery of I/Ca starts with values below 1 $\mu\text{mol/mol}$ and rises slowly to pre-OAE background levels near 3 $\mu\text{mol/mol}$. These data suggest that at this site, the proximal water masses that mix with the local surface waters were generally oxygenated before the OAE, whereas oxygen was rapidly removed from the local surface waters, where the iodine signal is captured, at the onset of the event itself, before slowly returning to background levels.

Eastbourne is among the most studied OAE 2 sites and was included in the first I/Ca investigation of the ancient ocean (Lu et al., 2010). However, several important observations have since emerged from multiproxy comparisons that have refined our view of those data (Blätler et al., 2011; Owens et al., 2013; Pogge von Strandmann et al., 2013). Relatively high

I/Ca values and an excursion to lower $\delta^{34}\text{S}_{\text{CAS}}$ values are reported from Eastbourne at levels corresponding with the lower part of the CIE (Figure 8) (Lu et al., 2010; Owens et al., 2013). These geochemical data likely record reoxygenation related to the Plenus Cold Event, which occurred during the early phase of OAE 2 and was initially proposed for the European Chalk Sea and the Western Interior Seaway based on southward invasion of boreal faunas (Gale and Christensen, 1996; Keller and Pardo, 2004; Forster et al., 2007). However, $p\text{CO}_2$ records based on stomata and $\Delta^{13}\text{C}$ indicate that the cooling and CO_2 drawdown were likely global during the first third of the CIE (Friedrich et al., 2006; Barclay et al., 2010; Jarvis et al., 2011). The high I/Ca values found at Eastbourne at a level close to the suggested base of the Plenus interval indicate that the spatial extent of oxygenated waters may have been more widespread than previously assumed during this event, although upper ocean geochemical conditions may not have evolved synchronously with bottom water conditions.

4.5. Data Model Comparisons

To help visualize patterns emerging from the data, the average and ranges of I/Ca are marked on the map in Figure 1 as a simple generalized representation of the overall conditions throughout the studied interval at each site. Three sites located in the NW proto-Atlantic and European shelf sea (Newfoundland Drifts and Eastbourne and South Ferriby, UK) were generally more oxygenated, as indicated by higher background I/Ca, compared with other regions. The area of this oxygen anomaly is small compared to the majority of the proto-Atlantic localities showing lower I/Ca values. By contrast, the paleo-Pacific ocean has been suggested to be largely oxic (Takashima et al., 2011; Hasegawa et al., 2013), with black shales developed in equatorial regions (Schlanger et al., 1987; Arthur et al., 1988).

Higher dissolved oxygen concentrations are also found in the northeastern proto-Atlantic and European shelf sea prior to OAE 2 in the Earth System Model simulations (Monteiro et al., 2012) (Figure 9). This modeled oxygen maximum occurs only as deep as ~500m, with the maximum depth decreasing south and away from the continental margin (Figure 9c). Upper water column oxygenation generally decreasing toward the equator is also consistent with proxy data. The I/Ca values are similar for South Ferriby and Eastbourne but are higher than those for Newfoundland Drifts (Figure 1). During OAE 2, oxygen depletion is enhanced throughout much of the ocean in GENIE (Figures 9d–9f). However, the northernmost regions of the proto-Atlantic and European pelagic shelf sea retain an oxygenated water column, consistent with data from South Ferriby showing only very minimal variations in baseline I/Ca during the CIE (Figure 6).

In the model simulations, oxygen depletion is most intense close to the equator on the eastern side of basins due to upwelling fueling biological productivity (and hence subsurface O₂ consumption), as well as subtropical regions of relatively restricted topography. At higher latitudes, the depth of seasonal mixing increases, keeping the upper water column oxygenated. For the northerly proto-Atlantic, mixing results in oxygenation down to depths of up to ~500 m, although true intermediate or deep water does not form in the cGENIE simulations (unlike the case in the far North Pacific and parts of the Southern Ocean). The proxy interpretation for sites such as South Ferriby is that they were predominantly supplied with oxygenated and iodate-rich surface currents, as opposed to the primarily upwelled and iodate-depleted waters at Demerara Rise and Tarfaya.

The notable exception to the otherwise general model data consistency is the Western Interior Seaway (Figure 1). Epeiric seas are poorly resolved in the cGENIE Earth System Model at this resolution (10° increments in longitude with variations but on average 5° spacing in

latitude), posing problems for such a shallow and restricted environment. A second caveat is that, as configured with a highly parameterized 2-D energy-moisture-balance atmospheric component (Edwards and Marsh, 2005), the model fails to exhibit interannual variability and is run to steady state. Hence, the possible role of fluctuating ocean currents and upwelling intensity that might explain redox changes and variability in I/Ca values cannot be addressed. Future modeling work could employ higher-resolution settings and involve simulations of ocean dynamics to improve data-model comparisons for epeiric seas.

4.6. Tempo of Local Redox Changes

During OAEs, the tipping point in the global carbon cycle marked by onset of the CIE does not necessarily coincide precisely with the deposition of black shales (Tsikos et al., 2004) or the buildup of low-oxygen water masses at specific locations. As correlated by the diagnostic carbon-isotope chemostratigraphic profiles, I/Ca records suggest highly dynamic local redox changes that were not always synchronous with the pace of global organic matter burial as recorded by the carbon isotope curves (Figure 10). Demerara Rise is excluded from this compilation due to the presence of diagenetic carbonate in the core. At two pelagic shelf sea sites (Eastbourne and South Ferriby), I/Ca ratios start to decrease below the onset level of the CIE but not necessarily at the same time, indicating that deoxygenation, likely linked to productivity, began to intensify before the global carbon cycle reached its tipping point and initiated the CIE.

At the Eastbourne site, I/Ca shifted to higher values rapidly and simultaneously with $\delta^{13}\text{C}$ during the middle of the CIE (Figure 10) and remained high during the later stage of the CIE. However, I/Ca reached maximum value at the onset of CIE at the Tarfaya site, decreased rapidly, and shows minimum values stratigraphically just above the depth in core with the highest $\delta^{13}\text{C}$

values. The most reducing local/regional conditions in at least part of the Western Interior Seaway are also registered postdating the peak CIE. I/Ca values during the CIE at Raia del Pedale were consistently low with very little variation and do not vary with changes in carbon isotope values. Similarly, I/Ca continued to rise after the CIE at the Newfoundland Drifts site, Eastbourne, and South Ferriby. This compilation of I/Ca data (Figure 10) indicates that the local oxygen levels in the upper ocean were highly heterogeneous across different sites and different ocean basins during OAE 2, indicating that redox changes did not necessarily follow the global $\delta^{13}\text{C}$ trend.

4.7. Marine Iodine Budget

Globally, the marine iodine budget may be affected by increased continental weathering and organic carbon (iodine) burial. If I/Ca records were predominantly artifacts related only to global changes in total iodine concentration (iodide + iodate), the I/Ca trends at different sites would show considerable similarities, as is observed for the isotopic records of Ca, Li, and C (Figures 2, 6, 8, and 10). Therefore, the differing I/Ca records among the studied sites probably have been affected by local redox conditions more than the potential large-scale changes in total iodine concentration. Sr isotopes ($^{87}\text{Sr}/^{86}\text{Sr}$) increased transiently at the onset of OAE 2, such as at Ocean Drilling Program (ODP) Site 551 in the northeast Atlantic (Bralower et al., 1997) and the southern Apennines of Italy (Frijia and Parente, 2008), suggesting a pulse of enhanced continental weathering, although the overall trend is nonradiogenic. Because Sr isotopes are significantly affected by hydrothermal activity and volcanism, which could overprint the effects of changing weathering rates, this isotopic ratio is not discussed in this study as a weathering proxy (Jenkyns, 2010). The observed I/Ca trends among sites are very different compared to

calcium, lithium, and carbon isotope records. Eastbourne and Raia del Pedale have both Li isotope and I/Ca data covering the rising interval of $\delta^{13}\text{C}$, a period of rapid global organic carbon burial. The two global proxies ($\delta^7\text{Li}$ and $\delta^{13}\text{C}$) show slightly better correlation ($R^2 > 0.50$), compared to I/Ca versus $\delta^{13}\text{C}$ ($R^2 < 0.15$; Figure 11).

Plotting Ca isotopes against $\delta^{13}\text{C}$ and I/Ca separately does not show any major correlation, likely due to the sample resolution and analytical uncertainty in Ca isotope records (Blättler et al., 2011). Therefore, any global surplus/deficit in the marine iodine budget related to weathering or organic carbon burial was masked by the signal related to dynamic local/regional redox changes in the upper ocean. Although some changes in the iodine budget during global redox shifts and organic carbon burial events are highly likely, this current data set seems to demonstrate that bulk carbonate I/Ca is primarily a proxy reflecting local and proximal upper ocean environmental conditions, at least during OAE 2.

5. Conclusions

Multiple I/Ca records suggest that global upper ocean redox conditions during the Cenomanian-Turonian Oceanic Anoxic Event were remarkably variable. The timing of deoxygenation in the upper ocean was not uniform across ocean basins, and the initial development of poorly oxygenated near-surface waters at some Atlantic locations predated the global carbon isotope excursion. A shallow oxygen oasis in the NE proto-Atlantic and European pelagic shelf sea is supported by both higher I/Ca values in multiple sites and by Earth System Modeling. Comparison between weathering indices and I/Ca records suggests that continental input was not a major driver of changes in the marine iodine budget on the time scale of the OAE. The highly variable stratigraphic I/Ca trends at the investigated sites indicate that I/Ca is

primarily a proxy for local redox conditions rather than for global iodine cycling during OAEs. I/Ca and $\delta^{34}\text{S}_{\text{CAS}}$ data both indicate important water mass redox changes, but the latter reflects processes operating on a global scale. This study further demonstrates the potential of I/Ca as a unique paleoceanographic proxy for the identification of relative subtle oxygenation changes in Earth's history (Loope et al., 2013; Hardisty et al., 2014; Zhou et al., 2014).

Acknowledgments

Z.L. thanks NSF OCE 1232620. J.D.O. is supported by an Agouron Postdoctoral Fellowship.

T.W.L. acknowledges support from the NSF-EAR and NASA-NAI. A.R. thanks the support of NERC via NE/J01043X/1. We are deeply grateful for the constructive and thorough reviews by Ian Jarvis and Maya Gomes. I/Ca data can be found in the supporting information.

References

- Adams, D. D., M. T. Hurtgen, and B. B. Sageman (2010), Volcanic triggering of a biogeochemical cascade during oceanic anoxic event 2, *Nat. Geosci.*, 3, 201–204.
- Alegret, L., and E. Thomas (2013), Benthic foraminifera across the Cretaceous/Paleogene boundary in the Southern Ocean (ODP Site 690): Diversity, food and carbonate saturation, *Mar. Micropaleontol.*, 105, 40–51.
- Arthur, M. A., E. D. Walter, and M. P. Lisa (1988), Geochemical and climatic effects of increased marine organic carbon burial at the Cenomanian/Turonian boundary, *Nature*, 335, 714–717.
- Arthur, M. A., H. C. Jenkyns, H.-J. Brumsack, and S. O. Schlanger (1990), Stratigraphy, geochemistry, and paleoceanography of organic carbon-rich Cretaceous sequences, in *Cretaceous Resources, Events and Rhythms*, NATO ASI Ser. C, vol. 304, edited by R. N. Ginsburg and B. Beaudoin, pp. 75–119, Kluwer Acad., Dordrecht, Netherlands.
- Barclay, R. S., J. C. McElwain, and B. B. Sageman (2010), Carbon sequestration activated by a volcanic CO₂ pulse during ocean anoxic event 2, *Nat. Geosci.*, 3, 205–208.
- Blättler, C. L., H. C. Jenkyns, L. M. Reynard, and G. M. Henderson (2011), Significant increases in global weathering during oceanic anoxic events 1a and 2 indicated by calcium isotopes, *Earth Planet. Sci. Lett.*, 309, 77–88.
- Bluhm, K., P. L. Croot, O. Huhn, G. Rohardt, and K. Lochte (2011), Distribution of iodide and iodate in the Atlantic sector of the southern ocean during austral summer, *Deep Sea Res., Part II*, 58, 2733–2748.

- Bralower, T. J., P. D. Fullagar, C. K. Paull, G. S. Dwyer, and R. M. Leckie (1997), Mid-Cretaceous strontium-isotope stratigraphy of deep-sea sections, *Geol. Soc. Am. Bull.*, 109, 1421–1442.
- Broecker, W. S., and E. Clark (2009), Ratio of coccolith CaCO₃ to foraminifera CaCO₃ in late Holocene deep sea sediments, *Paleoceanography*, 24, PA3205, doi:10.1029/2009PA001731.
- Broecker, W. S., and T.-H. Peng (1982), *Tracers in the Sea*, Lamont-Doherty Geological Observatory, Columbia Univ., Palisades, N. Y.
- Brumsack, H. (2006), The trace metal content of recent organic carbon-rich sediments: Implications for Cretaceous black shale formation, *Palaeogeogr. Palaeoclimatol. Palaeoecol.*, 232, 344–361.
- Campos, M., A. M. Farrenkopf, T. D. Jickells, and G. W. Luther (1996), A comparison of dissolved iodine cycling at the Bermuda Atlantic Time-Series station and Hawaii Ocean Time-Series Station, *Deep Sea Res., Part II*, 43, 455–466.
- Campos, M., R. Sanders, and T. Jickells (1999), The dissolved iodate and iodide distribution in the South Atlantic from the Weddell Sea to Brazil, *Mar. Chem.*, 65, 167–175.
- Chance, R., et al. (2010), Seasonal and interannual variation of dissolved iodine speciation at a coastal Antarctic site, *Mar. Chem.*, 118, 171–181.
- Chance, R., A. R. Baker, L. Carpenter, and T. D. Jickells (2014), The distribution of iodide at the sea surface, *Environ. Sci. Process. Impacts*, 16, 1841.
- Du Vivier, A., D. Selby, B. B. Sageman, I. Jarvis, D. R. Gröcke, and S. Voigt (2014), Marine ¹⁸⁷Os/¹⁸⁸Os isotope stratigraphy reveals the interaction of volcanism and ocean circulation during oceanic anoxic event 2, *Earth Planet. Sci. Lett.*, 389, 23–33.

- Edwards, N. R., and R. Marsh (2005), Uncertainties due to transport-parameter sensitivity in an efficient 3-D ocean-climate model, *Clim. Dyn.*, 24, 415–433, doi:10.1007/s00382-004-0508-8.
- Eldrett, J. S., D. Minisini, and S. C. Bergman (2014), Decoupling of the carbon cycle during ocean anoxic event 2, *Geology*, 42, 567–570.
- Elrick, M., R. Molina-Garza, R. Duncan, and L. Snow (2009), C-isotope stratigraphy and paleoenvironment changes across OAE 2 (mid-Cretaceous) from shallow-water platform carbonates of southern Mexico, *Earth Planet. Sci. Lett.*, 277, 295–306.
- Erba, E. (2004), Calcareous nannofossils and Mesozoic oceanic anoxic events, *Mar. Micropaleontol.*, 52, 85–106.
- Erbacher, J., D. C. Mosher, M. J. Malone, and O. L. S. Party (2004), Drilling probes past carbon cycle perturbations on the Demerara Rise, *Eos Trans. AGU*, 85, 57–68, doi:10.1029/2004EO060001.
- Erbacher, J., O. Friedrich, P. A. Wilson, H. Birch, and J. Mutterlose (2005), Stable organic carbon isotope stratigraphy across oceanic anoxic event 2 of Demerara Rise, western tropical Atlantic, *Geochem. Geophys. Geosyst.*, 6, Q06010, doi:10.1029/2004GC000850.
- Expedition 342 Scientists (2012), Paleogene Newfoundland sediment drifts, IODP Preliminary Reports, 342.
- Farrenkopf, A. M., and G. W. Luther (2002), Iodine chemistry reflects productivity and denitrification in the Arabian Sea: Evidence for flux of dissolved species from sediments of western India into the OMZ, *Deep Sea Res., Part II*, 49, 2303–2318.

- Farrenkopf, A. M., G. W. Luther, V. W. Truesdale, and C. H. Van der Weijden (1997), Sub-surface iodide maxima: Evidence for biologically catalyzed redox cycling in Arabian Sea OMZ during the SW intermonsoon, *Deep Sea Res., Part II*, 44, 1391–1409.
- Forster, A., S. Schouten, K. Moriya, P. A. Wilson, and J. S. Sinninghe Damsté (2007), Tropical warming and intermittent cooling during the Cenomanian/Turonian oceanic anoxic event 2: Sea surface temperature records from the equatorial Atlantic, *Paleoceanography*, 22, PA1219, doi:10.1029/2006PA001349.
- Forster, A., M. M. M. Kuypers, S. C. Turgeon, H.-J. Brumsack, M. R. Petrizzo, and J. S. Sinninghe Damsté (2008), The Cenomanian/Turonian oceanic anoxic event in the South Atlantic: New insights from a geochemical study of DSDP Site 530A, *Palaeogeogr. Palaeoclimatol. Palaeoecol.*, 267, 256–283.
- Friedrich, O., J. Erbacher, and J. Mutterlose (2006), Paleoenvironmental changes across the Cenomanian/Turonian boundary event (oceanic anoxic event 2) as indicated by benthic foraminifera from the Demerara Rise (ODP Leg 207), *Rev. Micropaléontol.*, 49, 121–139.
- Frijia, G., and M. Parente (2008), Strontium isotope stratigraphy in the upper Cenomanian shallow-water carbonates of the southern Apennines: Short-term perturbations of marine $^{87}\text{Sr}/^{86}\text{Sr}$ during the oceanic anoxic event 2, *Palaeogeogr. Palaeoclimatol. Palaeoecol.*, 261, 15–29.
- Gale, A. S., and W. K. Christensen (1996), Occurrence of the belemnite *Actinocamax plenus* in the Cenomanian of SE France and its significance, *Bull. Geol. Soc. Den.*, 43, 68–77.

- Gale, A. S., H. C. Jenkyns, W. J. Kennedy, and R. M. Corfield (1993), Chemostratigraphy versus biostratigraphy: Data from around the Cenomanian-Turonian boundary, *J. Geol. Soc. London*, 150, 29–32.
- Gill, B. C., T. W. Lyons, and H. C. Jenkyns (2011), A global perturbation to the sulfur cycle during the Toarcian oceanic anoxic event, *Earth Planet. Sci. Lett.*, 312, 484–496.
- Hardisty, D. S., Z. Lu, N. J. Planavsky, A. Bekker, P. Philippot, X. Zhou, and T. W. Lyons (2014), An iodine record of Paleoproterozoic surface ocean oxygenation, *Geology*, 42, 619–622.
- Harris, D. C. (2006), *Quantitative Chemical Analysis*, 6th ed., W. H. Freeman, New York.
- Hart, M. B., and P. N. Leary (1989), The stratigraphic and palaeogeographic setting of the late Cenomanian “anoxic” event, *J. Geol. Soc.*, 146, 305–310.
- Hasegawa, T., J. S. Crampton, P. Schioler, B. Field, K. Fukushi, and Y. Kakizaki (2013), Carbon isotope stratigraphy and depositional oxia through Cenomanian/Turonian boundary sequences (Upper Cretaceous) in New Zealand, *Cretaceous Res.*, 40, 61–80.
- Hetzel, A., M. E. Bottcher, U. G. Wortmann, and H.-J. Brumsack (2009), Paleo-redox conditions during OAE 2 reflected in Demerara Rise sediment geochemistry (ODP Leg 207), *Palaeogeogr. Palaeoclimatol. Palaeoecol.*, 273, 302–328.
- Higgins, M., R. S. Robinson, J. M. Husson, S. J. Carter, and A. Pearson (2012), Dominant eukaryotic export production during ocean anoxic events reflects the importance of recycled NH_4^+ , *Proc. Natl. Acad. Sci. U.S.A.*, 109, 2269–2274.
- Jarvis, I., J. S. Lignum, D. R. Gröcke, H. C. Jenkyns, and M. A. Pearce (2011), Black shale deposition, atmospheric CO_2 drawdown and cooling during the Cenomanian-Turonian

- oceanic anoxic event (OAE 2), *Paleoceanography*, 26, PA3201,
doi:10.1029/2010PA002081.
- Jenkyns, H. C. (2003), Evidence for rapid climate change in the Mesozoic-Palaeogene greenhouse world, *Philos. Trans. R. Soc. London, Ser. A*, 361, 1885–1916.
- Jenkyns, H. C. (2010), Geochemistry of oceanic anoxic events, *Geochem. Geophys. Geosyst.*, 11, Q03004, doi:10.1029/2009GC002788.
- Jenkyns, H. C., A. Matthews, H. Tsikos, and Y. Erel (2007), Nitrate reduction, sulfate reduction, and sedimentary iron isotope evolution during the Cenomanian-Turonian oceanic anoxic event, *Paleoceanography*, 22, PA3208, doi:10.1029/2006PA001355.
- Jones, C. E., and H. C. Jenkyns (2001), Seawater strontium isotopes, oceanic anoxic events, and seafloor hydrothermal activity in the Jurassic and Cretaceous, *Am. J. Sci.*, 301, 112–149.
- Joo, Y. J., and B. B. Sageman (2014), Cenomanian to Campanian carbon isotope chemostratigraphy from the Western Interior Basin, *J. Sediment. Res.*, 84, 529–542.
- Kauffman, E. G., and W. G. E. Caldwell (1993), The Western Interior Basin in space and time, in *Evolution of the Western Interior Basin*, *Geol. Assoc. Can. Spec. Pap.*, vol. 39, edited by W. E. Caldwell and E. G. Kauffman, pp. 1–30.
- Keller, G., and A. Pardo (2004), Age and paleoenvironment of the Cenomanian-Turonian global stratotype section and point at Pueblo, Colorado, *Mar. Micropaleontol.*, 51, 95–128.
- Kennedy, H. A., and H. Elderfield (1987a), Iodine diagenesis in pelagic deep-sea sediments, *Geochim. Cosmochim. Acta*, 51, 2489–2504.
- Kennedy, H. A., and H. Elderfield (1987b), Iodine diagenesis in nonpelagic deep-sea sediments, *Geochim. Cosmochim. Acta*, 51, 2505–2514.

- Kolonic, S., et al. (2005), Black shale deposition on the northwest African Shelf during the Cenomanian/Turonian oceanic anoxic event: Climate coupling and global organic carbon burial, *Paleoceanography*, 20, PA1006, doi:10.1029/2003PA000950.
- Kuroda, J., N. O. Ogawa, M. Tanimizu, M. F. Coffin, H. Tokuyama, H. Kitazato, and N. Ohkouchi (2007), Contemporaneous massive subaerial volcanism and late Cretaceous oceanic anoxic event 2, *Earth Planet. Sci. Lett.*, 256, 211–223.
- Kuypers, M. M. M., R. D. Pancost, I. A. Nijenhuis, and J. S. Sinninghe Damsté (2002), Enhanced productivity led to increased organic carbon burial in the euxinic North Atlantic basin during the late Cenomanian oceanic anoxic event, *Paleoceanography*, 17(4), 1051, doi:10.1029/2000PA000569.
- Little, S. H., D. Vance, T. W. Lyons, and J. McManus (2015), Controls on trace metal authigenic enrichment in reducing sediments: Insights from modern oxygen-deficient settings, *Am. J. Sci.*, 315, 77–119.
- Loope, G. R., L. R. Kump, and M. A. Arthur (2013), Shallow water redox conditions from the Permian-Triassic boundary microbialite: The rare earth element and iodine geochemistry of carbonates from Turkey and south China, *Chem. Geol.*, 351, 195–208.
- Lu, Z., H. C. Jenkyns, and R. E. M. Rickaby (2010), Iodine to calcium ratios in marine carbonate as a paleo-redox proxy during oceanic anoxic events, *Geology*, 38, 1107–1110.
- Luther, G. W., and T. Campbell (1991), Iodine speciation in the water column of the Black Sea, *Deep Sea Res., Part I*, 38, S875–S882.
- Luther, G. W., J. Wu, and J. B. Cullen (1995), Redox chemistry of iodine in seawater: Frontier molecular-orbital theory considerations, in *Aquatic Chemistry: Interfacial and*

- Interspecies Processes, *Advances in Chemistry Series*, vol. 224, edited by C. P. Huang, C. R. Omelia, and J. J. Morgan, pp. 135–155.
- Meyers, S. R., B. B. Sageman, and T. W. Lyons (2005), Organic carbon burial rate and the molybdenum proxy: Theoretical framework and application to Cenomanian-Turonian oceanic anoxic event 2, *Paleoceanography*, 20, PA2002, doi:10.1029/2004PA001068.
- Monteiro, F. M., R. D. Pancost, A. Ridgwell, and Y. Donnadieu (2012), Nutrients as the dominant control on the spread of anoxia and euxinia across the Cenomanian-Turonian oceanic anoxic event (OAE 2): Model-data comparison, *Paleoceanography*, 27, PA4209, doi:10.1029/2012PA002351.
- Montoya-Pino, C., S. Weyer, A. D. Anbar, J. Pross, W. Oschmann, B. van de Schootbrugge, and H. W. Arz (2010), Global enhancement of ocean anoxia during oceanic anoxic event 2: A quantitative approach using U isotopes, *Geology*, 38, 315–318.
- Ogg, J. G., and L. A. Hinnov (2012a), Jurassic, in *The Geologic Time Scale 2012*, edited by F. M. Gradstein et al., pp. 731–791, Elsevier, Amsterdam.
- Ogg, J. G., and L. A. Hinnov (2012b), Cretaceous, in *The Geologic Time Scale 2012*, edited by F. M. Gradstein et al., pp. 793–853, Elsevier, Amsterdam.
- Ohkouchi, N., K. Kawamura, Y. Kajiwara, E. Wada, M. Okada, T. Kanamatsu, and A. Taira (1999), Sulfur isotope records around Livello Bonarelli (northern Apennines, Italy) black shale at the Cenomanian-Turonian boundary, *Geology*, 27, 535–538.
- Orth, C. J., M. Attrep Jr., L. R. Quintana, W. P. Elder, E. G. Kauffman, R. Diner, and T. Willamil (1993), Elemental abundance anomalies in the late Cenomanian extinction interval: a search for the source(s), *Earth Planet. Sci. Lett.*, 117, 189–204.

- Owens, J. D., B. C. Gill, H. C. Jenkyns, S. M. Bates, S. Severmann, M. M. M. Kuypers, R. G. Woodfine, and T. W. Lyons (2013), Sulfur isotopes track the global extent and dynamics of euxinia during Cretaceous oceanic anoxic event 2, *Proc. Natl. Acad. Sci. U.S.A.*, 110, 18,407–18,412.
- Pancost, R. D., N. Crawford, S. Magness, A. Turner, H. C. Jenkyns, and J. R. Maxwell (2004), Further evidence for the development of photic-zone euxinic conditions during Mesozoic oceanic anoxic events, *J. Geol. Soc.*, 161, 353–364.
- Parente, M., G. Frijia, M. Di Lucia, H. C. Jenkyns, R. G. Woodfine, and F. Baroncini (2008), Stepwise extinction of larger foraminifers at the Cenomanian-Turonian boundary: A shallow-water perspective on nutrient fluctuations during oceanic anoxic event 2 (Bonarelli event), *Geology*, 36, 715–718.
- Paytan, A., M. Kastner, D. Campbell, and M. H. Thiemens (2004), Seawater sulfur isotope fluctuations in the Cretaceous, *Science*, 304, 1663–1665.
- Pearce, M. A., I. Jarvis, and B. A. Tocher (2009), The Cenomanian–Turonian boundary event, OAE 2 and paleoenvironmental change in epicontinental seas: New insights from the dinocyst and geochemical records, *Palaeogeogr. Palaeoclimatol. Palaeoecol.*, 280, 207–234.
- Pogge von Strandmann, P. A. E., H. C. Jenkyns, and R. G. Woodfine (2013), Lithium isotope evidence for enhanced weathering during oceanic anoxic event 2, *Nat. Geosci.*, 6, 668–672.
- Ridgwell, A., J. C. Hargreaves, N. R. Edwards, J. D. Annan, T. M. Lenton, R. Marsh, A. Yool, and A. Watson (2007), Marine geochemical data assimilation in an efficient Earth System Model of global biogeochemical cycling, *Biogeosciences*, 4(1), 87–104.

- Rue, E. L., G. J. Smith, G. A. Cutter, and K. W. Bruland (1997), The response of trace element redox couples to suboxic conditions in the water column, *Deep Sea Res., Part I*, 44, 113–134.
- Sageman, B. B., J. Rich, C. E. Savrda, T. Bralower, M. A. Arthur, and W. E. Dean (1998), Multiple Milankovitch cycles in the Bridge Creek Limestone (Cenomanian-Turonian), Western Interior Basin, in *Stratigraphy and Paleoenvironments of the Cretaceous Western Interior Seaway*, SEPM Concepts in Sedimentology and Paleontology, vol. 6, edited by M. A. Arthur and W. E. Dean, pp. 153–171.
- Sageman, B. B., S. R. Meyers, and M. A. Arthur (2006), Orbital time scale and new C-isotope record for Cenomanian-Turonian boundary stratotype, *Geology*, 34, 125–128.
- Schlanger, S. O., and H. C. Jenkyns (1976), Cretaceous oceanic anoxic events: Causes and consequences, *Geol. Mijnbouw*, 55, 179–194.
- Schlanger, S. O., M. A. Arthur, H. C. Jenkyns, and P. A. Scholle (1987), The Cenomanian–Turonian oceanic anoxic event, I. Stratigraphy and distribution of organic carbon-rich beds and the marine $\delta^{13}\text{C}$ excursion, in *Marine Petroleum Source Rocks*, edited by J. Brooks and A. J. Fleet, *Geol. Soc. London, Spec. Publ.*, 26, 371–399.
- Schnetger, B., and Y. Muramatsu (1996), Determination of halogens, with special reference to iodine, in geological and biological samples using pyrohydrolysis for preparation and inductively coupled plasma mass spectrometry and ion chromatography for measurement, *Analyst*, 121, 1627–1631.
- Scopelliti, G., A. Bellanca, R. Neri, F. Baudin, and R. Coccioni (2006), Comparative high-resolution chemostratigraphy of the Bonarelli level from the reference Bottaccione

- section (Umbria-Marche Apennines) and from an equivalent section in NW Sicily:
Consistent and contrasting responses to the OAE 2, *Chem. Geol.*, 228, 266–285.
- Scopelliti, G., A. Bellanca, E. Erba, H. C. Jenkyns, R. Neri, P. Tamagnini, V. Luciani, and D. Masetti (2008), Cenomanian-Turonian carbonate and organic-carbon isotope records, biostratigraphy and provenance of a key section in NE Sicily, Italy: Palaeoceanographic and palaeogeographic implications, *Palaeogeogr. Palaeoclimatol. Palaeoecol.*, 265, 59–77.
- Sinninghe Damsté J. S., and J. Koster (1998), A euxinic southern North Atlantic Ocean during the Cenomanian/Turonian oceanic anoxic event, *Earth Planet. Sci. Lett.*, 158, 165–173.
- Snow, L. J., R. A. Duncan, and T. J. Bralower (2005), Trace element abundances in the Rock Canyon Anticline, Pueblo, Colorado, marine sedimentary section and their relationship to Caribbean plateau construction and oxygen anoxic event 2, *Paleoceanography*, 20, PA3005, doi:10.1029/2004PA001093.
- Staudt, W. J., and M. A. A. Schoonen (1995), Sulfate incorporation into sedimentary carbonates, in *Geochemical Transformations of Sedimentary Sulfur: American Chemical Society Symposium Series*, vol. 612, edited by M. A. Vairavamurthy and M. A. A. Schoonen, pp. 332–345.
- Takashima, R., H. Nishi, T. Yamanaka, T. Tomosugi, A. G. Fernando, K. Tanabe, K. Moriya, F. Kawabe, and K. Hayashi (2011), Prevailing oxic environments in the Pacific Ocean during the mid-Cretaceous oceanic anoxic event 2, *Nat. Commun.*, 2, doi:10.1038/ncomms1233.

- Tian, R. C., J. C. Marty, E. Nicolas, J. Chiav éri, D. Ruiz-Ping, and M. D. Pizay (1996), Iodine speciation: A potential indicator to evaluate new production versus regenerated production, *Deep Sea Res., Part I*, 43, 723–738.
- Topper, R. P. M., J. Trabucho Alexandre, E. Tuenter, and P. T. Meijer (2011), A regional ocean circulation model for the mid-Cretaceous North Atlantic Basin: Implications for black shale formation, *Clim. Past*, 7, 277–297.
- Tribovillard, N., T. J. Algeo, F. Baudin, and A. Riboulleau (2012), Analysis of marine environmental conditions based on molybdenum-uranian covariation: Application to Mesozoic paleoceanography, *Chem. Geol.*, 324-325, 46–58.
- Tsikos, H., et al. (2004), Carbon-isotope stratigraphy recorded by the Cenomanian-Turonian oceanic anoxic event: Correlation and implications based on three key localities, *J. Geol. Soc.*, 161, 711–719.
- Turgeon, S., and H. Brumsack (2006), Anoxic versus dysoxic events reflected in sediment geochemistry during the Cenomanian-Turonian Boundary Event (Cretaceous) in the Umbria-Marche Basin of central Italy, *Chem. Geol.*, 234, 321–339.
- Turgeon, S., and R. A. Creaser (2008), Cretaceous oceanic anoxic event 2 triggered by a massive magmatic episode, *Nature*, 454, 323–326.
- van Bentum, E. C., A. Hetzel, H. J. Brumsack, A. Forster, G. J. Reichert, and J. S. Sinninghe Damst é (2009), Reconstruction of water column anoxia in the equatorial Atlantic during the Cenomanian-Turonian oceanic anoxic event using biomarker and trace metal proxies, *Palaeogeogr. Palaeoclimatol. Palaeoecol.*, 280, 489–498.
- van Helmond, N. A. G. M., I. Ruvalcaba Baroni, A. Sluijs, J. S. Sinninghe Damst é and C. P. Slomp (2014), Spatial extent and degree of oxygen depletion in the deep proto-North

- Atlantic basin during oceanic anoxic event 2, *Geochem. Geophys. Geosyst.*, 15, 4254–4266, doi:10.1002/2014GC005528.
- Waite, T. J., V. W. Truesdale, and J. Olafsson (2006), The distribution of dissolved inorganic iodine in the seas around Iceland, *Mar. Chem.*, 101, 54–67.
- Walker, J. C. G. (1986), Global geochemical cycles of carbon, sulfur and oxygen, *Mar. Geol.*, 70, 159–174.
- Weissert, H. (1989), C-isotope stratigraphy as monitor of paleoenvironmental changes: A case study from the early Cretaceous, *Surv. Geophys.*, 10, 1–16.
- Westermann, S., D. Vance, V. Cameron, C. Archer, and S. A. Robinson (2014), Heterogeneous oxygenation states in the Atlantic and Tethys Oceans during oceanic anoxic event 2, *Earth Planet. Sci. Lett.*, 404, 178–189.
- Wignall, P. B. (2001), Large igneous provinces and mass extinctions, *Earth Sci. Rev.*, 53, 1–33.
- Wong, G. T. F. (1995), Dissolved iodine across the Gulf Stream Front and in the South Atlantic Bight, *Deep Sea Res., Part I*, 42, 2005–2023.
- Wong, G. T. F., and P. G. Brewer (1977), Marine chemistry of iodine in anoxic basins, *Geochim. Cosmochim. Acta*, 41, 151–159.
- Wong, G. T. F., K. Takayanagi, and J. F. Todd (1985), Dissolved iodine in waters overlying and in the Orca Basin Gulf of Mexico, *Mar. Chem.*, 17, 177–183.
- Zheng, X.-Y., H. C. Jenkyns, A. S. Gale, D. J. Ward, and G. M. Henderson (2013), Changing ocean circulation and hydrothermal inputs during ocean anoxic event 2 (Cenomanian–Turonian): Evidence from Nd-isotopes in the European shelf sea, *Earth Planet. Sci. Lett.*, 375, 338–348.

Zhou, X., E. Thomas, R. E.M. Rickaby, A.M. E.Winguth, and Z. Lu (2014), I/Ca evidence for upper ocean deoxygenation during the Paleocene-Eocene Thermal Maximum (PETM), *Paleoceanography*, 29, 964–975, doi:10.1002/2014PA002702.

Tables

Table 1. OAE 2 Sections Used for I/Ca Measurements and Multiproxy Comparison^a

Label	Location	Deposition environment	Lithology	Reference
R	Raia del Pedale, Italy	Shallow water	Limestone	Parente et al., 2008
W	Aristocrat Angus core, Western Interior Seaway	Shallow water	Limestone/shale	Joo and Sageman, 2014
D	Demerara Rise, ODP 1258	Low-latitude, Pelagic	Organic-rich limestone/Black shale	Hetzel et al., 2009; Erbacher et al., 2005
T	Tarfaya, Morocco	Low-latitude, Pelagic	Organic-rich Chalk/Black shale	Jenkyns et al., 2007
E	Eastbourne, UK	Mid-latitude, Pelagic	Chalk	Pearce et al., 2009
F	South Ferriby, UK	Mid-latitude, Pelagic	Chalk/Black shale	Jenkyns et al., 2007
N	Newfoundland Drifts, IODP U1407	Mid-latitude, Pelagic	Chalk/Black shale	Expedition 342 Scientists, 2012

^aAbbreviations are used in the site map.

Figures

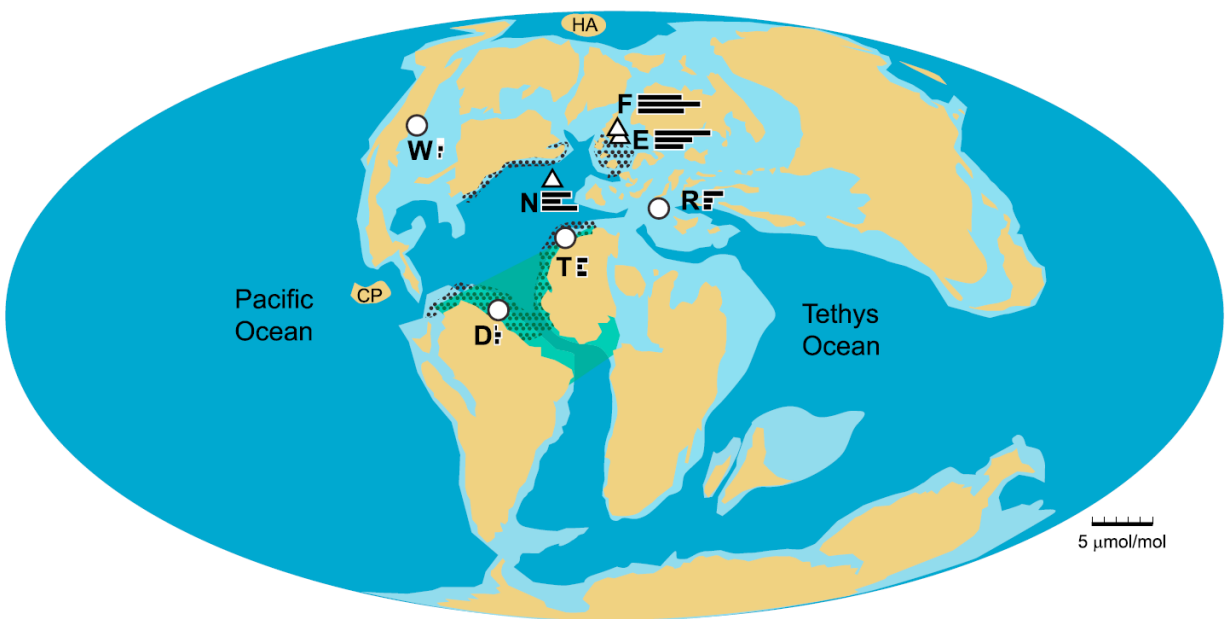


Figure 1. Global paleogeographic map of OAE 2 sections. The yellow represents the continents, the light blue stands for shallow oceans, and the dark blue for deep oceans. The black dots mark the modeled upwelling regions from Topper et al. (2011), and the green shading shows areas of euxinic conditions in the water column given in Jenkyns (2010). The studied sites are grouped into oxic (white triangles) and hypoxic (white circles) sites, and the site names are abbreviated. See Table 1 for abbreviations for site names. Average I/Ca values during pre-CIE, CIE, and post-CIE intervals are shown as uniformly scaled bars from bottom to top for individual sites. CP is Caribbean Plateau, and HA is High Arctic Large Igneous Province.

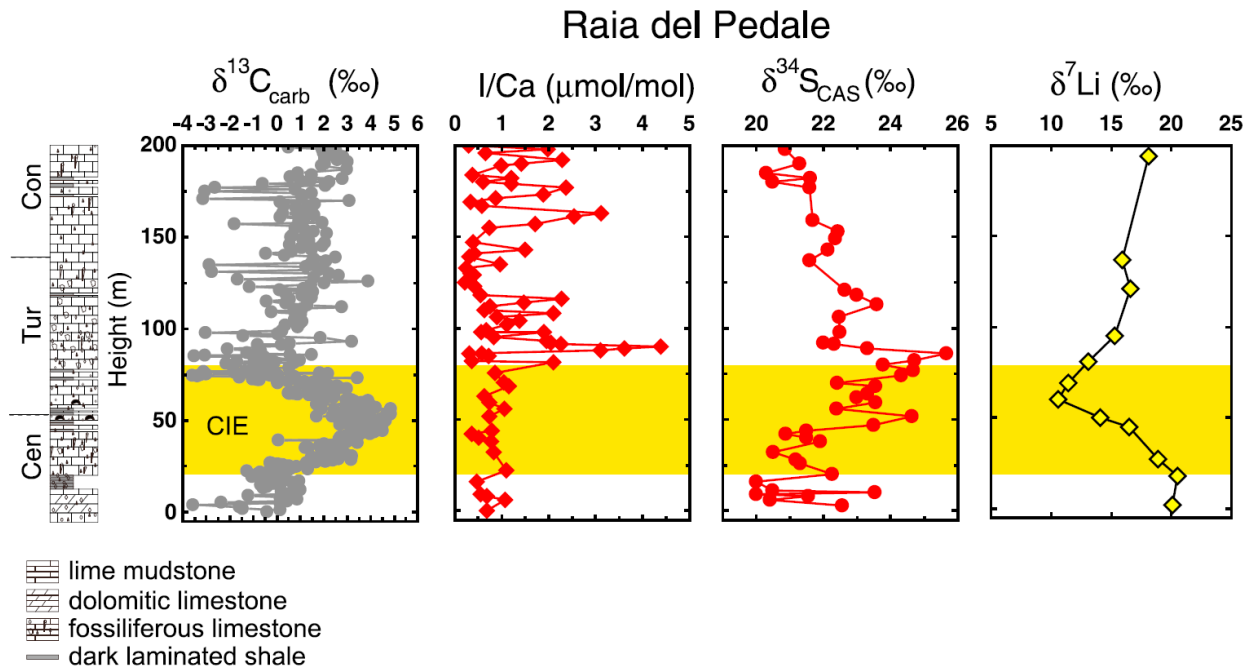


Figure 2. Chemostratigraphic plot for OAE 2 at Raia del Pedale. I/Ca data are from this study, $\delta^{13}\text{C}$ and $\delta^{34}\text{S}_{\text{CAS}}$ data are from Owens et al. (2013), and $\delta^7\text{Li}$ are from Pogge von Strandmann et al. (2013). The stratigraphic column on the left shows the facies variations (Owens et al., 2013), and the yellow boxes highlight the positive CIE.

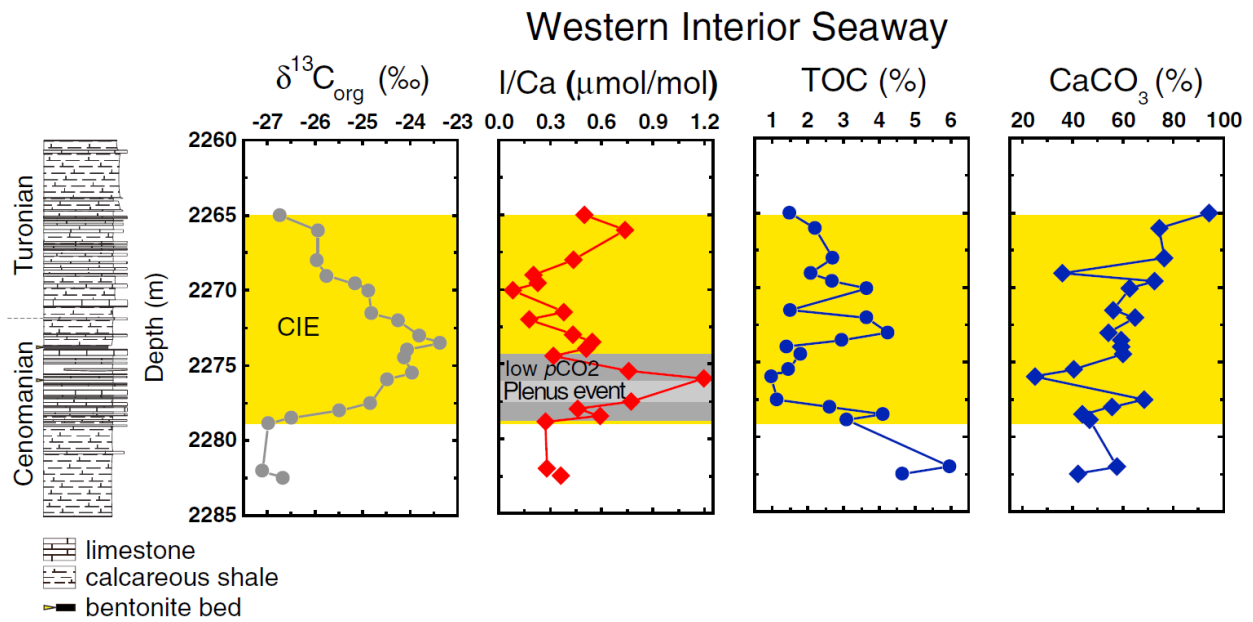


Figure 3. Preliminary I/Ca data from the Aristocrat Angus core in the Western Interior Seaway, plotted with wt % TOC, wt % CaCO₃, and δ¹³C_{org} (Joo and Sageman, 2014). The stratigraphic column is revised from Joo and Sageman (2014). The yellow boxes mark the CIE.

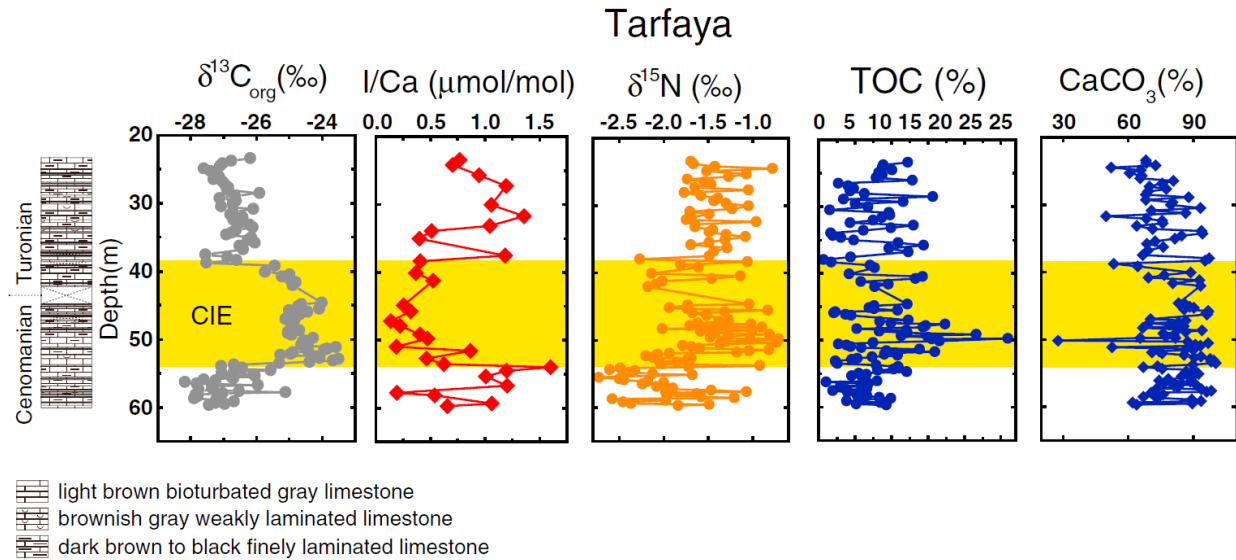


Figure 4. Geochemical and stable isotope data for OAE 2 at Tarfaya (core S57). $\delta^{13}\text{C}_{\text{org}}$ marks the CIE well and covers short periods before and after the CIE. The I/Ca data from bulk carbonate are generated in this study, compared with the $\delta^{15}\text{N}$, wt % TOC, and wt % CaCO_3 (Jenkyns et al., 2007). The highest TOC (%) correlates with the CaCO_3 (%) minimum and $\delta^{15}\text{N}$ maximum during the CIE. The stratigraphic column shows variable limestone, revised from Jenkyns et al. (2007). The CIE is bracketed in yellow boxes.

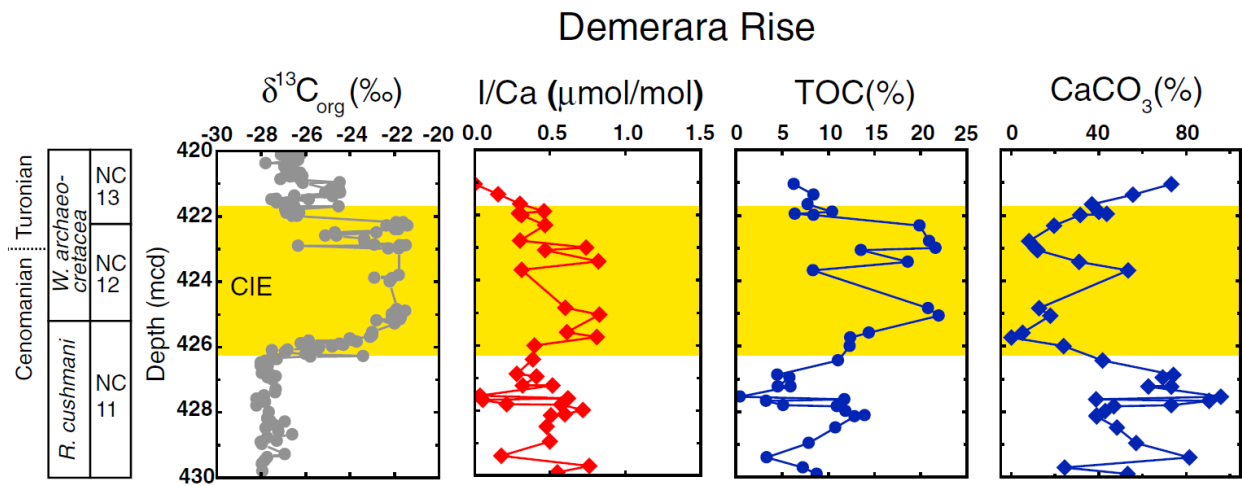


Figure 5. I/Ca for ODP Site 1258 on Demerara Rise, compared with $\delta^{13}\text{C}_{\text{org}}$, wt % TOC (Erbacher et al., 2005), and wt % CaCO_3 (iodp.tamu.edu). The biostratigraphic column to the left is from Erbacher et al. (2005). The scale is meter composite depth.

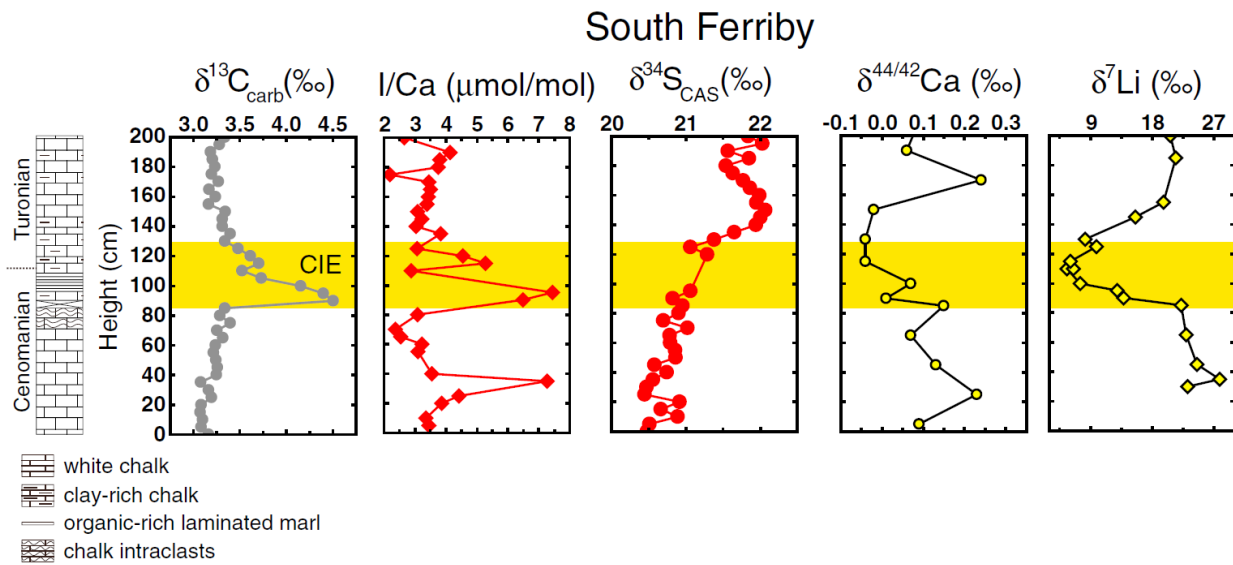


Figure 6. I/Ca data from South Ferriby, compared with $\delta^{13}\text{C}_{\text{carb}}$, $\delta^{34}\text{C}_{\text{CAS}}$, Ca, and Li isotopes (Blätler et al., 2011; Owens et al., 2013; Pogge von Strandmann et al., 2013). The stratigraphic column is adapted from Jenkyns et al. (2007). The yellow boxes bracket the CIE. A hiatus appears at the beginning of the CIE at ~85–90 cm and is highlighted in the stratigraphic column as a crossed box.

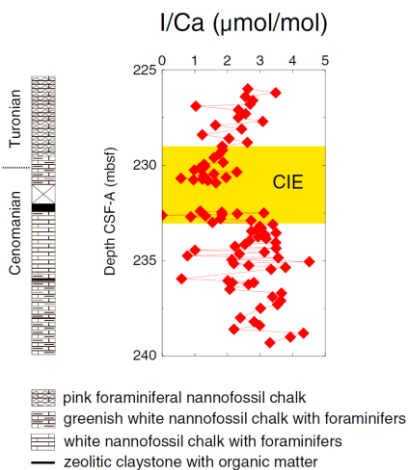


Figure 7. I/Ca record of Site U1407, IODP X342 on Newfoundland Drifts. The stratigraphic log is adapted from Expedition 342 Scientists (2012). A hiatus at ~231–232 is represented by a crossed box. The mbsf = meters below seafloor.

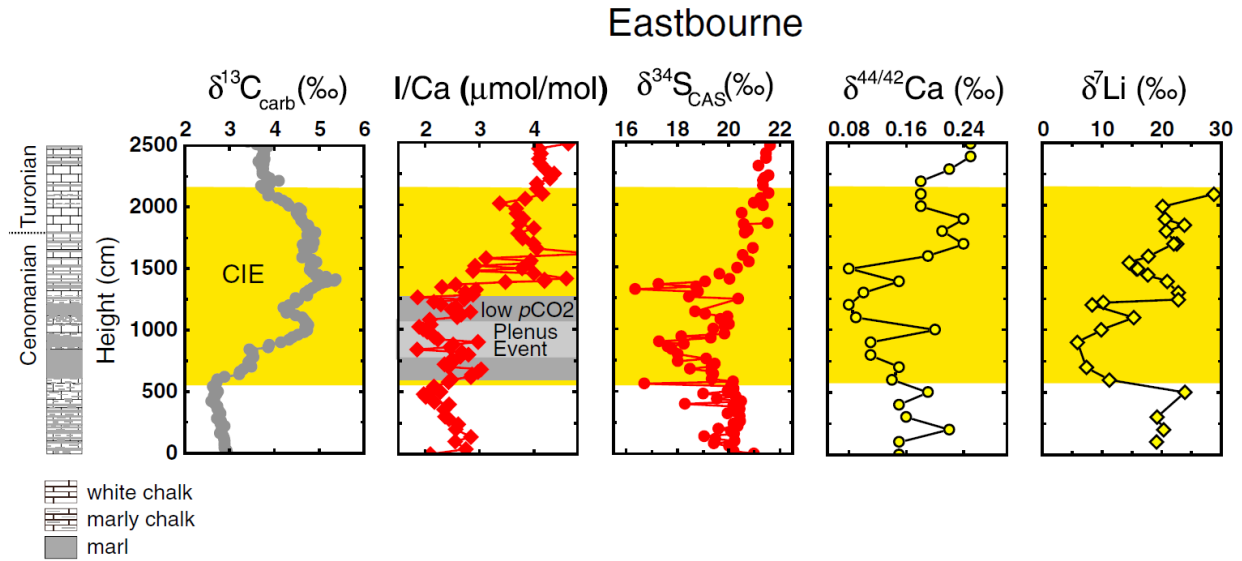


Figure 8. Geochemical and isotope data for Eastbourne. The $\delta^{13}\text{C}_{\text{carb}}$ marks the CIE well, and I/Ca and $\delta^{34}\text{S}_{\text{CAS}}$ indicate redox changes during the studied interval. Plenus Cold Event, also known as the Benthic Oxidic Event, is bracketed in light gray box (Tsikos et al., 2004; Owens et al., 2013). The ranges of low $p\text{CO}_2$ and Plenus Cold Event are adapted from Jarvis et al. (2011). The $\delta^{44/42}\text{Ca}$ and $\delta^7\text{Li}$ are regarded as proxies of continental weathering rates (Blättler et al., 2011; Pogge von Strandmann et al., 2013).

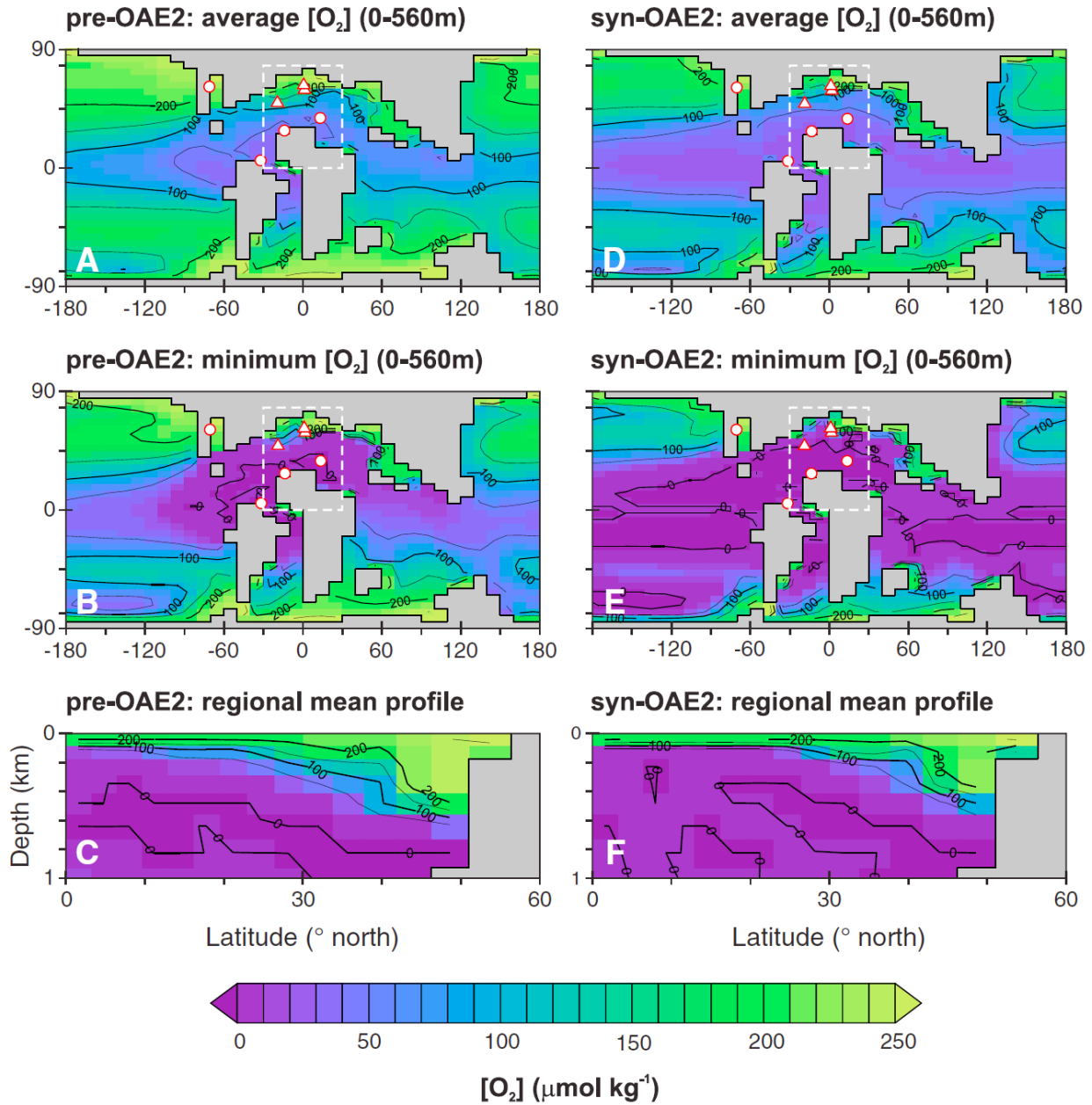


Figure 9. Modeled upper water column-dissolved oxygen distributions (a–c) before and (d–f) during OAE 2. Figures 9a and 9d show the averaged O_2 concentration over the upper 560m of water column; Figures 9b and 9e present the minimum (O_2) in the depth range of 0–560 m. Figures 9c and 9f show the cross-sectional views of dissolved oxygen in the proto-Atlantic upper ocean. The extent of longitudinal averaging in these zonal sections is marked by a white dashed rectangle in the map view panels.

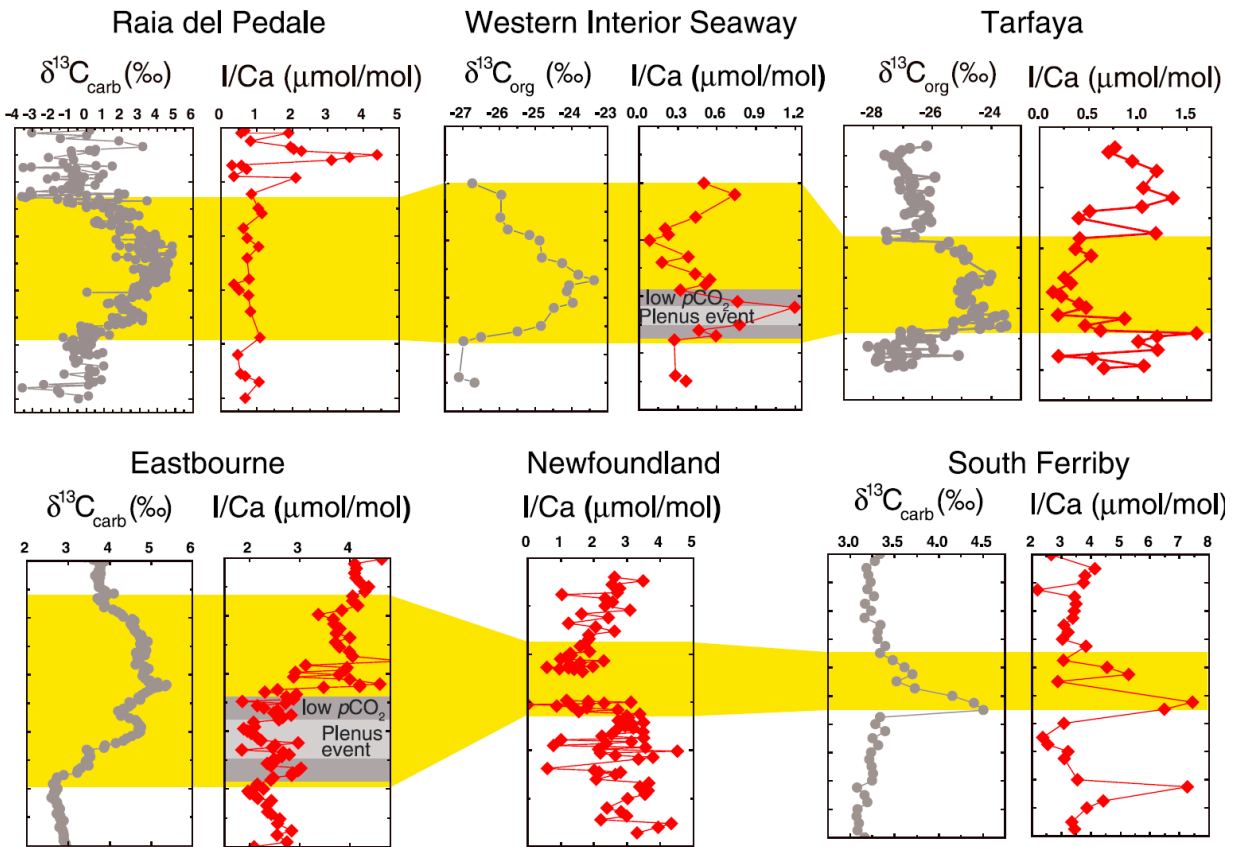


Figure 10. I/Ca records correlated by $\delta^{13}\text{C}$ showing distinct local surface water redox evolution.

The yellow boxes mark the CIE, except that the onset is missing at South Ferriby due to a hiatus.

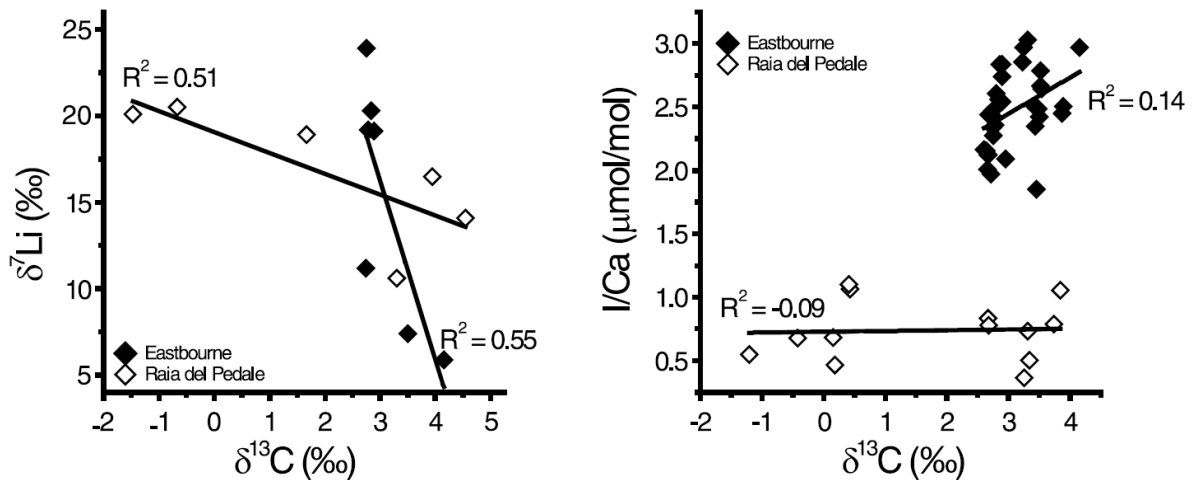


Figure 11. I/Ca and $\delta^7\text{Li}$ plotted against $\delta^{13}\text{C}$ during the rising limb of the CIE for Eastbourne and Raia del Pedale.

**Chapter 2: Records of organically bound iodine during the
Cenomanian–Turonian OAE 2: implications for bottom-water
conditions and iodine cycling**

Abstract:

Oceanic Anoxic Events (OAEs) were characterized by deposition of widespread organic-rich sediments (black shales). Carbonate-associated iodine (I/Ca) has been used to indicate local upper-ocean redox conditions, demonstrating highly dynamic spatial and temporal patterns at multiple sections across the Cenomanian–Turonian OAE 2 at ~94 Ma in the Late Cretaceous. We describe a new method of extracting organically bound iodine (I_{org}) from shale using volumes of samples on the order of tens of milligrams with the potential of high-resolution work across thin shale bands, and compare I/TOC with I/Ca. We generated I/TOC and I_{org} records from six sections: Tarfaya (Morocco), Furlo (central Italy), Demerara Rise (western equatorial Atlantic), Cape Verde Basin (eastern equatorial Atlantic), South Ferriby (UK), and Kerguelen Plateau (southern Indian Ocean). I/TOC in modern surface and subsurface sediment decreases with decreasing bottom-water oxygen, thus the iodine burial rate may have been influenced by redox changes. I/TOC indeed decreases into OAE 2, suggesting more reducing bottom-water conditions. Relatively higher I/TOC values (thus more oxic conditions) are recorded in two OAE 2 high-latitude and possibly in one low-latitude sites, where higher oxygen levels are also indicated by other redox indicators such as trace metal enrichment and iron speciation and Earth System Modeling. I/TOC and I/Ca record at Tarfaya both decreased during OAE 2, likely suggesting reducing water throughout the water column due to strong vertical mixing and shallow palaeo-depth. Bulk sediment I_{org} did not show uniform changes through the OAE 2 level at all six sites, suggesting that there was no global iodine drawdown linked to the enhanced organic carbon burial. These observations indicate that coeval carbonate and shale iodine records may be able to depict oxygenation changes in different parts of the water column, and reflect the change in marine iodine reservoir.

1. Introduction

1.1. OAE 2 and redox proxies

Oceanic Anoxic Events (OAEs) are characterized by widespread deposition of organic-rich sediments in marine environments known as black shales (Schlanger and Jenkyns, 1976; Jenkyns, 1980; Arthur et al., 1990; Jones and Jenkyns, 2001; Jenkyns, 2010). Black shales result from the combination of increased primary productivity coupled with enhanced preservation of organic matter in oxygen-depleted environments (e.g., Schlanger et al., 1987; Arthur et al., 1988). The geochemical signature of enhanced burial of organic matter manifests as a prominent positive carbon-isotope excursion (CIE) that is recorded in terrestrial and marine carbon reservoirs (Tsikos et al., 2004; Hasegawa, 1997; Barclay et al., 2010; Jarvis et al., 2011).

OAE 2 and other OAEs have been linked to the eruption of large igneous provinces (LIPs), which released large amounts of CO₂ to the atmosphere, increasing atmospheric temperature and strengthening hydrological cycling (e.g., Kerr, 1998; Kuroda et al., 2007; Turgeon and Creaser, 2008; Adams et al., 2010). As a result, continental weathering rates increased (Blattler et al., 2011; Pogge von Strandmann et al., 2013), delivering more nutrients to the ocean, stimulating marine productivity. Enhanced productivity shuttled more organic matter to the deep ocean, consuming more dissolved oxygen, inducing oceanic deoxygenation and widespread burial of organic carbon (Jenkyns, 2003; Adams et al., 2010; Jenkyns, 2010).

A wide range of proxies have been used to track vertical changes in water column redox condition. Trace-metal enrichment and Fe-speciation data have proven to be powerful tools to characterize redox changes during OAE 2 (van Helmond et al., 2014; Westermann et al., 2014; Junium et al., 2015; Poulton et al., 2015). Redox-sensitive trace-metal concentrations are commonly used to track the presence or absence of euxinia in the water column (Algeo and

Lyons, 2006; Algeo and Tribovillard, 2009). Iron speciation is a widely used bottom-water proxy which can be used to distinguish oxic, anoxic, and euxinic conditions (Poulton and Canfield, 2005, 2011). Biotic proxies such as foraminiferal assemblages have also been used as redox indicators (Friedrich et al., 2006; Takashima et al., 2009; Gertsch et al., 2010; El-Sabbagh et al., 2011; Bomou et al., 2013; Reolid et al., 2015). Biomarkers (e.g. isorenieratane) indicate photic-zone euxinia in the proto-North and South Atlantic Ocean (Sinninghe Damsté and Koster, 1998; Kuypers et al., 2002; Pancost et al., 2004; Hetzel et al., 2011). Bulk carbonate I/Ca is a relatively new proxy for redox reconstructions in the upper ocean, and is very sensitive to the transition between oxic and anoxic conditions (Zhou et al., 2015). Sedimentary iodine is also found bonded within organic matter, and in this paper, we test the potential of organically bound iodine to total organic-carbon ratio (I/TOC) as a proxy for bottom-water oxygenation.

1.2. Organically bound iodine in recent sediments

The iodine concentration in modern seawater is relatively uniform around 0.45 $\mu\text{mol/l}$, with slightly higher amounts in the deep ocean (Elderfield and Truesdale, 1980). Iodate is the predominant iodine species in oxygenated seawater, and is thermodynamically stable (Tsunogai, 1971; Wong, 1980). Iodate is slightly depleted in surface-ocean waters due to uptake by phytoplankton, and remains at constant concentration in an oxygenated water column (Bluhm et al., 2011). Iodine is taken up by marine plankton in the surface ocean at an average stoichiometry of $140 \pm 80 \mu\text{mol/mol}$ to carbon (I/TOC) (Elderfield and Truesdale, 1980), though the reason and the mechanisms of iodine uptake in phytoplankton are not clear. The relatively depleted iodate and high iodide concentration in the surface ocean may be associated with iodate reduction mistaken for nitrate by the enzyme nitrate reductase (Tsunogai and Sase, 1969), but this

hypothesis has been challenged by Waite and Truesdale (2003), who claimed that iodate reduction was independent on the presence or absence of nitrate reductase activity, but may be associated with photo-inhibition in phytoplankton, consuming excess electrons for photosynthetic needs. Iodine does not seem to be enriched in organic matter through the water column, considering the relatively constant total iodine concentration with water depth. I content in exported particles do not change significantly when particulate materials sink through the water column, with slightly decreasing values from 200-300 to 100-200 ppm (Brewer et al., 1980). I/TOC values of particulate matter including plankton and fecal pellets from the water column range from 30 to 310 $\mu\text{mol/mol}$, close to the average I/TOC values of marine plankton (60-220 $\mu\text{mol/mol}$), and is much lower than the values in marine surface sediments (Fig. 1).

At the seafloor, the I/TOC of surface sediments is dependent on the degree of oxygenation. Iodine is enriched in the organic fraction (not in mineral phases) of sediments deposited under well-oxygenated bottom water, with I/TOC above 2000 $\mu\text{mol/mol}$ (Price and Calvert, 1973; Kennedy and Elderfield, 1987b). Locations with oxygen-depleted bottom waters are reported to have lower I/TOC (Price and Calvert, 1973), on the same order of magnitude as the average ratio in plankton of $140 \pm 80 \mu\text{mol/mol}$ (Elderfield and Truesdale, 1980). I/TOC decreases rapidly from surface to subsurface sediments ($< 1 \text{ m}$) at oxygenated sites, whereas the ratios remain relatively stable at sites with low bottom-water oxygen contents (Price and Calvert, 1977). Price and Calvert (1973) predicted that the contrasting burial behavior of iodine in oxidizing versus reducing environments should be recorded in ancient sediments. In this study, we explore the possibility that I/TOC qualitatively records local bottom-water redox conditions during OAE 2. Organically bound total iodine content in sediments, I_{org} , may also provide

insights into the changes in the marine iodine reservoir during this time interval, which affects the interpretation of carbonate I/Ca as an upper-ocean redox proxy (Zhou et al., 2015).

2. Study sites

We studied OAE 2 in six sections at different environmental settings (Fig. 2). Five out of six sites are in the proto-North Atlantic or close to western Tethys, and one site is from the Southern Ocean. Although all these sites comprise organic-rich sediments, local paleoenvironments vary, including different oceanographic settings, latitudes, water depths and redox conditions. Such compilation should provide a comprehensive representation of OAE 2 sample locations.

A well-preserved sequence of glauconitic calcareous sandstone and organic-rich chalks was cored at Ocean Drilling Program (ODP) Site 1138 on the western margin of the central Kerguelen Plateau, a huge Early Cretaceous oceanic igneous plateau, in the palaeo-Indian Ocean sector of the Southern Ocean, at a modern water depth of 1141 m (Coffin et al., 2000; Holbourn and Kuhnt, 2002; Murphy and Thomas, 2012). The sediments from the Kerguelen Plateau studied here consist of black organic-rich claystones, virtually barren of calcareous foraminifera during OAE 2, although the overlying sediments contain moderately to well-preserved species (Holbourn and Kuhnt, 2002). We studied part of the black-shale interval, including the recovery stage of the positive CIE interval, according to organic-carbon isotopic data. The average TOC content at this section is 7.7%, intermediate among all the six studied sites, which range from 2.4% to 24.0%. CaCO₃ percentage remains close to 0 for most of the carbon isotope excursion (CIE) and recovers to ~40% at the end of the CIE, suggesting low production and/or low preservation of carbonate (Fig. 4).

All other sites are in pelagic proto-North and equatorial Atlantic Ocean and its shelf margins. Deep Sea Drilling Project (DSDP) Site 367 is located in the Cape Verde Basin, 330 km west of the African coast, at a current water depth of 4748 m, a palaeodepth of 3700 m (Lancelot et al., 1977; Chenet and Francheteau, 1979; Westermann et al., 2014). The studied cores consist of black, carbonaceous shale interbedded with silty turbidites, and total organic carbon (TOC) range from 4% to 48% (Lancelot et al., 1977; Jones et al., 2007). Clay and organic debris are common, with rare pyrite and traces of bioturbation, and rare to common foraminifera and nannofossils (Lancelot et al., 1977). The sediment covers the early stage of the CIE and several metres below. The maximum TOC value is the highest among the studied sections, up to 50% TOC (wt. %). CaCO_3 % across the studied sediment is below 5.5% (Fig. 4).

Tarfaya in southwest Morocco at the margin of northwest Africa, is a section of organic-rich shallow-marine sediments that span the Cenomanian–Turonian boundary (Kolonis et al., 2005). Core S57 (drilled by the Moroccan State Oil Company and Shell during exploration in the late 1970s and early 1980s; Kolonis et al., 2005) records the deepest part of the basin with a reconstructed paleo-water depth of ~250–300 m. The core comprises ~37 m of organic-rich calcareous sediment containing planktonic foraminifera and nannofossils, with light- and dark-colored layers that alternate at a decimeter scale (Tsikos et al., 2004). TOC (wt. %) fluctuates between 0 and 15% for most of the section with a peak value of 25% corresponding to the early stage of the CIE (Fig. 4). Other dominant sediment components in this section include carbonate, finely dispersed biogenic silica and clay (Leine, 1986; Tsikos et al., 2004).

The Furlo section of the pelagic Scaglia Bianca Formation was deposited at a latitude of ~20°N in western Tethys, central Italy (Lanci et al., 2010). The lower 17.5 metres of section consists of rhythmically developed whitish foraminiferal-nannofossil limestones, locally with

pink, grey and black cherts, the latter associated with thin (sub-centimetre scale) laminated black shales in parts of the section, and the TOC in some of these shales is ~20% (Turgeon and Brumsack, 2006; Jenkyns et al., 2007; Mort 2007a; Mitchell et al., 2008; Gambacorta et al., 2015). This is overlain by the Bonarelli Level, corresponding to OAE 2, characterized by interbedded black laminated organic-rich shale (TOC 0.5–18%), grey claystone and brown radiolarian sand, with a total thickness of ~ 1m (Fig. 4). A low-resolution organic $\delta^{13}\text{C}$ record shows a gradual rise from -26.5‰ to -25.5‰ in sediments below the Bonarelli Level, with values increasing abruptly to -23.5‰ in the onset of the positive CIE, and fluctuating between -24 and -23 ‰ through the organic-rich unit (Jenkyns et al., 2007).

South Ferriby is located in Lincolnshire, northeast UK, and its sediments (English Chalk) were deposited on a shallow epicontinental pelagic shelf, adjacent to the proto-Atlantic Ocean. The section comprises relatively condensed organic-lean foraminiferal-nannofossil carbonates with TOC mostly between 1 and 2%, interrupted by a thin (~10 cm) layer of organic-rich (max. TOC = ~8%), laminated marls (Jenkyns et al., 2007; Pogge von Strandmann et al., 2013). The carbon-isotope profile decreases upwards gradually from -23 to -25 ‰ in our studied interval, capturing part of the positive CIE (Fig. 4).

Site 1258 (ODP Leg 207) is situated on the northwest slope of the Demerara Rise off Suriname and French Guyana in the western equatorial Atlantic Ocean, currently located at a water depth of 3192 m (Erbacher et al., 2004; Friedrich et al., 2006). The Cenomanian to Turonian sequence mainly consists of laminated organic-rich black shales with local occurrence of limestones, chert, phosphatic nodules and well-preserved fish debris (Hetzl et al., 2009). Clay content varies throughout the section, and the carbonate content is usually equal to or less than

50% in these organic-rich layers with TOC level of ~0.5-25% (Erbacher et al., 2004). The abundance of foraminifera varies drastically between lamina (Nederbragt et al., 2007).

3. Methods

Various methods have in the past been used to decompose and extract iodine from sediment samples, such as dry ashing/alkaline fusion, microwave-assisted digestion and combustion (Knapp et al., 1998; Brown et al., 2005; Romar  -Hortas et al., 2009; Tinggi et al., 2011). The sample masses required for these methods are usually larger than 100 mg (e.g., Tullai et al., 1987; Knapp et al., 1998). We developed a new method for extracting organic iodine using samples of ~20 mg. Fine powders of sediments were weighed on a microbalance, decarbonated by adding 3% (v/v) nitric acid and then thoroughly rinsed with DI water. The decarbonated samples were transferred into Teflon vials and mixed with 2 ml of tetramethylammonium hydroxide (TMAH 25% in H₂O, Sigma-Aldrich TraceSELECT[®]). The vials were tightly sealed and heated in the oven at 90 °C for 4–6 weeks. The sealed vials were sonicated in a water bath for one hour daily. ~20 µl solution was subsampled from each Teflon vial and was diluted with DI water for preservation in refrigerator. Sub-sampling was carried out 1–5 times a week during the entire heating period. Iodine concentrations were measured in the sub-sampled solutions to determine the time interval required to extract organic iodine from samples.

The bulk-rock samples from six OAE 2 sections were extracted using the same method as described previously, except that sub-sampling was skipped and the heating time was shortened to 20 days, which is demonstrated to be sufficient to completely extract iodine from the sample. Before iodine analysis by ICP-MS, the stored solutions were mixed with a freshly made matrix including internal standards (5ppb Cs). Potassium iodide standard (KI, Alfa Aesar, 99.99% in

purity) was diluted to 1 ppb of iodine, which was tuned to be 80–100 kcps. The standard deviation for each measurement was mostly less than 1% and was always less than 5%.

4. Results and discussion

4.1. Method development

We selected two samples for a preliminary test of the extraction method, one from a pre-OAE interval, one from within the OAE interval, and a duplicate for each sample. A potassium iodide solution was set up as a control and processed with the same method as the OAE 2 samples. The iodine concentrations in subsampled solutions increased in the first 20 days and remained almost constant afterwards (Fig. 3a). This result suggested that 20 days was enough to extract all the iodine from organic matter. The variation in KI concentrations (RSD = 5%) reflects the uncertainty in sub-sampling, preserving and measuring iodine on an ICP-MS, and suggests no major loss during the experiment (Fig. 3a). Compared to the variability between OAE samples and the change in concentration during heating, the variation in the KI control was negligible.

We also investigated the effect of sample mass on measured I/TOC values using the same two samples mentioned in the previous paragraph. Samples are weighed for ~5, 10, 20, 30, 40, and 50 mg, and then treated following the same extraction method as done to all the OAE 2 samples. The result suggests relative constant I/TOC values with sample masses from 5 to 50 mg (Fig. 3b). Most of the data fall within the standard deviation of each set of I/TOC values, 6.6% and 5.1% for the pre-OAE and OAE samples respectively. So 20 mg of samples is appropriate for such study. I/TOC values were calculated from the measured iodine concentration and TOC from each sample, and I_{org} values represent organic iodine content in bulk sediment.

4.2. I/TOC as a qualitative bottom water oxygenation proxy

The positive correlation between I/TOC and bottom-water oxygenation in recent sediments offers a potential opportunity to reconstruct palaeo-redox near the seafloor (Price and Calvert, 1973) (Fig. 1). Proxies distinguishing between oxic and anoxic settings, including foraminiferal assemblage, trace metal enrichment, and iron speciation, are sometimes not in consensus for specific geological event, such as OAE 2. If proved to be reliable, I/TOC may have its advantage to be used in this redox window. However, it is important to discuss fundamentals and limitations of I/TOC as an oxygenation indicator so that proper interpretations can be made on proxy data, including: (1) causes of the correlation between surface-sediment I/TOC and bottom-water oxygen level; (2) preservation of the I/TOC gradient (oxygen gradient) among different sites in shallow subsurface sediments during early diagenesis; (3) the influence of long-term burial.

The surficial enrichment of iodine in oxic sediments (relative to marine plankton) has been generally interpreted as the result of organic-matter degradation and iodine recycling, but the detailed biogeochemical processes have not been clearly elucidated. Price and Calvert (1973) speculated that this enrichment is related to iodine sorption on the organic fraction, controlled by unspecified enzyme reactions at the surface of dead cells that occur only in an oxidizing environment. Similarly, sources of iodine in surficial sediments are suggested to be from remineralization of organic matter just below the sediment-seawater interface, rather than from bottom water (Kennedy and Elderfield, 1987b). Ullman and Aller (1985) introduced an alternative hypothesis, i.e., adsorption of iodate by Fe-oxyhydroxides on the surface of oxic sediments. However, enrichment of iodine associated with Fe-oxyhydroxides is rarely reported

in the marine environment, compared to its enrichment associated with organic matter, so we are not able to discuss the effect of iron in detail.

Iodine is found enriched in surface marine sediments, and iodine in sediments tends to be lost during early diagenesis, but the rate of iodine loss gets much lower, almost reaching a constant iodine content below a certain sediment depth, usually within a couple meters below the sediment-water interface (Price et al., 1970). In more oxygenated bottom waters, I/TOC decreases more rapidly in sediments below the sea floor, usually within 1 m, whereas low-oxygen sites show a more stable I/TOC depth profile in shallow subsurface sediments (Price and Calvert, 1977). The large difference in I/TOC between oxic and low-oxygen sites appears to be largely erased within the top meter of the sediment column (Price and Calvert, 1977), but the I/TOC signature of the bottom-water O₂ gradient between sites seems to be preserved in subsurface sediments (Fig. 1). We have not attempted to use these literature data to establish a quantitative calibration for subsurface I/TOC vs bottom-water O₂ because some of the down-core I/TOC profiles did not reach a constant value at the base of the cored interval (Price and Calvert, 1977). Furthermore, higher sedimentation rates may cause preservation of a smaller proportion of the enriched surface I/TOC (i.e. bottom-water O₂ signature) (Kennedy and Elderfield, 1987b). Hence, the absolute values of subsurface I/TOC may be affected by non-redox-related factors, but bottom-water O₂ gradient acts as an important role on the I/TOC gradient between different sites.

I/TOC data in ancient sediments cannot be directly compared with those in modern sediments due to iodine loss during diagenetic alteration of organic matter. I/TOC values for the OAE 2 samples are more than an order of magnitude lower than those in modern subsurface sediments (Fig. 1), possibly indicating preferential release of iodine during burial of organic

matter over tens of millions of years. Regardless of the unknowns mentioned above, there is potential for preservation of the spatial pattern and temporal changes in bottom-water oxygen in I/TOC values in the sediment deposited during OAEs. OAE 2, characterized by deposition of very organic-rich sediments, is among the best opportunities to test this new proxy. Given that the redox window of the oxic–anoxic conditions is where this proxy is likely to behave sensitively, as recorded in modern sediments, I/TOC may have the potential to be complimentary to other local bottom-water proxies, especially in organic-rich sediments.

4.3. Oceanographic patterns of I/TOC during pre- and post-OAE 2 intervals

We report I/TOC and I_{org} data across OAE 2 at 6 sites (Fig. 2). $\delta^{13}\text{C}$ and TOC data are plotted for each site (Fig 4). Firstly, we discuss the spatial pattern of I/TOC during the background, i.e. below and above the OAE 2 sediment. Subsequently, we discuss the temporal changes of I/TOC at the individual sites.

I/TOC values for the pre- and post-OAE intervals display a wide range, from ~ 1 $\mu\text{mol/mol}$ to >50 $\mu\text{mol/mol}$, effectively separating the study sites into two groups. Sites at relatively low latitudes (Tarfaya, Furlo and Demerara Rise), have background I/TOC below 5 $\mu\text{mol/mol}$, with the exception of the Cape Verde Basin. Two sites at higher latitudes (Kerguelen Plateau and South Ferriby) have background I/TOC of ~ 15 – 50 $\mu\text{mol/mol}$. Based on these contrasting I/TOC values, we interpret that bottom water was more oxic at the high-latitude sites and Cape Verde Basin, before and after the OAE, whereas most low-latitude sites had relatively oxygen-depleted bottom waters.

Benthic foraminiferal assemblages at Kerguelen Plateau suggest that the bottom water might have been generally oxygenated with episodes of short-term dysoxic conditions (Coffin et

al., 2000; Holbourn and Kuhnt, 2002). No proxy data are available in the literature directly addressing the bottom-water conditions at South Ferriby, although several studies imply a latitudinal increase of oxygenation on the seafloor from tropical sites to both North Atlantic and Northern Tethyan margins (Kuhnt and Wiedmann, 1995; Westermann et al., 2010; van Helmond et al., 2014; Westermann et al., 2014). The high I/TOC at South Ferriby (northernmost Atlantic site, in European pelagic shelf sea) fits into such a pattern. The Cape Verde Basin background I/TOC of ~10–20 $\mu\text{mol/mol}$, lower than the range for Kerguelen Plateau and South Ferriby, indicates relatively reducing bottom waters before the OAE. The strong enrichment of Mo relative to U in the sediments during the same interval suggest that a strong particulate shuttle existed in the water column, delivering Mo enriched Mn-Fe-oxyhydroxide to the sediments (Algeo and Tribovillard, 2009; Westermann et al., 2014). Whereas $\text{Fe}_{\text{HR}}/\text{Fe}_{\text{T}}$ values were consistently low at ~0.4, suggesting anoxic conditions close to the oxic/anoxic boundary (Poulton and Canfeld, 2011). The bottom-water redox conditions of the Cape Verde Basin during the background interval likely represent a transitional state between the oxic and anoxic end-member sites, according to its intermediate I/TOC values among the six sites. Coincidentally, iron-isotope data also identified this site as a mixture of two types of iron supply, i.e., the hydrothermal and shuttle inputs from shelf to the deep ocean basin (Owens et al., 2012).

The low I/TOC background values at Tarfaya, Furlo, and Demerara Rise, indicate less oxygenated bottom-water conditions at these two sites. Elevated redox-sensitive trace-metal concentrations and repetitive deposition of laminated organic-rich sediments indicate suboxic to anoxic bottom water in the Tarfaya Basin (Kolonic et al., 2005), and the presence of isorenieratane and the high degree of pyritization in sediments indicate at least intermittent photic-zone euxinia (Kolonic et al., 2005; Poulton et al., 2015). Transient occurrences of

relatively oxic bottom waters, suggested by much higher resolution studies (Kolonic et al., 2005; Kuhnt et al., 2005), are not captured in our I/TOC record. Fe-speciation data suggest bottom-water anoxia existed before OAE 2 at Tarfaya (Poulton et al., 2015).

Several proxies indicate that bottom waters could have been anoxic before, during and after the OAE 2 at Demerara Rise with brief oxygenation and in the black shales at Furlo, thus we do not specifically distinguish the conditions during the background interval and the OAE. The presence of the biomarkers isorenieratene and chlorobactene suggest photic-zone euxinia during OAE 2 at the relatively shallow Site 1260 on Demerara Rise, where lycopane to n-alkane ratios much higher than in modern oxygen minimum zones indicate prolonged anoxia in bottom water throughout late Cenomanian to early Turonian, across OAE 2 (van Bentum et al., 2009). Trace-metal evidence and iron speciation also suggest anoxic, and possibly euxinic conditions at Demerara Rise during OAE 2 (Bunte, 2009). During the pre-OAE interval, trace metals show little to no enrichment at Furlo, and Fe-speciation data suggest anoxic bottom water throughout the event (Westermann et al., 2014). This evidence is consistent with the relatively low I/TOC across the sections at Demerara Rise and Furlo, as well as the low $\delta^{15}\text{N}$ at these two sites (Jenkyns et al., 2007).

4.4. I/TOC vs. modeled seafloor oxygen

The general oceanographic pattern of background I/TOC agrees with the bottom-water oxygenation simulated in Earth System Model cGENIE for the Late Cretaceous with a deeper Panama (Monteiro et al., 2012). The three sites with high I/TOC values: Kerguelen Plateau, South Ferriby, and Cape Verde Basin, are located in or near areas with modeled bottom-water oxygen higher than 100 $\mu\text{mol/l}$, while the other three sites are in areas with modeled seafloor oxygen below 50 $\mu\text{mol/l}$. Most parts of the proto-North Atlantic was probably anoxic in the late

Cretaceous, because the deep water in North Atlantic was likely formed at relatively low latitudes during the Cretaceous Period, hence containing less oxygen (Monteiro et al., 2012).

In this model (Monteiro et al., 2012), the northeast corner of the proto-Atlantic had relatively oxic water extending from the surface ocean to ~0.5 km (Zhou et al., 2015), as supported by the highest I/TOC at South Ferriby (Fig. 4). Kerguelen Plateau was located at high southern latitudes, where relatively low temperatures could have favored higher levels of dissolved oxygen in seawater and possible formation of bottom water near this location. Nd-isotope results suggest deep-water formation in the Indian sector of the Southern Ocean at least from the late Albian to the late Cenomanian (Murphy and Thomas, 2012), which may have delivered O₂-rich deep water to Kerguelen, recorded as high I/TOC at the this site.

The background I/TOC values (>10 μmol/mol) at Cape Verde are higher than expected, considering its low-latitude location. Interestingly, a modeled high O₂ anomaly on the seafloor appeared persistently at the equatorial West African margin, even in reconstructions where high-latitude bottom waters became almost anoxic (Monteiro et al., 2012). Regardless of the relatively high background I/TOC, low pre-OAE Fe_{HR}/Fe_T (~0.4), and the proximity to the modeled bottom-water O₂ anomaly, the Cape Verde region probably was susceptible to the influence of anoxic bottom water, as demonstrated by I/TOC rapidly declining during the OAE, ultimately in the mid-stage of the OAE reaching levels similar to those at Demerara Rise.

4.5. Temporal changes in I/TOC across the OAE 2

Compared to the background intervals, OAE 2, as constrained by the δ¹³C excursion, shows lower I/TOC at all study sites, most likely indicating widespread increase in planktonic carbon flux and less oxygenated bottom-water conditions. The two high latitude sites, Kerguelen

and South Ferriby, have minimum I/TOC values of ~10–25 $\mu\text{mol/mol}$ during the OAE, significantly higher than the minimum I/TOC at the other sites (0–5 $\mu\text{mol/mol}$). It therefore seems likely that the latitudinal redox gradient in bottom waters persisted during the OAE 2.

The extent and timing of upper ocean oxygenation changes indicated by I/Ca are often not synchronous when calibrated against the carbon-isotope curve that characterizes OAE 2 (Zhou et al., 2015). Compared to I/Ca records, I/TOC values show slightly better covariance with the $\delta^{13}\text{C}$ profile during the OAE at almost all sites, which suggests that local bottom-water redox conditions were tied more closely to global organic-carbon burial. This result is unsurprising, because upper-ocean oxygenation is heavily influenced by interactions with the atmosphere and ocean circulation, whereas bottom-water oxygenation during the OAE should reflect widespread organic-matter burial and oxygen consumption in the ocean interior.

4.6. Seawater iodine inventory

The marine iodine inventory could have changed during the OAE 2 global organic-carbon burial event, since the main output of iodine from seawater is organic matter in marine sediments (Muramatsu and Wedepohl, 1998). There is no consensus as to whether iodine would be draw-down as was the case with redox-sensitive trace metals (Algeo, 2004; Ma, et al., 2014), or whether it would be more efficiently remobilized and recycled like phosphate (Mort et al., 2007b). The iodine budget has implications for the interpretation of the carbonate I/Ca record as I/Ca values are affected by marine iodine reservoir, but it is difficult to evaluate budget changes from I/Ca data alone because organic matter is the major sink of marine iodine (Zhou et al., 2015). Organically bound iodine concentrations (I_{org}) may record, at least in part, the amount of buried iodine during the OAE 2.

Average I_{org} values are highest at the Kerguelen and Cape Verde sites (Fig. 4). South Ferriby has relatively low I_{org} but low TOC, which leads to high I/TOC. Consequently, the ideal sedimentary iodine sink may be relatively oxic and organic-rich settings, where iodine can be enriched in the organic fraction of surface sediments under oxic bottom-water conditions (Price and Calvert, 1973). I_{org} was elevated at Kerguelen and Cape Verde during the OAE, regardless of decreasing I/TOC, possibly due to strong iodine enrichment driven by adsorption on abundant organic matter on the seafloor, overpowering the effect of deoxygenation. I_{org} shows better correlation with TOC at Kerguelen and South Ferriby than at rest of the sites during the OAE 2, which may suggest that TOC becomes the main control for iodine enrichment when the bottom water is oxygenated (Fig. 6). At Furlo, Demerara Rise and Tarfaya, I_{org} values either remain at the same level as at pre-OAE interval or decreases during the OAE, with the intensification of low oxygen conditions on the seafloor as indicated by the decreasing I/TOC at these sites. So the records of I_{org} and I/TOC provide a good understanding of the connection between the iodine inventory and oceanic oxygenation, but such changes during the OAE cannot be easily predicted due to its complexity. An Earth System Model such as cGENIE may be able to provide the ultimate answer by simulating both bottom-water oxygenation and the global iodine cycle.

5. Conclusions

I/TOC has been suggested to correlate with bottom-water oxygenation in the modern ocean. We developed a method to extract organic iodine from small volumes of sediment. I/TOC data from six sites across the Cenomanian–Turonian OAE 2 showed relatively more oxic conditions at high-latitude sites, consistent with other redox indicators and model simulations. Bottom waters became more reducing during the OAE 2 at all sites, as illustrated by lower I/TOC values. Compared to upper-ocean oxygenation indicated by carbonate I/Ca, temporal

changes in bottom-water conditions were relatively synchronous with global organic-carbon burial and oxygen utilization in the ocean interior during the OAE 2. Total organically bound iodine content did not show consistent changes through the OAE 2 interval at different sites, so no firm conclusions as to the possible extent of global iodine burial can be drawn. Relatively organic-rich sediment deposited under oxygenated bottom water may be an important sink of seawater iodine. Such a topic may be worthy of with more modeling work.

Acknowledgements

XZ and ZL are supported by NSF EAR 1349252.

References

- Adams, D.D., Hurtgen, M.T., and Sageman, B.B., 2010, Volcanic triggering of a biogeochemical cascade during Oceanic Anoxic Event 2: *Nature Geoscience*, v. 3, no. 3, p. 201–204, doi: Doi 10.1038/Ngeo743.
- Algeo, T.J., 2004, Can marine anoxic events draw down the trace element inventory of seawater? *Geology*, v. 32, no. 12, p. 1057–1060, doi: 10.1130/G20896.1.
- Algeo, T.J., and Lyons, T.W., 2006, Mo-total organic carbon covariation in modern anoxic marine environments: Implications for analysis of paleoredox and paleohydrographic conditions: *Paleoceanography*, v. 21, no. 1, doi: 10.1029/2004PA001112.
- Algeo, T.J., and Tribouillard, N., 2009, Environmental analysis of paleoceanographic systems based on molybdenum-uranium covariation: *Chemical Geology*, v. 268, no. 3-4, p. 211–225, doi: 10.1016/j.chemgeo.2009.09.001.
- Arthur, M.A., Dean, W.E., and Pratt, L.M., 1988, Geochemical and climatic effects of increased marine organic carbon burial at the Cenomanian/Turonian boundary: *Nature*, v. 335, p. 714–717.
- Arthur, M.A., Jenkyns, H.C., Brumsack, H.J., and Schlanger, S.O., 1990, Stratigraphy, geochemistry, and paleoceanography of organic carbon-rich Cretaceous sequences, *in* Ginsburg, R.N. and Beaudoin, B. eds., *Cretaceous Resources, Events and Rhythms*, Kluwer Academic Publishers, p. 75–119.
- Barclay, R.S., McElwain, J.C., and Sageman, B.B., 2010, Carbon sequestration activated by a volcanic CO₂ pulse during Ocean Anoxic Event 2: *Nature Geoscience*, v. 3, p. 205–208, doi:10.1038/ngeo757.
- van Bentum, E.C., Hetzel, A., Brumsack, H.J., Forster, A., Reichert, G.J., and Damste, J.S.S.,

- 2009, Reconstruction of water column anoxia in the equatorial Atlantic during the Cenomanian-Turonian oceanic anoxic event using biomarker and trace metal proxies: *Palaeogeography Palaeoclimatology Palaeoecology*, v. 280, no. 3-4, p. 489–498, doi: DOI 10.1016/j.palaeo.2009.07.003.
- Blattler, C.L., Jenkyns, H.C., Reynard, L.M., and Henderson, G.M., 2011, Significant increases in global weathering during Oceanic Anoxic Events 1a and 2 indicated by calcium isotopes: *Earth and Planetary Science Letters*, v. 309, no. 1-2, p. 77–88, doi: 10.1016/j.epsl.2011.06.029.
- Bluhm, K., Croot, P.L., Huhn, O., Rohardt, G., and Lochte, K., 2011, Distribution of iodide and iodate in the Atlantic sector of the southern ocean during austral summer: *Deep-Sea Research Part II-Topical Studies in Oceanography*, v. 58, no. 25-26, p. 2733–2748, doi: 10.1016/j.dsr2.2011.02.002.
- Bomou, B., Adatte, T., Tantawy, A.A., Mort, H., Fleitmann, D., Huang, Y., and Föllmi, K.B., 2013, The expression of the Cenomanian-Turonian oceanic anoxic event in Tibet: *Palaeogeography, Palaeoclimatology, Palaeoecology*, v. 369, p. 466–481, doi: 10.1016/j.palaeo.2012.11.011.
- Brewer, P.G., Nozaki, Y., Spencer, D.W., and Fler, A.P., 1980, SEDIMENT TRAP EXPERIMENTS IN THE DEEP NORTH-ATLANTIC - ISOTOPIC AND ELEMENTAL FLUXES: *Journal of Marine Research*, v. 38, no. 4, p. 703–728.
- Brown, C.F., Geiszler, K.N., and Vickerman, T.S., 2005, Extraction and quantitative analysis of iodine in solid and solution matrixes.: *Analytical chemistry*, v. 77, no. 21, p. 7062–6, doi: 10.1021/ac050972v.
- Bunte, von F.A., 2009, Geochemical signatures of black shales deposited during Oceanic

- Anoxic Event 2 (Cenomanian/Turonian) in the tropical Atlantic (Demerara Rise, ODP Leg 207) and in northern Germany (Wunstorf): Carl von Ossietzky Universität Oldenburg.
- Chenet, P.Y., and Francheteau, J., 1979, Bathymetric reconstruction method: application to the Central Atlantic Basin between 10°N and 40°N: Initial Reports of the Deep Sea Drilling Project, v. 51-53, p. 1501–1514.
- Coffin, M.F., Frey, F.A., and Wallace, P.J., 2000, 6. Site 1138: Proceedings of the Ocean Drilling Program, Initial Reports, v. 183.
- Elderfield, H., and Truesdale, V.W., 1980, On the Biophilic Nature of Iodine in Seawater: Earth and Planetary Science Letters, v. 50, no. 1, p. 105–114.
- El-Sabbagh, A., Tantawy, A.A., Keller, G., Khozyem, H., Spangenberg, J., Adatte, T., and Gertsch, B., 2011, Stratigraphy of the Cenomanian–Turonian Oceanic Anoxic Event OAE 2 in shallow shelf sequences of NE Egypt: Cretaceous Research, v. 32, no. 6, p. 705–722, doi: 10.1016/j.cretres.2011.04.006.
- Erbacher, J., Friedrich, O., Wilson, P.A., Birch, H., and Mutterlose, J., 2005, Stable organic carbon isotope stratigraphy across Oceanic Anoxic Event 2 of Demerara Rise, western tropical Atlantic: Geochemistry Geophysics Geosystems, v. 6, doi: 10.1029/2004gc000850.
- Erbacher, J., Mosher, D.C., and Malone, M.J., 2004, 5. Site 1258: Proceedings of the Ocean Drilling Program Initial Reports, v. 207.
- Friedrich, O., Erbacher, J., and Mutterlose, J., 2006, Paleoenvironmental changes across the Cenomanian/Turonian Boundary Event (Oceanic Anoxic Event 2) as indicated by benthic foraminifera from the Demerara Rise (ODP Leg 207): Revue de Micropaléontologie, v. 49, no. 3, p. 121–139, doi: 10.1016/j.revmic.2006.04.003.
- Gambacorta, G., Jenkyns, H.C., Russo, F., Tsikos, H., Wilson, P.A., Faucher, G. and Erba, E.,

- 2015, Carbon- and oxygen-isotope records of mid-Cretaceous Tethyan pelagic sequences from the Umbria–Marche and Belluno Basins (Italy). *Newsletters Stratigr.*, 48, 299–323.
- Gertsch, B., Keller, G., Adatte, T., Berner, Z., Kassab, A., Tantawy, A., El-Sabbagh, A., and Stueben, D., 2010, Cenomanian–Turonian transition in a shallow water sequence of the Sinai, Egypt: *International Journal of Earth Sciences*, v. 99, no. 1, p. 165–182, doi: 10.1007/s00531-008-0374-4.
- Grimm, M.R., 1952, Iodine Content of Some Marine Algae: Cornell University, 318–323 p.
- van Helmond, N.A.G.M., Ruvalcaba Baroni, I., Sluijs, A., Sinninghe Damsté J.S., and Slomp, C.P., 2014, Spatial extent and degree of oxygen depletion in the deep proto-North Atlantic basin during Oceanic Anoxic Event 2: *Geochemistry, Geophysics, Geosystems*, v. 15, p. 4254–4266, doi: 10.1002/2014GC005528.
- Hasegawa, T., 1997, Cenomanian-Turonian carbon isotope events recorded in terrestrial organic matter from northern Japan. *Palaeogeography, Palaeoclimatology, Palaeoecology*, v. 130, p. 251–273.
- Hetzl, A., Bottcher, M.E., Wortmann, U.G., and Brumsack, H.J., 2009, Paleo-redox conditions during OAE 2 reflected in Demerara Rise sediment geochemistry (ODP Leg 207): *Palaeogeography Palaeoclimatology Palaeoecology*, v. 273, p. 302–328, doi: DOI 10.1016/j.palaeo.2008.11.005.
- Hetzl, A., März, C., Vogt, C., and Brumsack, H.J., 2011, Geochemical environment of Cenomanian - Turonian black shale deposition at Wunstorf (northern Germany): *Cretaceous Research*, v. 32, no. 4, p. 480–494, doi: 10.1016/j.cretres.2011.03.004.
- Holbourn, A., and Kuhnt, W., 2002, Cenomanian–Turonian palaeoceanographic change on the Kerguelen Plateau: a comparison with Northern Hemisphere records: *Cretaceous Research*,

- v. 23, no. 3, p. 333–349, doi: 10.1006/cres.2002.1008.
- Jarvis, I., Lignum, J.S., Gröcke, D.R., Jenkyns, H.C., and Pearce, M.A., 2011, Black shale deposition, atmospheric CO₂ drawdown and cooling during the Cenomanian-Turonian Oceanic Anoxic Event (OAE 2): *Paleoceanography*, v. 26, no. 3, p. PA3201, doi: 10.1029/2010PA002081.
- Jenkyns, H.C., 1980. Cretaceous anoxic events: from continents to oceans. *Journal of the Geological Society*, v. 137, p. 171–188.
- Jenkyns, H.C., 2003, Evidence for rapid climate change in the Mesozoic-Palaeogene greenhouse world: *Philosophical Transactions of the Royal Society a-Mathematical Physical and Engineering Sciences*, v. 361, no. 1810, p. 1885–1916, doi: 10.1098/rsta.2003.1240.
- Jenkyns, H.C., 2010, Geochemistry of oceanic anoxic events: *Geochemistry Geophysics Geosystems*, v. 11, doi: 10.1029/2009gc002788.
- Jenkyns, H.C., Matthews, A., Tsikos, H., and Erel, Y., 2007, Nitrate reduction, sulfate reduction, and sedimentary iron isotope evolution during the Cenomanian-Turonian oceanic anoxic event: *Paleoceanography*, v. 22, no. 3, doi: 10.1029/2006pa001355.
- Jones, E.J.W., Bigg, G.R., Handoh, I.C., and Spathopoulos, F., 2007, Distribution of deep-sea black shales of Cretaceous age in the eastern Equatorial Atlantic from seismic profiling: *Palaeogeography, Palaeoclimatology, Palaeoecology*, v. 248, no. 1-2, p. 233–246, doi: 10.1016/j.palaeo.2006.12.006.
- Jones, C.E., and Jenkyns, H.C., 2001, Seawater strontium isotopes, oceanic anoxic events, and seafloor hydrothermal activity in the Jurassic and Cretaceous: *American Journal of Science*, v. 301, no. 2, p. 112–149.
- Junium, C.K., Freeman, K.H., and Arthur, M.A., 2015, Controls on the stratigraphic distribution

- and nitrogen isotopic composition of zinc, vanadyl and free base porphyrins through Oceanic Anoxic Event 2 at Demerara Rise: *Organic Geochemistry*, v. 80, p. 60-71, doi:10.1016/j.orggeochem.2014.10.009.
- Kennedy, H.A., and Elderfield, H., 1987a, Iodine Diagenesis in Non-Pelagic Deep-Sea Sediments: *Geochimica et Cosmochimica Acta*, v. 51, no. 9, p. 2505–2514.
- Kennedy, H.A., and Elderfield, H., 1987b, Iodine Diagenesis in Pelagic Deep-Sea Sediments: *Geochimica et Cosmochimica Acta*, v. 51, no. 9, p. 2489–2504.
- Kerr, A.C., 1998, Oceanic plateau formation: a cause of mass extinction and black shale deposition around the Cenomanian-Turonian boundary? *Journal of the Geological Society*, v. 155, p. 619–626, doi: 10.1144/gsjgs.155.4.0619.
- Knapp, G., Maichin, B., Fecher, P., Hasse, S., and Schramel, P., 1998, Iodine determination in biological materials: Options for sample preparation and final determination: *Journal of Analytical Chemistry*, v. 362, no. 6, p. 508–513.
- Kolonic, S., Wagner, T., Forster, A., Sinninghe Damsté J.S., Walsworth-Bell, B., Erba, E., Turgeon, S., Brumsack, H.-J., Chellai, E.H., Tsikos, H., Kuhnt, W., and Kuypers, M.M.M., 2005, Black shale deposition on the northwest African Shelf during the Cenomanian/Turonian oceanic anoxic event: Climate coupling and global organic carbon burial: *Paleoceanography*, v. 20, no. 1, p. PA1006, doi: 10.1029/2003PA000950.
- Kuhnt, W., Luderer, F., Nederbragt, S., Thurow, J., and Wagner, T., 2005, Orbital-scale record of the late Cenomanian-Turonian oceanic anoxic event (OAE-2) in the Tarfaya Basin (Morocco): *International Journal of Earth Sciences*, v. 94, p. 147–159, doi: 10.1007/s00531-004-0440-5.
- Kuhnt, W., and Wiedmann, J., 1995, Cenomanian-Turonian source rocks: paleobiogeographic

- and paleoenvironmental aspects: AAPG, Studies in Geology, v. 40, p. 213–231.
- Kuroda, J., Ogawa, N.O., Tanimizu, M., Coffin, M.F., Tokuyama, H., Kitazato, H., and Ohkouchi, N., 2007, Contemporaneous massive subaerial volcanism and late cretaceous Oceanic Anoxic Event 2: Earth and Planetary Science Letters, v. 256, no. 1-2, p. 211–223, doi: 10.1016/j.epsl.2007.01.027.
- Kuypers, M.M.M., Pancost, R.D., Nijenhuis, I.A., and Damste, J.S.S., 2002, Enhanced productivity led to increased organic carbon burial in the euxinic North Atlantic basin during the late Cenomanian oceanic anoxic event: Paleoceanography, v. 17, no. 4, doi: 10.1029/2000pa000569.
- Lancelot, Y., Seibold, E., Cepek, P., Dean, W.E., Eremeev, V., Gardner, J., Jansa, L.F., Johnson, D., Krasheninnikov, V., Pflaumann, U., Rankin, J.G., Trabant, P., and Bukry, D., 1977, Site 367: Cape Verde Basin: Deep Sea Drilling Project Initial Reports, v. 41, no. March, p. 163–232.
- Lanci, L., Muttoni, G., and Erba, E., 2010, Astronomical tuning of the Cenomanian Scaglia Bianca Formation at Furlo, Italy: Earth and Planetary Science Letters, v. 292, no. 1-2, p. 231–237, doi: 10.1016/j.epsl.2010.01.041.
- Leine, L., 1986, Geology of the Tarfaya oil shale deposit, Morocco: Geologie en Mijnbouw, v. 65, p. 57–74.
- Lu, Z., Hensen, C., Fehn, U., and Wallmann, K., 2008, Halogen and ¹²⁹I systematics in gas hydrate fields at the northern Cascadia margin (IODP Expedition 311): Insights from numerical modeling: Geochemistry, Geophysics, Geosystems, v. 9, doi: 10.1029/2008GC002156.
- Ma, C., Meyers, S. R., Sageman, B. B., Singer, B. S., and Jicha, B. R., 2014, Testing the

- astronomical time scale for oceanic anoxic event 2, and its extension into Cenomanian strata of the Western Interior Basin (USA): *GSA Bulletin*; v. 126, no. 7-8, p. 974–989, doi: 10.1130/B30922.1.
- Mitchell, R.N., Bice, D.M., Montanari, A., Cleaveland, L.C., Christianson, K.T., Coccioni, R., and Hinnov, L.A., 2008, Oceanic anoxic cycles? Orbital prelude to the Bonarelli Level (OAE 2): *Earth and Planetary Science Letters*, v. 267, no. 1-2, p. 1–16, doi: 10.1016/j.epsl.2007.11.026.
- Monteiro, F.M., Pancost, R.D., Ridgwell, A., and Donnadieu, Y., 2012, Nutrients as the dominant control on the spread of anoxia and euxinia across the Cenomanian-Turonian oceanic anoxic event (OAE 2): *Model-data comparison: Paleocyanography*, v. 27, doi: 10.1029/2012pa002351.
- Mort, H., Jacquat, O., Adatte, T., Steinmann, P., Föllmi, K., Matera, V., Berner, Z., and Stüben, D., 2007a, The Cenomanian/Turonian anoxic event at the Bonarelli Level in Italy and Spain: enhanced productivity and/or better preservation? *Cretaceous Research*, v. 28, no. 4, p. 597–612, doi: 10.1016/j.cretres.2006.09.003.
- Mort, H.P., Adatte, T., Föllmi, K.B., Keller, G., Steinmann, P., Matera, V., Berner, Z., and Stüben, D., 2007b, Phosphorus and the roles of productivity and nutrient recycling during oceanic anoxic event 2: *Geology*, v. 35, no. 6, p. 483–486, doi: Doi 10.1130/G23475a.1.
- Muramatsu, Y., and Wedepohl, K.H., 1998, The distribution of iodine in the earth's crust: *Chemical Geology*, v. 147, no. 3-4, p. 201–216.
- Murphy, D.P., and Thomas, D.J., 2012, Cretaceous deep-water formation in the Indian sector of the Southern Ocean: *Paleocyanography*, v. 27, no. 1, p. PA1211, doi: 10.1029/2011PA002198.

- Nederbragt, A.J., Thurow, J., and Pearce, R., 2007, Sediment composition and cyclicity in the Mid-Cretaceous at Demerara Rise, ODP Leg 207: Proc. ODP Sci. Results, v. 207, p. 1–31, doi: 10.2973/odp.proc.sr.207.103.2007.
- Owens, J.D., Lyons, T.W., Li, X., MacLeod, K.G., Gordon, G., Kuypers, M.M.M., Anbar, A., Kuhnt, W., and Severmann, S., 2012, Iron isotope and trace metal records of iron cycling in the proto-North Atlantic during the Cenomanian-Turonian oceanic anoxic event (OAE-2): *Paleoceanography*, v. 27, no. 3, p. 1–13, doi: 10.1029/2012PA002328.
- Pancost, R.D., Crawford, N., Magness, S., Turner, A., Jenkyns, H.C., and Maxwell, J.R., 2004, Further evidence for the development of photic-zone euxinic conditions during Mesozoic oceanic anoxic events: *Journal of the Geological Society*, v. 161, p. 353–364.
- Pogge von Strandmann, P.A.E., Jenkyns, H.C., and Woodfine, R.G., 2013, Lithium isotope evidence for enhanced weathering during Oceanic Anoxic Event 2: *Nature Geoscience*, v. 6, no. 8, p. 668–672, doi: 10.1038/ngeo1875.
- Poulton, S.W., and Canfield, D.E., 2011, Ferruginous conditions: A dominant feature of the ocean through Earth's history: *Elements*, v. 7, no. 2, p. 107–112, doi: 10.2113/gselements.7.2.107.
- Poulton, S.W., and Canfield, D.E., 2005, Development of a sequential extraction procedure for iron: Implications for iron partitioning in continentally derived particulates: *Chemical Geology*, v. 214, no. 3-4, p. 209–221, doi: 10.1016/j.chemgeo.2004.09.003.
- Poulton, S.W., Henkel, S., März, C., Urquhart, H., Flögel, S., Kasten, S., Sinninghe Damsté J.S., and Wagner, T., 2015, A continental-weathering control on orbitally driven redox-nutrient cycling during Cretaceous Oceanic Anoxic Event 2: *Geology*, v. 43, no. 11, p. 963–966, doi: 10.1130/G36837.1.
- Price, N.B., and Calvert, S.E., 1973, Geochemistry of iodine in oxidized and reduced recent

- marine sediments: *Geochimica et Cosmochimica Acta*, v. 37, no. 9, p. 2149–2158, doi: 10.1016/0016-7037(73)90013-6.
- Price, N.B., and Calvert, S.E., 1977, The contrasting geochemical behaviours of iodine and bromine in recent sediments from the Namibian shelf: *Geochimica et Cosmochimica Acta*, v. 41, no. 12, p. 1769–1775, doi: 10.1016/0016-7037(77)90209-5.
- Price, N.B., Calvert, S. E., and Jones, P.G.W., 1970, The distribution of iodine and bromine in the sediments of the Southwestern Barents Sea: *Journal of Marine Research*, v. 28, no. 1, p. 22–34.
- Reolid, M., Sánchez-Quiñónez, C. a., Alegret, L., and Molina, E., 2015, Palaeoenvironmental turnover across the Cenomanian-Turonian transition in Oued Bahloul, Tunisia: foraminifera and geochemical proxies: *Palaeogeography, Palaeoclimatology, Palaeoecology*, v. 417, p. 491–510, doi: 10.1016/j.palaeo.2014.10.011.
- Romar í-Hortas, V., Moreda-Piñeiro, A., and Bermejo-Barrera, P., 2009, Microwave assisted extraction of iodine and bromine from edible seaweed for inductively coupled plasma-mass spectrometry determination: *Talanta*, v. 79, no. 3, p. 947–952, doi: 10.1016/j.talanta.2009.05.036.
- Schlanger, S.O., Arthur, M.A., Jenkyns, H.C., and Scholle, P.A., 1987, The Cenomanian–Turonian oceanic anoxic event, I. Stratigraphy and distribution of organic carbo-rich beds and the marine $\delta^{13}\text{C}$ excursion, *in* Brooks, J. and Fleet, A.J. eds., *Marine Petroleum Source Rocks*, p. 371–399.
- Schlanger, S.O., and Jenkyns, H.C., 1976, Cretaceous oceanic anoxic events: causes and consequences: *Geol. Mijnb*, v. 55, p. 179–194.
- Sinninghe Damste, J.S., and Koster, J., 1998, A euxinic southern North Atlantic Ocean during

- the Cenomanian/Turonian oceanic anoxic event: *Earth and Planetary Science Letters*, v. 158, no. 3-4, p. 165–173.
- Takashima, R., Nishi, H., Hayashi, K., Okada, H., Kawahata, H., Yamanaka, T., Fernando, A.G., and Mampuku, M., 2009, Litho-, bio- and chemostratigraphy across the Cenomanian/Turonian boundary (OAE 2) in the Vocontian Basin of southeastern France: *Palaeogeography, Palaeoclimatology, Palaeoecology*, v. 273, no. 1-2, p. 61–74, doi: 10.1016/j.palaeo.2008.12.001.
- Tinggi, U., Schoendorfer, N., Davies, P.S.W., Scheelings, P., and Olszowy, H., 2011, Determination of iodine in selected foods and diets by inductively coupled plasma-mass spectrometry: *Pure and Applied Chemistry*, v. 84, no. 2, p. 291–299, doi: 10.1351/PAC-CON-11-08-03.
- Topper, R.P.M., Alexandre, J.T., Tuenter, E., and Meijer, P.T., 2011, A regional ocean circulation model for the mid-Cretaceous North Atlantic Basin: implications for black shale formation: *Climate of the Past*, v. 7, no. 1, p. 277–297, doi: 10.5194/cp-7-277-2011.
- Tsikos, H., Jenkyns, H.C., Walsworth-Bell, B., Petrizzo, M.R., Forster, A., Kolonic, S., Erba, E., Silva, I.P., Baas, M., Wagner, T., and Damste, J.S.S., 2004, Carbon-isotope stratigraphy recorded by the Cenomanian-Turonian Oceanic Anoxic Event: correlation and implications based on three key localities: *Journal of the Geological Society*, v. 161, p. 711–719.
- Tsunogai, S., 1971, Iodine in the deep water of the ocean: *Deep Sea Research and Oceanographic Abstracts*, v. 18, no. 9, p. 913–919, doi: 10.1016/0011-7471(71)90065-9.
- Tsunogai, S., and Sase, T., 1969, Formation of Iodide-Iodine in Ocean: *Deep-Sea Research*, v. 16, no. 5, p. 489.
- Tullai, S., Tubbs, L.E., and Fehn, U., 1987, Iodine Extraction from Petroleum for Analysis of I-

- 129/I-127 Ratios by Ams: Nuclear Instruments & Methods in Physics Research Section B-Beam Interactions with Materials and Atoms, v. 29, no. 1-2, p. 383–386.
- Turgeon, S.C., and Creaser, R.A., 2008, Cretaceous oceanic anoxic event 2 triggered by a massive magmatic episode: *Nature*, v. 454, p. 323–329, doi: 10.1038/Nature07076.
- Turgeon, S. and Brumsack, H.-J., 2006, Anoxic vs dysoxic events reflected in sediment geochemistry during the Cenomanian–Turonian Boundary Event (Cretaceous) in the Umbria–Marche Basin of central Italy. *Chemical Geology*, v. 234, p.321–339.
- Ullman, W.J., and Aller, R.C., 1985, The Geochemistry of Iodine in near-Shore Carbonate Sediments: *Geochimica et Cosmochimica Acta*, v. 49, no. 4, p. 967–978.
- Waite, T.J., and Truesdale, V.W., 2003, Iodate reduction by *Isochrysis galbana* is relatively insensitive to de-activation of nitrate reductase activity - are phytoplankton really responsible for iodate reduction in seawater? *Marine Chemistry*, v. 81, no. 3-4, p. 137–148, doi: 10.1016/s0304-4203(03)00013-6.
- Westermann, S., Caron, M., Fiet, N., Fleitmann, D., Matera, V., Adatte, T., and Föllmi, K.B., 2010, Evidence for oxic conditions during oceanic anoxic event 2 in the northern Tethyan pelagic realm: *Cretaceous Research*, v. 31, no. 5, p. 500–514, doi: 10.1016/j.cretres.2010.07.001.
- Westermann, S., Vance, D., Cameron, V., Archer, C., and Robinson, S.A., 2014, Heterogeneous oxygenation states in the Atlantic and Tethys oceans during Oceanic Anoxic Event 2: *Earth and Planetary Science Letters*, v. 404, p. 178–189, doi: 10.1016/j.epsl.2014.07.018.
- Wong, G.T.F., 1980, The stability of dissolved inorganic species of iodine in seawater: *Marine Chemistry*, v. 9, no. 1, p. 13–24, doi: 10.1016/0304-4203(80)90003-1.
- Zhou, X., Jenkyns, H.C., Owens, J.D., Junium, C.K., Zheng, X., Sageman, B.B., Hardisty, D.S.,

Lyons, T.W., Ridgwell, A., and Lu, Z., 2015, Upper ocean oxygenation dynamics from I/Ca ratios during the Cenomanian-Turonian OAE 2: *Paleoceanography*, v. 30, p. 510–526.

doi:10.1002/2014PA002741.

Tables

Table 1. Evidence of anoxia at each site except for the evidence for oxygenation in seawater at Site South Ferriby as indicated.

Site	Evidence	Pre-CIE	CIE	Post-CIE	References
Demerara Rise	I/Ca	Low I/Ca values			Zhou et al., 2015
	Trace metals	Low Mn content	Enrichment of Fe and Co, low Mn content	Low Mn content	Hetzel et al., 2009
	Biomarkers	Presence of lycopane	Presence of Isorenieratane, chlorobactane and lycopane	Presence of lycopane	van Bentum, 2009
	Foraminifera		Low abundance in benthic foraminifera		Friedrich et al., 2006
Tarfaya	I/Ca	Low I/Ca values	Low I/Ca values	Low I/Ca values	Zhou et al., 2015
	Iron speciation		FeHR/FeT higher than 0.4, FePy/FeHR fluctuating around 0.7 (0.4-0.9)		Poulton et al., 2015
	Biomarkers		Presence of Isorenieratane and chlorobactane	Presence of Isorenieratane and chlorobactane	Kolonic et al., 2005; Poulton et al., 2015
	Foraminifera	Low abundance of benthic foraminifera			
Furlo	I/Ca	Low I/Ca values		Low I/Ca values	
	Iron speciation	FeHR/FeT higher than 0.4, FePy/FeHR lower than 0.8	FeHR/FeT higher than 0.4, FePy/FeHR lower than 0.8		Westermann et al., 2014
	Trace metals		High U, V, Mo contents, low Mn content		Turgeon and Brumsack, 2006
Cape Verde	Iron speciation		FeHR/FeT higher than 0.4, FePy/FeHR between 0.1 and 0.7		Westermann et al., 2014
	Trace metals	High V contents	High U, V, Mo contents		Westermann et al., 2014
Kerguelen Plateau	Foraminifera		Barren foraminifera		Holbourn and Kuhnt, 2002
South Ferriby	I/Ca	High I/Ca suggest relatively oxygenated upper ocean	I/Ca peaks may suggest local water oxygenation or invasion of iodate-rich waters	High I/Ca suggest relatively oxygenated upper ocean	Zhou et al., 2015
	Trace metals	High Mn content	Low Mn content suggest dysoxic bottom water	High Mn content	Turgeon and Brumsack, 2006

Figures

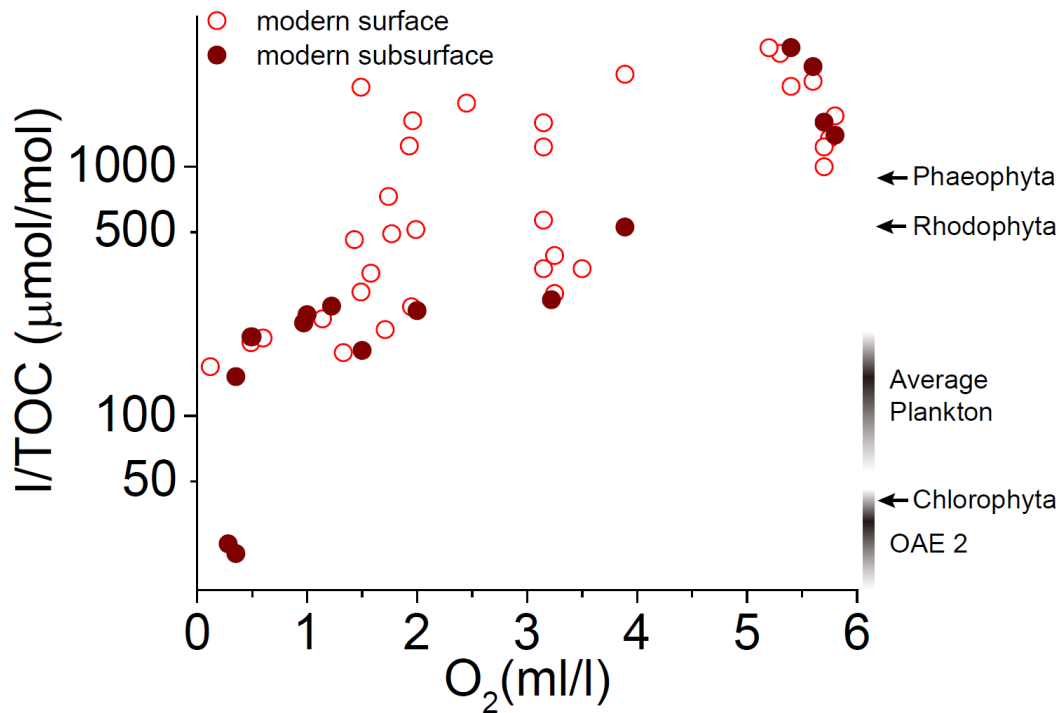


Figure 1. I/TOC of modern marine sediments plotted with bottom-water oxygen concentration immediately overlying the sea floor. The open circles are surface sediments of the southwest African continental shelf (Price and Calvert, 1973), tropical eastern Pacific and coastal areas of North Atlantic (Kennedy and Elderfield, 1987a). Closed circles are subsurface sediments from Namibian shelf (Price and Calvert, 1977), Cascadia margin (Lu et al., 2008), and coastal areas of tropical North Atlantic (Kennedy and Elderfield, 1987a). The highest I/TOC values in different groups of algae, average I/TOC values in plankton, and the range of OAE 2 I/TOC values are pointed out as short arrows and a grey shading, respectively (Grimm, 1952).

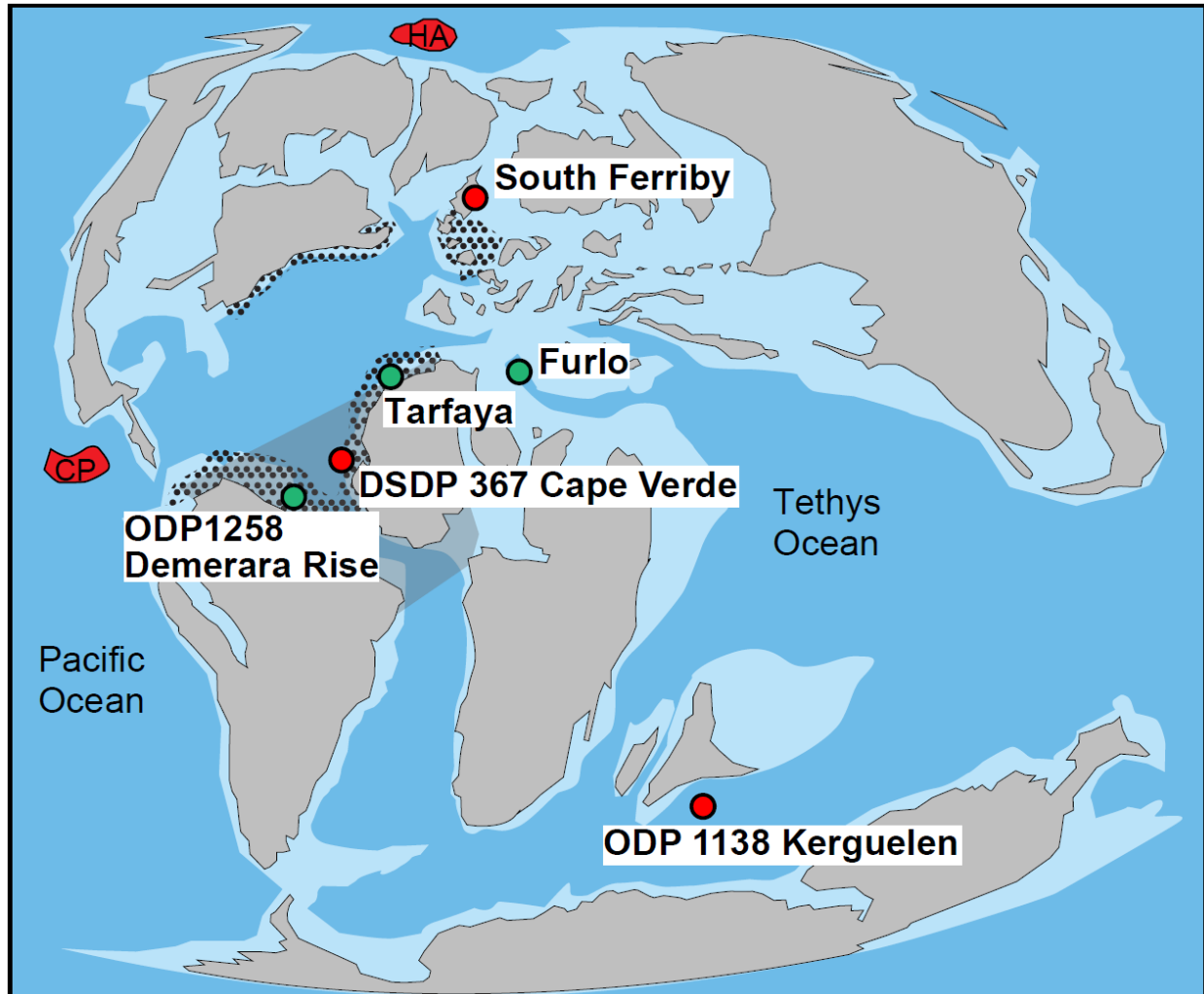


Figure 2. Paleogeographic map for the Late Cretaceous. The beige shading represents continents, light blue neritic (shelf) sea, and dark blue deep sea. The six OAE 2 sections are divided into two groups; the green circles represent relatively reducing locations, and the red circles show relatively oxygenated ones. The full name is put beside each site. The black dots mark the modeled upwelling regions from Topper et al. (2011), and the gray shading shows areas of prolonged euxinic conditions in the water column given in Jenkyns (2010). HA = High Arctic Large Igneous Province, CP = Caribbean Plateau.

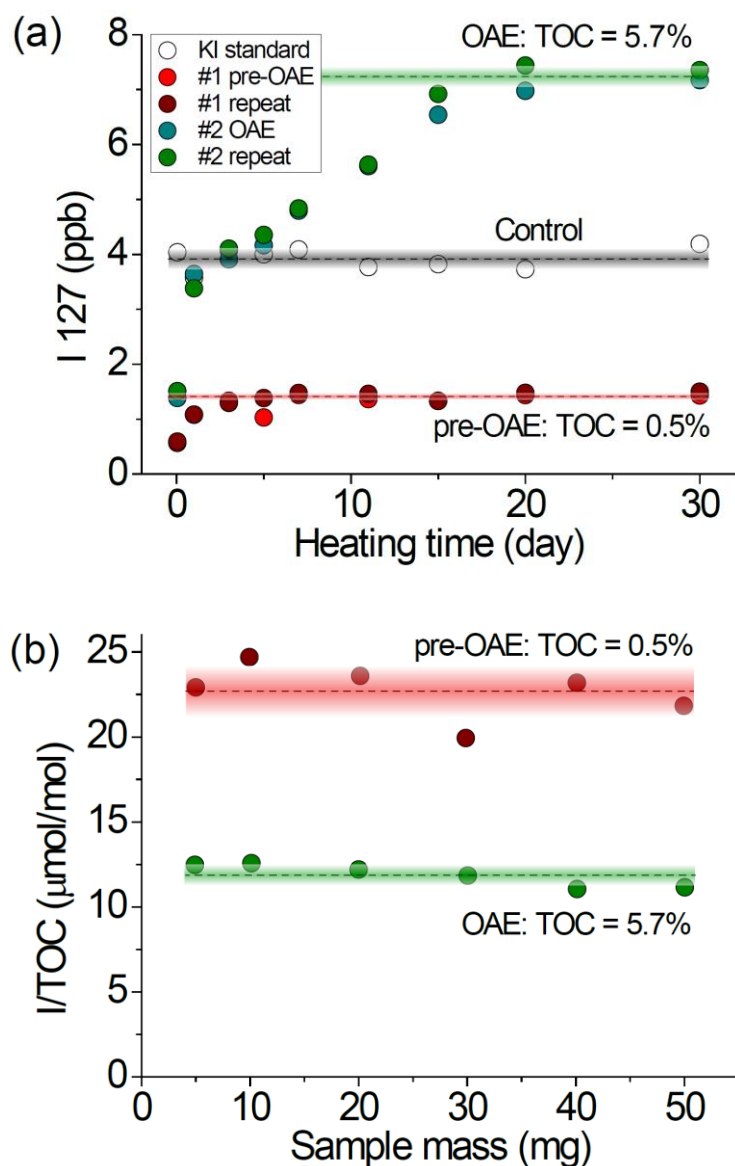


Figure 3. (a). Iodine extraction results of the test run of two OAE 2 samples. Closed circles in red and wine represent the sample from the pre-OAE interval; closed circles in green and blue are the two identical samples from within the OAE; and the open circles denote the KI standard. The plot shows changes in iodine concentration released from the samples with time. The dashed line and colored bars on top of each set of circles are the average value and standard deviation of the data. (b). Effect of sample mass on I/TOC values of the two OAE 2 samples. Legends are the same as figure (a).

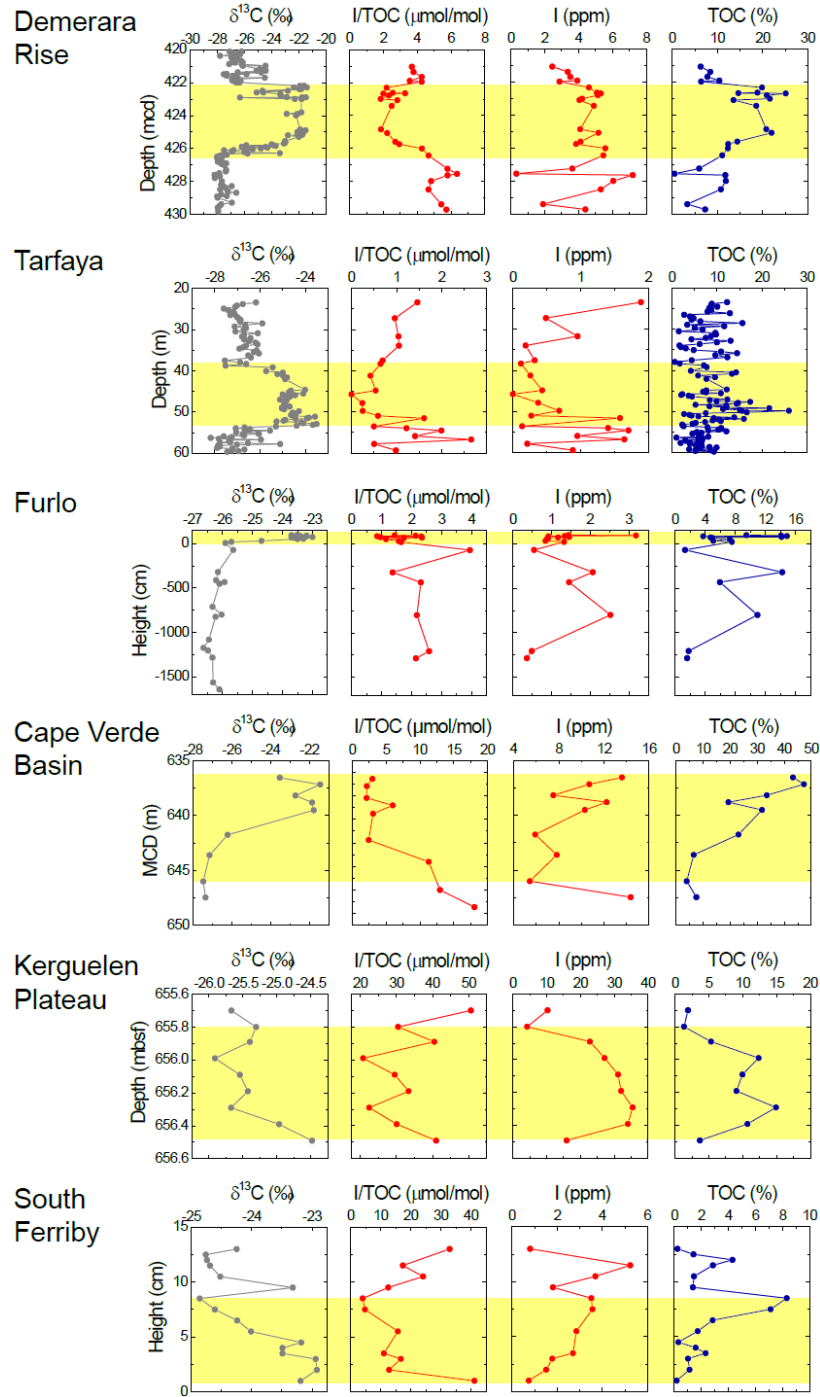


Figure 4. Stratigraphic records of $\delta^{13}\text{C}$, I/TOC, I_{org} , and TOC at the six study sites. I/TOC and I_{org} data are from this study, $\delta^{13}\text{C}$ and TOC data are from Holbourn and Kuhnt (2002); Kuypers et al. (2002); Tsikos et al. (2004); Erbacher et al. (2005); and Jenkyns et al. (2007). The yellow boxes bracket the CIE or part of the CIE at each site.

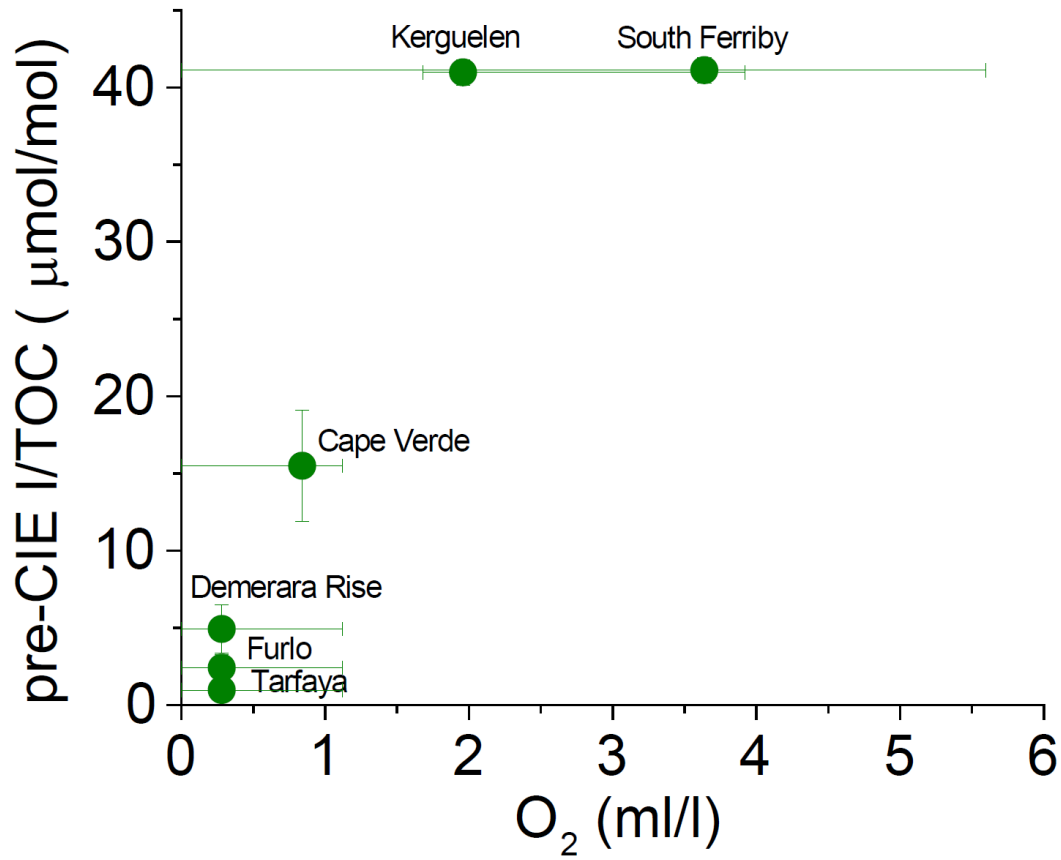


Figure 5. Pre-CIE average I/TOC values plotted against modeled bottom-water oxygen for the Late Cretaceous with a deeper Panama, after Monteiro et al. (2012). Vertical error bars represent the standard deviation of the average pre-CIE I/TOC value from each site; horizontal error bars are calculated from the surrounding modeled bottom-water O_2 concentrations of each site.

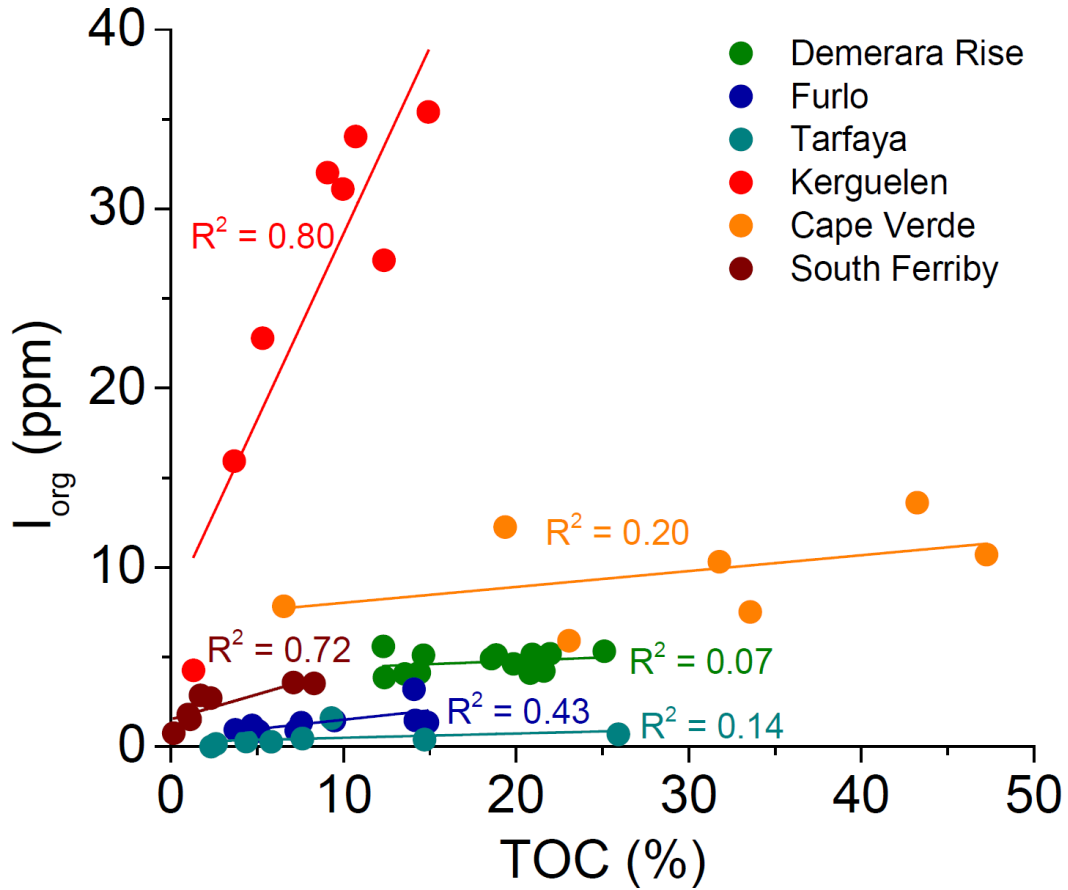


Figure 6. Organically bound iodine concentration in bulk sediment (I_{org}) plotted against corresponded TOC content for samples during OAE 2. I_{org} data are from this study, TOC data are from published papers. Circle data points in green, royal blue, dark cyan, red, orange, and wine colors represent the site of Demerara Rise, Furlo, Tarfaya, Kerguelen Plateau, Cape Verde Basin, and South Ferriby, respectively. The colored lines across each data set are linear fittings with R^2 on the side.

Chapter 3: I/Ca evidence for upper ocean deoxygenation during the PETM

Published As:

Zhou, X., Thomas, E., Rickaby, R.E.M., Winguth, A.M.E., and Lu, Z., 2014, I/Ca evidence for upper ocean deoxygenation during the PETM: *Paleoceanography*, v. 29, no. 10, p. 964–975, doi: 10.1002/2014PA002702.

Abstract

Anthropogenic global warming affects marine ecosystems in complex ways, and declining ocean oxygenation is a growing concern. Forecasting the geographical and bathymetric extent, rate, and intensity of future deoxygenation and its effects on oceanic biota, however, remains highly challenging because of the complex feedbacks in the Earth-ocean biota system. Information on past global warming events such as the Paleocene-Eocene Thermal Maximum (PETM, ~55.5Ma), a potential analog for present and future global warming, may help in such forecasting. Documenting past ocean deoxygenation, however, is hampered by the lack of sensitive proxies for past oceanic oxygen levels throughout the water column. As yet no evidence has been presented for pervasive deoxygenation in the upper water column through expansion of oxygen minimum zones (OMZs). We apply a novel proxy for paleoredox conditions, the iodine to calcium ratio (I/Ca) in bulk coarse fraction sediment and planktonic foraminiferal tests from pelagic sites in different oceans, and compared our reconstruction with modeled oxygen levels. The reconstructed iodate gradients indicate that deoxygenation occurred in the upper water column in the Atlantic, Indian Oceans, and possibly the Pacific Ocean, as well during the PETM, due to vertical and potentially lateral expansion of OMZs.

1. Introduction

Global warming reportedly leads to deoxygenation in the modern and future oceans (Helm et al., 2011). With present global warming, OMZs are shoaling worldwide (Whitney et al., 2007; Bograd et al., 2008; Gilly et al., 2013), strongly impacting the structure of pelagic ecosystems (Stramma et al., 2012). It is important to predict future oceanic oxygen levels because of the consequences of decreased oxygen levels for marine life (including fisheries) (Keeling et al., 2010; Falkowski et al., 2011). The geological record of past global warming episodes may be used to obtain information on the extent and severity of oceanic deoxygenation and its effects on marine biota (Reid et al., 2009), as has been done for ocean acidification (Hoenisch et al., 2012).

Reconstruction of global oceanic oxygen levels of the past is difficult, however. Trace elements and isotopic proxies measured on bulk sediment reflect local to regional oxygen conditions in bottom or pore waters, or potentially the relative area of the global sea floor affected by anoxia/hypoxia (Algeo and Lyons, 2006; Anbar and Gordon, 2008). In the present oceans, we see low-oxygen conditions in semienclosed, poorly ventilated basins such as the Black Sea, but the largest oceanic regions with anoxic-dysoxic waters are the oxygen minimum zones (OMZs), midwater regions with O_2 concentrations <0.5 ml/L that intercept continental margins generally at bathyal depths (200–1000 m) (Levin, 2003; Gooday et al., 2010). Modern OMZs are well developed in the high-productivity regions of the eastern Pacific Ocean, the Arabian Sea, and the Bay of Bengal (Levin, 2003). Below OMZs, bottom waters may well be oxygenated: the eastern equatorial Pacific OMZ, for instance, has its minimum oxygen levels between 200 and 700 m in a region where the water depth is more than 4000 m (Gilly et al., 2013).

The geological record contains examples of oceanic deoxygenation during rapid global warming episodes of the past, such as the Mesozoic Oceanic Anoxic Events (OAEs) (Jenkyns,

2010). The Paleocene-Eocene Thermal Maximum (PETM, ~55.5 Ma) has been considered a less intense counterpart of the OAEs (Jenkyns, 2010) and our best analog for future global warming (Hoenisch et al., 2012). More complete global records can be constructed for this younger event than for Mesozoic events (McInerney and Wing, 2011; Dunkley Jones et al., 2013). Laminated, organic-rich shales, as typical for OAEs, were deposited during the PETM in marginal basins in the Tethys (Speijer and Wagner, 2002), Peri-Tethys (Gavrilov et al., 1997; Dickson et al., 2014), and in the Arctic Ocean (Moran et al., 2006; Stein et al., 2006). Decreased bioturbation indicates lowered oxygen levels along continental margins in New Zealand (Nicolo et al., 2010) but is not associated with benthic foraminiferal assemblages indicative of low-oxygen levels (Alegret et al., 2009, 2010). Along the New Jersey shelf, oxygen levels declined, but anoxia was not reached (Stassen et al., 2012). Low-oxygen conditions occurred in the semirestricted Arctic before, during, and after the PETM (Sluijs et al., 2006), as well as in its marginal basins (Akhmet'ev et al., 2010; McNeil et al., 2013; Nagy et al., 2013). The widespread anoxic to hypoxic conditions in arginal basins have been linked to eutrophication (New Jersey; Gibbs et al., 2006; Stassen et al., 2012), possibly due to increased nutrient inputs as supplied by a more active hydrological cycle during the extreme warmth of the PETM (Ravizza et al., 2001; Wieczorek et al., 2013).

Globally, oxygen levels in open ocean basins may have dropped slightly during the late PETM, as argued from Mo-isotope evidence (Dickson et al., 2012) and from modeling (Winguth et al., 2012). Sediment chemical evidence suggests that bottom waters were suboxic at abyssal to bathyal depths in the Atlantic and Southern Oceans across the PETM with intensification during the event but not in the Pacific (Chun et al., 2010; Paelike et al., 2014), and there is no evidence for global bottom water anoxia during the peak of the PETM (Thomas, 2007).

In contrast to marginal basins, suboxic conditions in open oceans have not been linked to eutrophication: warming, changes in ocean stratification circulation, and oxidation of methane hydrates have been invoked as causes for suboxia (Paelike et al., 2014). Site-specific reconstruction of paleoredox conditions at surface water and midwater depths cannot be performed using traditional proxies, unless full euxinia occurs within the photic zone and the organic biomarker isorenieretane can be used (Summons and Powell, 1987; Koopmans et al., 1996).

We use the novel proxy I/Ca in the first attempt to reconstruct paleo-oxygenation levels in the upper ocean (Lu et al., 2010; Hardisty et al., 2014). The I/Ca in marine bulk carbonate is sensitive to relatively subtle redox changes. We use I/Ca in bulk coarse fraction carbonate (dominantly planktonic foraminifera) and in monogeneric planktonic foraminiferal tests to investigate potential changes in the oxygenation state of mixed-layer and thermocline ocean waters during the PETM. Deriving a fully quantitative relationship between dissolved oxygen and foraminiferal I/Ca is beyond the scope of this work, because there are currently no cultivation studies of planktonic foraminifera and no core top I/Ca studies paired with water column iodine speciation analyses for the modern ocean. Therefore, our inferences from I/Ca remain qualitative. Our main goal is to test the potential of I/Ca in foraminifera as a paleoceanographic proxy for oxygenation changes at multiple open ocean locations. We assess various factors that might complicate the use of this proxy and demonstrate the potential of I/Ca to reflect past deoxygenation through agreement with model simulations of oxygenation levels (Winguth et al., 2012).

2. Iodine in Seawater and Foraminifera

2.1. Marine Chemistry of Iodine

The I/Ca proxy is based on knowledge of iodine speciation in the modern oceans. In modern seawater, the total iodine content, the sum of iodate and iodide concentrations, is invariant at around $0.45 \mu\text{mol/L}$ (Kuepper et al., 2011). In the upper ocean, the iodate concentration is inversely correlated to the iodide concentration. Iodate as a micronutrient is used by marine organisms (Kuepper et al., 2011). High primary productivity and decomposition of organic matter may cause up to ~50% iodate loss in surface ocean waters, and iodide production deeper in the water column, as observed at many locations including Hawaii and Bermuda (Campos et al., 1996), the Weddell Sea (Campos et al., 1999; Bluhm et al., 2011), the Mediterranean Sea (Tian et al., 1996), the Arabian Sea (Farrenkopf and Luther, 2002), and Antarctic coastal waters (Chance et al., 2010).

In addition to the biologic uptake/release, iodine speciation is also strongly affected by redox conditions. Under hypoxic conditions, more than 75% of iodate is converted to iodide (Truesdale and Bailey, 2000), and iodide is the dominant species below the oxygenated surface water in anoxic basins (Wong and Brewer, 1977). Iodine occurs mostly as iodate in oxic bottom waters, and upwelling of oxygenated deep water may compensate for iodate reduction in surface waters (Truesdale and Bailey, 2002).

The vertical iodate concentration profile is thus influenced by productivity and the presence/absence of an oxygen minimum zone (OMZ). If there is no OMZ (Figure 1a), the iodate concentration increases downward from the mixed layer, where primary productivity occurs, to greater depths (Jickells et al., 1988). O_2 generally decreases with depth due to respiration, but iodate is not used as an oxidant before complete O_2 consumption, and its concentration increases to the wholeocean value. In contrast, when there is an OMZ at relatively

shallow levels (Figure 1b), the iodate concentration decreases from the mixed layer down to the upper OMZ (Smith et al., 1990). When the OMZ is located deeper in the water column (Figure 1c), the iodate concentration increases from the mixed layer downward, then decreases to zero in the OMZ (Rue et al., 1997).

2.2. Water Column Depth Gradient in Planktonic Foraminiferal I/Ca

Primary productivity and oxygen levels act as first-order controls on the iodate concentration in ocean waters; thus, they should be the dominant control of I/Ca in planktonic foraminiferal tests. We thus expect I/Ca to be lower in mixed-layer dwelling planktonic foraminifera at higher productivity (Figure 1a). Oxygen levels are generally positively correlated to seawater iodate concentrations, thus I/Ca in foraminifera. The development of OMZs, particularly the shallow ones, should cause an overall decrease in planktonic foraminiferal I/Ca, with lower values in thermocline calcifiers (D) than in mixed-layer calcifiers (M) (Figure 1).

Changes in I/Ca can be anticipated for simple scenarios in which productivity and oxygen levels vary simultaneously. A combination of increased productivity and deoxygenation should lead to sharply lower I/Ca in planktonic foraminifera, with these two factors working in the same direction. In contrast, the net effect of decreased productivity and deoxygenation (as potentially caused by increased ocean stratification) depends on the relative magnitude of the changes, because they have opposite effects. Changes in I/Ca in mixed-layer (M) compared to I/Ca in deep-dwelling (D) planktonic foraminifera thus reflect changes in the iodate depth gradient, related to productivity and the vertical extent of OMZs (Figure 1).

3. Methods

3.1. Samples, Sites, and Age Models

We used bulk coarse fraction samples (BCF, >63 μm) and single genus planktonic foraminiferal tests, targeting the redox conditions above and within the thermocline, broadly named upper ocean waters. The BCF consists dominantly of planktonic foraminiferal tests calcified in upper ocean waters (Ezard et al., 2011). We picked three planktonic genera, mixed-layer calcifiers *Acarinina* spp. and *Morozovella* spp. (M), and deep calcifier *Subbotina* spp. (D) (Ezard et al., 2011), and calculated the difference in I/Ca between D and M (D-M). For some pre-CIE (carbon isotope excursion) samples from Sites 1262 and 865, we sieved BCF samples in eight size fractions from 63 to >250 μm and analyzed these separately for I/Ca.

We focused on well-studied open ocean sites in the Pacific (Site 865), Southeast Atlantic Walvis Ridge (Sites 1262 and 1263), Southern Ocean Weddell Sea (Site 690), and Indian Ocean (Site 738) (Figure 2). A few samples from Site 762 (Indian Ocean) were analyzed to compare with modeled productivity. Age models are based on correlation through carbon isotope records (Zachos et al., 2005), with numerical ages relative to the base of the carbon isotope excursion (CIE) during the PETM for Sites 690, 1262, and 1263 as in Röhl et al. (2007), for Site 738 as in Larrasoana et al. (2012), and for Site 865 as in Penman et al. (2014). The age model for Site 762 is poorly constrained and is based on the bulk stable isotope record in Thomas et al. (1992). To constrain background I/Ca, we extended the records to 1–2 Myr into the Paleocene before the onset of the carbon isotope excursion (CIE).

3.2. Cleaning Procedures

For each sample, 3–5 mg of coarse fraction material was weighed, crushed, and rinsed with deionized water to remove residual pore water before dissolution and not further cleaned by

oxidative or reductive reagents. The single genus planktonic tests were picked and then cleaned using the procedure following the Mg/Ca protocol (Barker et al., 2003). The shells were gently crushed between two clean glass slides to open the chambers. After clay removal in an ultrasonic water bath, NaOH-buffered H₂O₂ solutions were added to the samples, which were then heated in boiling water for 20 min. Carbonate materials were then thoroughly rinsed. We did not use reductive cleaning, because contribution of iodine from Mn oxides is negligible (see below).

3.3. Inductively Coupled Plasma Mass Spectrometry Measurements

I/Ca was measured on a quadrupole inductively coupled plasma mass spectrometry (Bruker M90) at Syracuse University. After cleaning, carbonate samples were dissolved in 3% nitric acid and diluted to form solutions with ~50 ppm Ca for analyses. Fresh calibration standards, matching the sample matrix, were prepared for every batch of samples. The sensitivity of iodine is tuned to about 80–120 kHz for 1 ppb standard, and the standard deviation for three blanks in a row is ~0.3 kHz. The precision of ¹²⁷I is typically better than 1% and is not reported separately for each sample. The long-term accuracy is guaranteed by frequent repeats of the reference material JCp-1 (Lu et al., 2010). The detection limit of I/Ca is typically below 0.1 μmol/mol.

3.4. Partial Dissolution, Mn Oxide Coatings, and Temperature

To test the potential influence of postdepositional partial dissolution of shell carbonate on I/Ca, 200–250 tests of *Acarinina* spp. and *Morozovella* spp. were picked from Paleocene samples. They were crushed, homogenized, and divided into six subsamples. Two were not acidified, and the others were soaked in 0.1ml of 0.08 N HNO₃ for 3 min, repeated up to 4 times.

After partial dissolution, the tests were cleaned as normal samples and dissolved for measurement.

To evaluate potential contamination of I from Mn oxides, we determined the temporal trend in I/Ca after reductive cleaning (Boyle and Keigwin, 1985) in six coarse fraction samples from between 100 and 150 kyr after the onset of the CIE at Site 1262; 2–4mg of micronodules were separated from carbonate material by picking then treated the same as bulk coarse fraction samples for detecting any oxides associated iodine signal.

To evaluate temperature dependence of the iodate partition coefficient, calcite crystals were synthesized in deionized water by mixing CaCl_2 and Na_2CO_3 solutions at three different temperatures (6, 19, and 33 °C). Crystals grew in a refrigerated or heated water bath over a period of 2 weeks, reaching a size of ~0.3 mm. The calcite was thoroughly rinsed before dissolution for I/Ca analysis.

4. Results

The general patterns in BCF and single genus records are similar at Sites 865 and 690 (Figure 3), although I/Ca values are higher at Site 865 throughout the records. At both sites, the I/Ca values in deep-dwelling planktonic foraminifera (D) are higher than those in mixed-layer dwelling foraminifera, resulting in D-M values that are generally >0 (Figure 4), increasing during the PETM. At both sites, the I/Ca in monogeneric records dropped at the start of the CIE. At Site 865, the BCF record also shows a decrease; at Site 690 such a decrease may exist, but our data do not cover the peak CIE. At this site, two samples in the peak PETM (<25 kyr) show a much larger decline in I/Ca in M than in D so that the D-M reaches a maximum (~2 $\mu\text{mol/mol}$, Figure 4).

At Site 1262, the BCF and monogeneric I/Ca values are even higher than at Site 865 and decrease during the CIE (Figure 3). At this site, however, there are no clear and consistent offsets between I/Ca in D and M, and D-M is generally negative, with a few positive points ~100 kyr after the start of the CIE (Figure 4). In the Paleocene, I/Ca values in BCF are significantly higher than those in all monogeneric records. In two Paleocene samples from Site 1262, the I/Ca values of the <125 μm size fraction are considerably higher than those in larger size fractions (Figure 5), in contrast to a coeval sample from Site 865, where values do not change with size. Site 1262 was at a paleodepth of ~3400m (Zachos et al., 2005), i.e., close to the carbonate compensation depth and possibly below the lysocline at that time, and carbonate dissolution (even before the PETM) could have led to preferential dissolution of planktonic over benthic foraminifera (Nguyen et al., 2009). Visual inspection of these samples showed that benthic foraminifera are indeed dominant in the smaller size fractions. Iodate in oxic bottom waters is much higher than in surface waters (Figure 1), and these high values in BCF as compared to the monogeneric planktonic records reflect the common presence of benthic foraminifera in BCF at Site 1262 (Figure 3).

At Site 1263, close to Site 1262 but at a paleodepth of ~1500m (Zachos et al., 2005), the BCF record shows large, random fluctuations during the PETM, possibly also due to preferential dissolution of planktonic foraminifera and a higher benthic/planktonic ratio in BCF. Overall, the values of monogeneric M (*Morozovella* spp.) were higher than those of D (*Subbotina* spp.), leading to overall negative D-M (Figure 4), with the exception of a few positive data points, coeval with those at Site 1262, ~100 kyr after the onset of the CIE. D-M may have decreased at the onset of the CIE.

The record at Site 738 is similar to that at Site 1263, with large fluctuations in the I/Ca in the BCF record during the PETM. At this site, however, there is no clear, consistent offset between D and M I/Ca values, and the monogeneric records show a decrease in I/Ca during the PETM. D-M values fluctuate and are relatively higher in the Paleocene and relatively lower within about 100 kyr after the onset of the CIE.

The effects of dissolution and Mn oxide coatings on I/Ca signal are found to be minimal and are not further discussed. The partition coefficient of iodate decreases at higher temperatures for the synthetic calcite. The potential contribution of PETM warming to I/Ca changes in the records are estimated using the synthetic calcite data, and experimental results are shown in the supporting information.

5. Discussion

5.1. Pre-PETM Productivity Versus I/Ca

The Paleocene I/Ca values in the monogeneric records differ substantially between sites (Figure 3), with values at Sites 690, 1263, and 738 generally lower (values 2–4 $\mu\text{mol/mol}$) and Sites 865 and 1262 higher (6–8, Figure 3). We expect planktonic I/Ca to reflect paleoproductivity when there is no overriding effect of oxygenation levels, with lower I/Ca at higher productivity (Chance et al., 2010) (Figure 1a). In order to test whether the differences in I/Ca in our planktonic foraminiferal tests from different sites could be related to differences in productivity, we compared the average I/Ca in mixed-layer planktonic (*Acarinina* spp.) with the export productivity modeled for these sites in Community Climate System Model Version 3 (CCSM3) (Winguth et al., 2012) (Figures 2 and 6). The patterns in Paleocene modeled productivity generally resemble present-day patterns of export production (Doney et al., 2006).

The modeled productivity and I/Ca in planktonic foraminifera are negatively correlated as predicted (Figure 6). Modeling and the I/Ca data indicate that Sites 1262 and 865 had relatively low productivity compared to Sites 690, 738, and 762. Microfossil evidence agrees with the hypothesis that productivity was lower at Site 865 than at Site 690 (Bralower et al., 1995). Site 762 (Indian Ocean) had somewhat higher productivity than at Sites 738 (Indian Ocean) and 690 (Weddell Sea). Productivity thus may have been one of the dominant controls on iodate concentrations in the upper oceans during the Paleocene, as in modern oceans.

5.2. Productivity Changes During the PETM

Because productivity and oxygenation changes are often intertwined, the interpretation of I/Ca as a paleoredox signal requires a thorough review of productivity changes during the PETM. It is not clear how primary and export production in the open ocean changed during the PETM, and changes may not have been globally uniform (Winguth et al., 2012). At many sites, there is conflicting evidence on productivity, e.g., decreasing productivity inferred from nannofossil assemblages at Weddell Sea Site 690 (Bralower, 2002), but potentially short-term increasing productivity from Sr/Ca in nannofossils at the same site (Stoll et al., 2007).

On a global scale, primary productivity may have decreased in vast open ocean areas (Gibbs et al., 2006; Paytan et al., 2007; Thomas, 2007; Winguth et al., 2012; Norris et al., 2013) and remained close to be constant in other regions (Stoll et al., 2007; Gibbs et al., 2010). The trophic resource continuum may have expanded so that globally more extreme oligotrophic as well as eutrophic conditions occurred (Hallock, 1987; Boersma et al., 1998).

5.3. PETM Open Ocean Deoxygenation

Records from the open ocean Pacific (865), Weddell Sea (690), SE Atlantic (1262 and 1263), and Indian (738) sites, although not yet at high resolution, generally show decreased I/Ca in monogeneric mixed-layer and thermocline dwelling planktonic foraminiferal records over the CIE (Figure 3), with minimum values around the peak CIE. Such a decrease in I/Ca likely indicates widespread deoxygenation in the upper ocean, since neither microfossil records (Kelly et al., 1996; Bralower, 2002; Gibbs et al., 2006) nor modeling (Winguth et al., 2012) support widespread increased pelagic productivity during the PETM. The decrease in I/Ca at Site 690 is very large, dropping to values of $\sim 1 \mu\text{mol/mol}$ (Figure 3) and probably cannot be explained by productivity spikes as indicated by barite accumulation rates (Ma et al., 2014) (Figure 6). Data on magnetotactic bacteria suggest Fe dust-induced increased productivity at Site 738 (Larrasoana et al., 2012), but there is only one data point for the barite proxy (Ma et al., 2014). Productivity declined at nearby Site 1135 according to nanofossil evidence (Jiang and Wise, 2009).

The I/Ca decrease at Site 865 is relatively small, which may be explained by increased productivity instead of deoxygenation, but microfossil evidence strongly indicates a decrease in productivity (Kelly et al., 1996; Kelly, 2002). There is some evidence for increased productivity during the PETM at Site 690 (Stoll and Bains, 2003), but this is controversial (Bralower et al., 2004; Stoll et al., 2007). Barite accumulation rates somewhat increased at several Pacific Sites but that might indicate increased remineralization and not increased primary productivity (Ma et al., 2014). Therefore, we suggest that Site 865 went through mild deoxygenation during the PETM, a condition possibly typical for oligotrophic parts of the Pacific Ocean.

We thus interpret the observed general decrease in I/Ca at the onset of the PETM as most probably indicative of widespread deoxygenation in the upper ocean waters. Ocean stratification induced by warming may be the mechanism for lowering oxygen levels (Norris et al., 2013), and

the elevated respiration rates at higher temperatures may also play a role (John et al., 2013). The deoxygenation likely was stronger in the Atlantic and Indian Oceans than in the Pacific Ocean in agreement with geochemical evidence (Paelike et al., 2014), possibly due to increased stratification.

5.4. Iodate Gradients and OMZs

We next use the difference in I/Ca values of deep dwellers and mixed-layer dwellers (D-M) to reconstruct iodate gradients and detect whether an OMZ was present and then compare the results with dissolved oxygen profiles modeled with CCSM3 at 4xCO₂ (Figures 1, 4, and 7) (Winguth et al., 2012). The average D-M through the studied interval is positively correlated with the minimum oxygen levels in the water column estimated from the model (insert in Figure 7). Qualitatively, the ranking of oxygen levels among these sites is comparable in proxy data versus model output, although absolute values of dissolved oxygen cannot be derived until the proxy is quantitatively calibrated.

Sites 865 and 690 have predominantly positive D-M values before, during, and after the PETM, indicating that no strong OMZ was present or it was deep (Figure 1c). We argued above that deoxygenation occurred at Sites 690 and 865 during the PETM, especially for the very low I/Ca at Site 690, but the D-M values remained positive at both sites. This could be explained through comparison with the iodate profile in modern OMZs (Figures 1a and 1c). The iodate concentrations may increase from the surface to near the upper boundary of the OMZ, then drop rapidly to zero within the OMZ (Rue et al., 1997). If Sites 690 and 865 had normal open ocean iodate profiles in the Paleocene and then switched to OMZ-type iodate profiles during the PETM, I/Ca of both deep (D) and mixed-layer (M) genera would have decreased while

maintaining positive D-M values, as long as the deeper dwellers lived above the iodate reversal around the upper boundary of OMZ.

Monogeneric records show declining I/Ca at the onset of the PETM at Site 738. D-M values varied around zero due to the lack of a clear difference between D and M values. Potentially, an OMZ was present throughout the studied interval. The OMZ might have been deeper before the PETM, corresponding to mostly positive D-M values, and then shoaled across the onset of the PETM as indicated by a change to largely negative D-M values (Figure 4).

Sites 1262 and 1263, on a depth transect along Walvis Ridge, have negative D-M values in most samples, indicative of OMZ presence throughout the studied interval. Exceptions are a few positive values at about 125 kyr after the onset of the CIE at both sites (Figure 4). Bulk sediment Mn and U enrichment factors indicate that bottom waters at Site 1263 (paleodepth 1500 m) were suboxic before, during, and after the PETM, whereas Site 1262 (3400 m) developed suboxic bottom water conditions during the event (Chun et al., 2010).

The pre-PETM planktonic I/Ca values at Site 1263 (2–3 $\mu\text{mol/mol}$) are much lower than those at the deeper Site 1262 (~ 6 $\mu\text{mol/mol}$) (Figure 3), although the sites were geographically close, so that there probably was no large difference in productivity. Surface water iodate concentrations ranging from 0.05 to 0.35 μM were reported within a small region during a modern hypoxic event in the southern Benguela system (Truesdale and Bailey, 2000). Although the oceanographic setting for Walvis Ridge is not identical to the setting for this modern event, highly dynamic I/Ca spatial variability in nearby sites is not impossible.

The difference in I/Ca is thus probably caused by the presence of a shallow OMZ over Site 1263 throughout the studied period, as supported by the low I/Ca values, the negative D-M values, and the modeling results (Figures 3, 4, and 7). The D-M values at Site 1263 dropped

rapidly before the onset of CIE and then increased gradually in the first 100 kyr of the event. This trend is mainly driven by the changes in I/Ca values of the deep dwellers and not the relatively stable I/Ca values in the mixed-layer genera (Figure 3). The period of intensified deoxygenation, as indicated by lower I/Ca, appears to have been relatively short (<100 kyr) at 1263, as compared to other open ocean sites (Figure 3).

A possible scenario at Site 1263 is that the upper ocean iodate concentration was lowered by the shoaling of an OMZ during the PETM and that migration of *Subbotina* spp. could not compensate for the iodate gradient change. We thus conclude that the OMZ in the Walvis Ridge region (Site 1263) may have expanded vertically, both upward and downward, as indicated by I/Ca and Mn data (Chun et al., 2010).

The upward extension of OMZs might have been widespread, influencing pelagic ecosystems (John et al., 2013). Such a trajectory was predicted for the future (Stramma et al., 2012), contributing to the different composition of pelagic ecosystems during Greenhouse climates (Norris et al., 2013). A vertical compression of the zone above the OMZ thus may also have been one of the drivers for the observed changes in planktonic foraminiferal assemblages during hyperthermal events, commonly attributed to changes in ocean stratification (Kelly et al., 1998; Kelly, 2002; Petrizzo, 2007; Stap et al., 2010). In addition, the enrichment in fish debris in sediment above the base of the CIE at Shatsky Rise sites (Colosimo et al., 2006) could reflect a mortality event due to expansion of the OMZ, rather than due to carbonate dissolution, with % fish debris not precisely correlated with %CaCO₃.

Methane oxidation was proposed as one of the major causes of low-oxygen conditions at intermediate depth such as the New Zealand margin (Nicolo et al., 2010). This current data set does not shed new light on a potential role of methane as a cause of ocean deoxygenation during

the PETM, because we focus on the open ocean conditions rather than on continental margin locations. The rapid release of methane and other hydrocarbon during the Deepwater Horizon oil spill in the Gulf of Mexico in 2010 did result in minor O₂ depletion, but the low-O₂ anomaly did not propagate to the upper ocean (Kessler et al., 2011). This event differs from the PETM in many aspects but could be seen as indicative that the upper water column in open ocean settings could escape deoxygenation related to methane oxidation. The observation that deoxygenation may have been more severe in Atlantic and Indian Oceans, however, might suggest that hydrate dissociation could have been a causal factor in these more enclosed basins, but not in the much larger Pacific Ocean.

5.5. Shell Recrystallization

Planktonic foraminifera in carbonate-rich pelagic sections usually undergo recrystallization within the upper sediment column. Pore waters deeper than a few centimeters below seafloor do not contain iodate but only contain iodide (Kennedy and Elderfield, 1987) which cannot be incorporated in the carbonate structure (Lu et al., 2010). Recrystallization in pore waters thus would lower the I/Ca values. We argue that such diagenetic loss of carbonate iodate probably would not interfere with the observed trends. Recrystallization typically is less important in benthic and deep-dwelling planktonics than in mixed-layer species. If recrystallization had impacted the I/Ca records, the D-M values would have increased, incorrectly indicating oxygenated water masses. Specifically, relatively low I/Ca values combined with positive D-M values would be suspicious. The two data points at Site 690 very close to the onset of CIE may be an example, although 690 is generally considered to have well-preserved tests. Recrystallization is known for Site 865 (Kozdon et al., 2013), but the I/Ca values

are the highest among all sites, indicating that the proxy may not be very susceptible to diagenetic alteration.

5.6. Depth Habitat

The discussions about I/Ca and D-M values are based on the assumption that there was no major shift in habitat of planktonic foraminifera. This assumption may not hold for PETM, given the warming and increased stratification. Specifically, Kelly et al. (1996, 1998, 2005) describe significant changes in the foraminifer assemblages at Sites 865 and 690, including the appearance of warm water taxa such as *Morozovella* at high latitudes, and shifts in the relative abundances of species of *Acarinina*. The mixed-layer genera, taxa, however, contain photosymbionts and thus would not be expected to migrate below the zone where light penetrates, thus keeping a vertical distance from the thermocline calcifiers (see also discussion in Penman et al. (2014)). The deep-dwellers could have adjusted to warming by migrating to deeper levels, whereas the expansion of OMZ likely limited such downward migration. Indeed, an abrupt decrease in abundance or absence of the deep-dwelling *Subbotina* during the peak CIE is observed at many localities (Kelly et al., 1998; Arenillas et al., 1999; Kelly et al., 2005; Luciani et al., 2007; Petrizzo, 2007) and thus might have been caused by loss of deeper habitat space. At this moment we cannot evaluate the influence of habitat change on the interpretation of I/Ca records in detail, especially the temporal trends in D-M values. Higher-resolution records combined with faunal assemblage analyses are needed to fully evaluate this topic and could provide new light on the question of planktonic depth migration during climate change.

5.7. Symbiont Bearing Planktonic Foraminifera

Active photosymbionts could increase the iodate concentration in the direct microenvironment of calcification of the test, but we do not have information on the magnitude of such an effect from culture studies. A potential loss of photosymbionts, as argued for the Middle Eocene Climate Optimum (Edgar et al., 2013), could have caused a decline in I/Ca in species that carried photosymbionts. If that had been the only cause of the I/Ca decline at the onset of the PETM, the decline would have been seen in mixed-layer dwellers only, in contrast to observations (Figure 3). At Site 690, the decline in I/Ca in M species was somewhat larger than that in D species (Figure 3), so a loss of photosymbionts might have contributed to the I/Ca decline, specifically for the two samples with maximum D-M (Figure 4).

5.8. Whole-Ocean Change in Iodine

The decline in I/Ca could potentially have been caused by a decline in total iodine concentration in seawater, but there is no evidence for globally high organic burial rates (Paytan et al., 2007), which would be the main sink for iodine. The iodine content of foraminifera from organic-rich sections across the PETM, however, should be investigated to further constrain the burial flux. The pore water iodine concentration is typically up to 3 orders of magnitude higher than the seawater iodine concentration in modern methane hydrate fields (Lu et al., 2008), and the destabilization of hydrate might have released sedimentary pore water iodine into the ocean, slightly increasing (rather than decreasing) the total iodine concentration in seawater. If this had occurred, we would have underestimated the degree of deoxygenation.

6. Conclusions

Our records demonstrate that foraminiferal I/Ca may be a useful paleoceanographic proxy for changes in oxygenation in the upper ocean, tracing the horizontal and vertical extent of OMZs. The difference between the I/Ca of mixed-layer and deeper-dwelling planktonic foraminifera can provide insight into the evolution of the OMZ at a site, and our I/Ca records demonstrate that OMZs expanded during the PETM. This proxy thus has promise for reconstructing paleodeoxygenation at various depths in the water column under oxic/suboxic conditions, complementing the use of bulk sediment proxies (e.g., Mn and Mo) and organic biomarkers (e.g., isorenieretane) for anoxic/euxinic conditions.

Acknowledgments

This work is supported by NSF OCE 1232620 to Lu and NSF OCE 1232413 to Thomas. Thomas and Rickaby also thank the Leverhulme Trust (UK). All model simulations were done on NCAR computers, supported by NSF. Data can be found in the supporting information. Two anonymous reviewers helped to improve the manuscript greatly.

References

- Akhmet'ev, M. A., N. I. Zaporozhets, A. I. Iakovleva, G. N. Aleksandrova, V. N. Beniamovsky, T. V. Oreshkina, Z. N. Gnibidenko, and Z. A. Dolya (2010), Comparative analysis of marine paleogene sections and biota from West Siberia and the Arctic Region, *Stratigr. Geol. Correl.*, 18(6), 635–659.
- Alegret, L., S. Ortiz, and E. Molina (2009), Extinction and recovery of benthic foraminifera across the Paleocene-Eocene Thermal Maximum at the Alamedilla section (Southern Spain), *Palaeogeogr. Palaeoclimatol. Palaeoecol.*, 279(3-4), 186–200.
- Alegret, L., S. Ortiz, I. Arenillas, and E. Molina (2010), What happens when the ocean is overheated? The foraminiferal response across the Paleocene-Eocene Thermal Maximum at the Alamedilla section (Spain), *Geol. Soc. Am. Bull.*, 122(9-10), 1616–1624.
- Algeo, T. J., and T. W. Lyons (2006), Mo-total organic carbon covariation in modern anoxic marine environments: Implications for analysis of paleoredox and paleohydrographic conditions, *Paleoceanography*, 21, PA1016, doi:10.1029/2004PA001112.
- Anbar, A. D., and G. W. Gordon (2008), Redox renaissance, *Geology*, 36(3), 271–272.
- Arenillas, I., E. Molina, and B. Schmitz (1999), Planktic foraminiferal and ^{13}C isotopic changes across the Paleocene/ Eocene boundary at Possagno (Italy), *Int. J. Earth Sci.*, 88(2), 352–364.
- Bains, S., R. M. Corfield, and R. D. Norris (1999), Mechanisms of climate warming at the end of the Paleocene, *Science*, 285 (2048), 724–727.
- Barker, S., M. Greaves, and H. Elderfield (2003), A study of cleaning procedures used for foraminiferal Mg/Ca paleothermometry, *Geochem. Geophys. Geosyst.*, 4(9), 8407, doi:10.1029/2003GC000559.

- Bluhm, K., P. L. Croot, O. Huhn, G. Rohardt, and K. Lochte (2011), Distribution of iodide and iodate in the Atlantic sector of the southern ocean during austral summer, *Deep Sea Res., Part II*, 58(25-26), 2733–2748.
- Boersma, A., I. Premoli-Silva, and P. Hallock (1998), *Trophic Models for the Well-Mixed Warm Oceans Across the Paleocene/Eocene Epoch Boundary*, Columbia Univ. Press, New York.
- Bograd, S. J., C. G. Castro, E. Di Lorenzo, D. M. Palacios, H. Bailey, W. Gilly, and F. P. Chavez (2008), Oxygen declines and the shoaling of the hypoxic boundary in the California Current, *Geophys. Res. Lett.*, 35, L12607, doi:10.1029/2008GL034185.
- Boyle, E. A., and L. D. Keigwin (1985), Comparison of Atlantic and Pacific paleochemical records for the last 215,000 years—Changes in deep ocean circulation and chemical inventories, *Earth Planet. Sci. Lett.*, 76(1-2), 135–150.
- Bralower, T. J. (2002), Evidence of surface water oligotrophy during the Paleocene-Eocene thermal maximum: Nannofossil assemblage data from Ocean Drilling Program Site 690, Maud Rise, Weddell Sea, *Paleoceanography*, 17(2), 1023, doi:10.1029/2001PA000662.
- Bralower, T. J., J. C. Zachos, E. Thomas, M. Parrow, C. K. Paull, D. C. Kelly, I. P. Silva, W. V. Sliter, and K. C. Lohmann (1995), Late Paleocene to Eocene paleoceanography of the equatorial Pacific Ocean—Stable isotopes recorded at Ocean Drilling Program Site-865, Allison Guyot, *Paleoceanography*, 10(4), 841–865, doi:10.1029/95PA01143.
- Bralower, T. J., D. C. Kelly, and D. J. Thomas (2004), Comment on "Coccolith Sr/Ca records of productivity during the Paleocene-Eocene thermal maximum from the Weddell Sea" by Heather M. Stoll and Santo Bains, *Paleoceanography*, 19, PA1014, doi:10.1029/2003PA000953.

- Campos, M., A. M. Farrenkopf, T. D. Jickells, and G. W. Luther (1996), A comparison of dissolved iodine cycling at the Bermuda Atlantic time-series station and Hawaii Ocean time-series station, *Deep Sea Res., Part II*, 43(2-3), 455–466.
- Campos, M., R. Sanders, and T. Jickells (1999), The dissolved iodate and iodide distribution in the South Atlantic from the Weddell Sea to Brazil, *Mar. Chem.*, 65(3-4), 167–175.
- Chance, R., et al. (2010), Seasonal and interannual variation of dissolved iodine speciation at a coastal Antarctic site, *Mar. Chem.*, 118(3–4), 171–181.
- Chun, C. O. J., M. L. Delaney, and J. C. Zachos (2010), Paleoredox changes across the Paleocene-Eocene thermal maximum, Walvis Ridge (ODP Sites 1262, 1263, and 1266): Evidence from Mn and U enrichment factors, *Paleoceanography*, 25, PA4202, doi:10.1029/2009PA001861.
- Colosimo, A. B., T. J. Bralower, and J. C. Zachos (2006), Evidence for lysocline shoaling at the Paleocene/Eocene Thermal Maximum on Shatsky Rise, Northwest Pacific, in *Proc. Ocean Drill. Program Part B Sci. Results*, vol. 198, edited by T. J. Bralower, I. Premoli Silva, and M. J. Malone, pp. 1–36, College Station, Tex., doi:10.2973/odp.proc.sr.198.112.2006.
- Dickson, A. J., A. S. Cohen, and A. L. Coe (2012), Seawater oxygenation during the Paleocene-Eocene Thermal Maximum, *Geology*, 40(7), 639–642.
- Dickson, A. J., R. L. Rees-Owen, C. März, A. L. Coe, A. S. Cohen, R. D. Pancost, K. Taylor, and E. Shcherbinina (2014), The spread of marine anoxia on the northern Tethys margin during the Paleocene-Eocene Thermal Maximum, *Paleoceanography*, 29, 471–488, doi:10.1002/2014PA002629.

- Doney, S. C., K. Lindsay, I. Fung, and J. John (2006), Natural variability in a stable, 1000-yr global coupled climate-carbon cycle simulation, *J. Clim.*, 19(13), 3033–3054.
- Dunkley Jones, T., D. J. Lunt, D. N. Schmidt, A. Ridgwell, A. Sluijs, P. J. Valdes, and M. Maslin (2013), Climate model and proxy data constraints on ocean warming across the Paleocene–Eocene Thermal Maximum, *Earth Sci. Rev.*, 125, 123–145.
- Edgar, K. M., S. M. Bohaty, S. J. Gibbs, P. F. Sexton, R. D. Norris, and P. A. Wilson (2013), Symbiont 'bleaching' in planktonic foraminifera during the Middle Eocene Climatic Optimum, *Geology*, 41(1), 15–18.
- Ezard, T. H. G., T. Aze, P. N. Pearson, and A. Purvis (2011), Interplay between changing climate and species' ecology drives macroevolutionary dynamics, *Science*, 332(6027), 349–351.
- Falkowski, P. G., et al. (2011), Ocean deoxygenation: Past, present and future, *Eos Trans. AGU*, 92, 409–410, doi:10.1029/2011EO460001.
- Farrenkopf, A. M., and G. W. Luther (2002), Iodine chemistry reflects productivity and denitrification in the Arabian Sea: Evidence for flux of dissolved species from sediments of western India into the OMZ, *Deep Sea Res., Part II*, 49(12), 2303–2318.
- Gavrilov, Y. O., L. A. Kodina, I. Y. Lubchenko, and N. G. Muzylev (1997), The late Paleocene anoxic event in epicontinental seas of peri-Tethys and formation of the sapropelite unit: Sedimentology and geochemistry, *Lithol. Min. Resour.*, 32(5), 427–450.
- Gibbs, S. J., T. J. Bralower, P. R. Bown, J. C. Zachos, and L. M. Bybell (2006), Shelf and open-ocean calcareous phytoplankton assemblages across the Paleocene-Eocene Thermal Maximum: Implications for global productivity gradients, *Geology*, 34(4), 233–236.

- Gibbs, S. J., H. M. Stoll, P. R. Bown, and T. J. Bralower (2010), Ocean acidification and surface water carbonate production across the Paleocene-Eocene thermal maximum, *Earth Planet. Sci. Lett.*, 295(3-4), 583–592.
- Gilly, W. F., J. M. Beman, S. Y. Litvin, and B. H. Robison (2013), Oceanographic and biological effects of shoaling of the oxygen minimum zone, in *Annual Review of Marine Science*, vol. 5, edited by C. A. Carlson and S. J. Giovannoni, pp. 393–420, Annual Reviews, Palo Alto, Calif.
- Gooday, A. J., B. J. Bett, E. Escobar, B. Ingole, L. A. Levin, C. Neira, A. V. Raman, and J. Sellanes (2010), Habitat heterogeneity and its influence on benthic biodiversity in oxygen minimum zones, *Mar. Ecol.*, 31(1), 125–147.
- Hallock, P. (1987), Fluctuations in the trophic resource continuum: A factor in global diversity cycles?, *Paleoceanography*, 2(5), 457–471, doi:10.1029/PA002i005p00457.
- Hardisty, D. S., Z. Lu, N. Planavsky, A. Bekker, P. Philippot, X. Zhou, and T. W. Lyons (2014), An iodine record of Paleoproterozoic surface ocean oxygenation, *Geology*, doi:10.1130/G35439.1.
- Helm, K. P., N. L. Bindoff, and J. A. Church (2011), Observed decreases in oxygen content of the global ocean, *Geophys. Res. Lett.*, 38, L23602, doi:10.1029/2011GL049513.
- Hoenisch, B., et al. (2012), The geological record of ocean acidification, *Science*, 335(6072), 1058–1063.
- Jenkyns, H. C. (2010), Geochemistry of oceanic anoxic events, *Geochem. Geophys. Geosyst.*, 11, Q03004, doi:10.1029/2009GC002788.
- Jiang, S. J., and S. W. Wise (2009), Distinguishing the influence of diagenesis on the paleoecological reconstruction of nanoplankton across the Paleocene/Eocene Thermal

- Maximum: An example from the Kerguelen Plateau, southern Indian Ocean, *Mar. Micropaleontol.*, 72(1–2), 49–59.
- Jickells, T. D., S. S. Boyd, and A. H. Knap (1988), Iodine cycling in the Sargasso Sea and the Bermuda inshore waters, *Mar. Chem.*, 24(1), 61–82.
- John, E. H., P. N. Pearson, H. K. Coxall, H. Birch, B. S. Wade, and G. L. Foster (2013), Warm ocean processes and carbon cycling in the Eocene, *Philos. Trans. R. Soc. A*, 371(2001), 20130099.
- Keeling, R. F., A. Kortzinger, and N. Gruber (2010), Ocean deoxygenation in a warming world, *Annu. Rev. Mar. Sci.*, 2, 199–229.
- Kelly, D. C. (2002), Response of Antarctic (ODP Site 690) planktonic foraminifera to the Paleocene-Eocene thermal maximum: Faunal evidence for ocean/climate change, *Paleoceanography*, 17(4), 1071, doi:10.1029/2002PA000761.
- Kelly, D. C., T. J. Bralower, J. C. Zachos, I. P. Silva, and E. Thomas (1996), Rapid diversification of planktonic foraminifera in the tropical Pacific (ODP Site 865) during the late Paleocene thermal maximum, *Geology*, 24(5), 423–426.
- Kelly, D. C., T. J. Bralower, and J. C. Zachos (1998), Evolutionary consequences of the latest Paleocene thermal maximum for tropical planktonic foraminifera, *Palaeogeogr. Palaeoclimatol. Palaeoecol.*, 141(1-2), 139–161.
- Kelly, D. C., J. C. Zachos, T. J. Bralower, and S. A. Schellenberg (2005), Enhanced terrestrial weathering/runoff and surface ocean carbonate production during the recovery stages of the Paleocene-Eocene Thermal Maximum, *Paleoceanography*, 20, PA4023, doi:10.1029/2005PA001163.

- Kennedy, H. A., and H. Elderfield (1987), Iodine diagenesis in pelagic deep-sea sediments, *Geochim. Cosmochim. Acta*, 51(9), 2489–2504.
- Kessler, J. D., et al. (2011), A persistent oxygen anomaly reveals the fate of spilled methane in the deep Gulf of Mexico, *Science*, 331(6015), 312–315.
- Koopmans, M. P., J. Koster, H. M. E. van Kaam Peters, F. Kenig, S. Schouten, W. A. Hartgers, J. W. de Leeuw, and J. S. S. Damste (1996), Diagenetic and catagenetic products of isorenieratene: Molecular indicators for photic zone anoxia, *Geochim. Cosmochim. Acta*, 60(22), 4467–4496.
- Kozdon, R., D. C. Kelly, K. Kitajima, A. Strickland, J. H. Fournelle, and J. W. Valley (2013), In situ delta O-18 and Mg/Ca analyses of diagenetic and planktonic foraminiferal calcite preserved in a deep-sea record of the Paleocene-Eocene thermal maximum, *Paleoceanography*, 28, 517–528, doi:10.1002/palo.20048.
- Kuepper, F. C., et al. (2011), Commemorating two centuries of iodine research: An interdisciplinary overview of current research, *Angew. Chem. Int. Ed.*, 50(49), 11,598–11,620.
- Larrasoana, J. C., A. P. Roberts, L. Chang, S. A. Schellenberg, J. FitzGerald, R. D. Norris, and J. C. Zachos (2012), Magnetotactic bacterial response to Antarctic dust supply during the Palaeocene-Eocene Thermal Maximum, *Earth Planet. Sci. Lett.*, 333–334, 122–133.
- Levin, L. A. (2003), Oxygen minimum zone benthos: Adaptation and community response to hypoxia, *Oceanogr. Mar. Biol.*, 41, 1–45.
- Lu, Z., C. Hensen, U. Fehn, and K. Wallmann (2008), Halogen and ¹²⁹I systematics in gas hydrate fields at the northern Cascadia margin (IODP Expedition 311): Insights from

- numerical modeling, *Geochem. Geophys. Geosyst.*, 9, Q10006,
doi:10.1029/2008GC002156.
- Lu, Z., H. C. Jenkyns, and R. E.M. Rickaby (2010), Iodine to calcium ratios in marine carbonate as a paleo-redox proxy during oceanic anoxic events, *Geology*, 38(12), 1107–1110.
- Luciani, V., L. Giusberti, C. Agnini, J. Backman, E. Fornaciari, and D. Rio (2007), The Paleocene-Eocene Thermal Maximum as recorded by Tethyan planktonic foraminifera in the Forada section (northern Italy), *Mar. Micropaleontol.*, 64(3–4), 189–214.
- Ma, Z., E. Gray, E. Thomas, B. Murphy, J. C. Zachos, and A. Paytan (2014), Carbon sequestration during the Paleocene Eocene Thermal Maximum by an efficient biological pump, *Nat. Geosci.*, 7, 382–388.
- McInerney, F. A., and S. L. Wing (2011), The Paleocene-Eocene Thermal Maximum: A perturbation of carbon cycle, climate, and biosphere with implications for the future, in *Annual Review of Earth and Planetary Sciences*, vol. 39, edited by R. Jeanloz and K. H. Freeman, pp. 489–516, Annual Reviews, Palo Alto, Calif.
- McNeil, D. H., M. G. Parsons, and J. Russel-Houston (2013), The Paleocene-Eocene thermal maximum in the Arctic Beaufort–Mackenzie Basin—Palynomorphs, carbon isotopes and benthic foraminiferal turnover, *Bull. Can. Pet. Geol.*, 61(2), 157–186.
- Moran, K., et al. (2006), The Cenozoic palaeoenvironment of the Arctic Ocean, *Nature*, 441(7093), 601–605.
- Nagy, J., D. Jargvoll, H. Dypvik, M. Jochmann, and L. Riber (2013), Environmental changes during the Paleocene-Eocene Thermal Maximum in Spitsbergen as reflected by benthic foraminifera, *Polar Res.*, 32, 19737.

- Nguyen, T.M. P., M. R. Petrizzo, and R. P. Speijer (2009), Experimental dissolution of a fossil foraminiferal assemblage (Paleocene-Eocene Thermal Maximum, Dababiya, Egypt): Implications for paleoenvironmental reconstructions, *Mar. Micropaleontol.*, 73(3-4), 241–258.
- Nicolo, M. J., G. R. Dickens, and C. J. Hollis (2010), South Pacific intermediate water oxygen depletion at the onset of the Paleocene-Eocene thermal maximum as depicted in New Zealand margin sections, *Paleoceanography*, 25, PA4210, doi:10.1029/2009PA001904.
- Norris, R. D., S. K. Turner, P.M. Hull, and A. Ridgwell (2013), Marine ecosystem responses to Cenozoic global change, *Science*, 341(6145), 492–498.
- Paelike, C., M. L. Delaney, and J. Zachos (2014), Deep-sea redox across the Paleocene-Eocene thermal maximum, *Geochem. Geophys. Geosyst.*, 15, 1038–1053, doi:10.1002/2013GC005074.
- Paytan, A., K. Averyt, K. Faul, E. Gray, and E. Thomas (2007), Barite accumulation, ocean productivity, and Sr/Ba in barite across the Paleocene-Eocene Thermal Maximum, *Geology*, 35(12), 1139–1142.
- Penman, D. E., B. Hönisch, R. E. Zeebe, E. Thomas, and J. C. Zachos (2014), Rapid and sustained surface ocean acidification during the Paleocene-Eocene Thermal Maximum, *Paleoceanography*, 29, 357–369, doi:10.1002/2014PA002621.
- Petrizzo, M. R. (2007), The onset of the Paleocene-Eocene Thermal Maximum (PETM) at Sites 1209 and 1210 (Shatsky Rise, Pacific Ocean) as recorded by planktonic foraminifera, *Mar. Micropaleontol.*, 63(3-4), 187–200.

- Ravizza, G., R. N. Norris, J. Blusztajn, and M. P. Aubry (2001), An osmium isotope excursion associated with the late Paleocene thermal maximum: Evidence of intensified chemical weathering, *Paleoceanography*, 16(2), 155–163, doi:10.1029/2000PA000541.
- Reid, P. C., et al. (2009), Impacts of the oceans on climate change, in *Advances in Marine Biology*, vol. 56, edited by D. W. Sims, pp. 1–150, Elsevier Acad. Press Inc., San Diego, Calif.
- Röhl, U., T. Westerhold, T. J. Bralower, and J. C. Zachos (2007), On the duration of the Paleocene-Eocene thermal maximum (PETM), *Geochem. Geophys. Geosyst.*, 8, Q12002, doi:10.1029/2007GC001784.
- Rue, E. L., G. J. Smith, G. A. Cutter, and K. W. Bruland (1997), The response of trace element redox couples to suboxic conditions in the water column, *Deep Sea Res., Part I*, 44(1), 113–134.
- Sluijs, A., et al. (2006), Subtropical arctic ocean temperatures during the Palaeocene/Eocene thermal maximum, *Nature*, 441(7093), 610–613.
- Smith, J. D., E. C. V. Butler, D. Airey, and G. Sandars (1990), Chemical-properties of a low-oxygen water column in port-hacking (Australia)—Arsenic, iodine and nutrients, *Mar. Chem.*, 28(4), 353–364.
- Speijer, R. P., and T. Wagner (2002), Sea-level changes and black shales associated with the late Paleocene thermal maximum (LPTM): Organic geochemical and micropaleontologic evidence from the southern Tethyan margin (Egypt-Israel), in *Catastrophic Events and Mass Extinctions: Impacts and Beyond*, edited by C. Koeberl and K. MacLeod, *Geol. Soc. Am. Spec. Pap.*, 356, 533–549.

- Stap, L., L. J. Lourens, E. Thomas, A. Sluijs, S. Bohaty, and J. C. Zachos (2010), High-resolution deep-sea carbon and oxygen isotope records of Eocene Thermal Maximum 2 and H2, *Geology*, 38(7), 607–610.
- Stassen, P., E. Thomas, and R. P. Speijer (2012), Integrated stratigraphy of the Paleocene-Eocene thermal maximum in the New Jersey Coastal Plain: Toward understanding the effects of global warming in a shelf environment, *Paleoceanography*, 27, PA4210, doi:10.1029/2012PA002323.
- Stein, R., B. Boucsein, and H. Meyer (2006), Anoxia and high primary production in the Paleogene central Arctic Ocean: First detailed records from Lomonosov Ridge, *Geophys. Res. Lett.*, 33, L18606, doi:10.1029/2006GL026776.
- Stoll, H. M., and S. Bains (2003), Coccolith Sr/Ca records of productivity during the Paleocene-Eocene thermal maximum from the Weddell Sea, *Paleoceanography*, 18(2), 1049, doi:10.1029/2002PA000875.
- Stoll, H. M., N. Shimizu, D. Archer, and P. Ziveri (2007), Coccolithophore productivity response to greenhouse event of the Paleocene-Eocene Thermal Maximum, *Earth Planet. Sci. Lett.*, 258(1-2), 192–206.
- Stramma, L., E. D. Prince, S. Schmidtko, J. Luo, J. P. Hoolihan, M. Visbeck, D. W. R. Wallace, P. Brandt, and A. Koertinger (2012), Expansion of oxygen minimum zones may reduce available habitat for tropical pelagic fishes, *Nat. Clim. Change*, 2(1), 33–37.
- Summons, R. E., and T. G. Powell (1987), Identification of aryl isoprenoids in source rocks and crude oils—Biological markers for the green sulfur bacteria, *Geochim. Cosmochim. Acta*, 51(3), 557–566.

- Thomas, E. (2007), Cenozoic mass extinctions in the deep sea: What disturbs the largest habitat on Earth?, in *Large Ecosystem Perturbations: Causes and Consequences*, edited by S. Monechi, R. Coccioni, and M. Rampino, *Geol. Soc. Am. Spec. Pap.*, 424, 1–24.
- Thomas, E., N. J. Shackleton, and M. A. Hall (1992), Data report: Carbon isotope stratigraphy of Paleogene bulk sediments, Hole 762C (Exmouth Plateau, eastern Indian Ocean), in *Proc. Ocean Drill. Program Part B Sci. Results*, vol. 122, edited by U. von Rad et al., pp. 897–901, College Station, Tex., doi:10.2973/odp.proc.sr.122.195.1992.
- Tian, R. C., J. C. Marty, E. Nicolas, J. Chiaverini, D. RuizPino, and M. D. Pizay (1996), Iodine speciation: A potential indicator to evaluate new production versus regenerated production, *Deep Sea Res., Part I*, 43(5), 723–738.
- Truesdale, V. W., and G. W. Bailey (2000), Dissolved iodate and total iodine during an extreme hypoxic event in the Southern Benguela system, *Estuarine Coastal Shelf Sci.*, 50(6), 751–760.
- Truesdale, V. W., and G. W. Bailey (2002), Iodine distribution in the Southern Benguela system during an upwelling episode, *Cont. Shelf Res.*, 22(1), 39–49.
- Whitney, F. A., H. J. Freeland, and M. Robert (2007), Persistently declining oxygen levels in the interior waters of the eastern subarctic Pacific, *Prog. Oceanogr.*, 75(2), 179–199.
- Wieczorek, R., M. S. Fantle, L. R. Kump, and G. Ravizza (2013), Geochemical evidence for volcanic activity prior to and enhanced terrestrial weathering during the Paleocene Eocene Thermal Maximum, *Geochim. Cosmochim. Acta*, 119, 391–410.
- Winguth, A. M. E., E. Thomas, and C. Winguth (2012), Global decline in ocean ventilation, oxygenation, and productivity during the Paleocene-Eocene Thermal Maximum: Implications for the benthic extinction, *Geology*, 40(3), 263–266.

Wong, G. T. F., and P. G. Brewer (1977), Marine chemistry of iodine in anoxic basins, *Geochim. Cosmochim. Acta*, 41(1), 151–159.

Zachos, J. C., et al. (2005), Rapid acidification of the ocean during the Paleocene-Eocene thermal maximum, *Science*, 308(5728), 1611–1615.

Figures

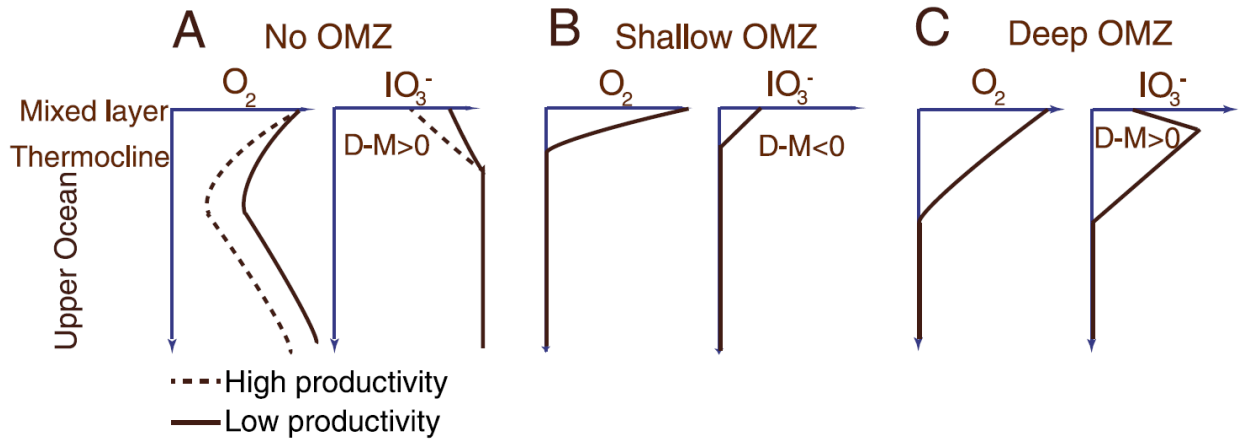


Figure 1. (a–c) Schematic seawater iodate and oxygen concentration profiles. D-M stands for the difference between I/Ca of deep (*Subbotina*) and mixed-layer (*Acarinina*, *Morozovella*) calcifiers.

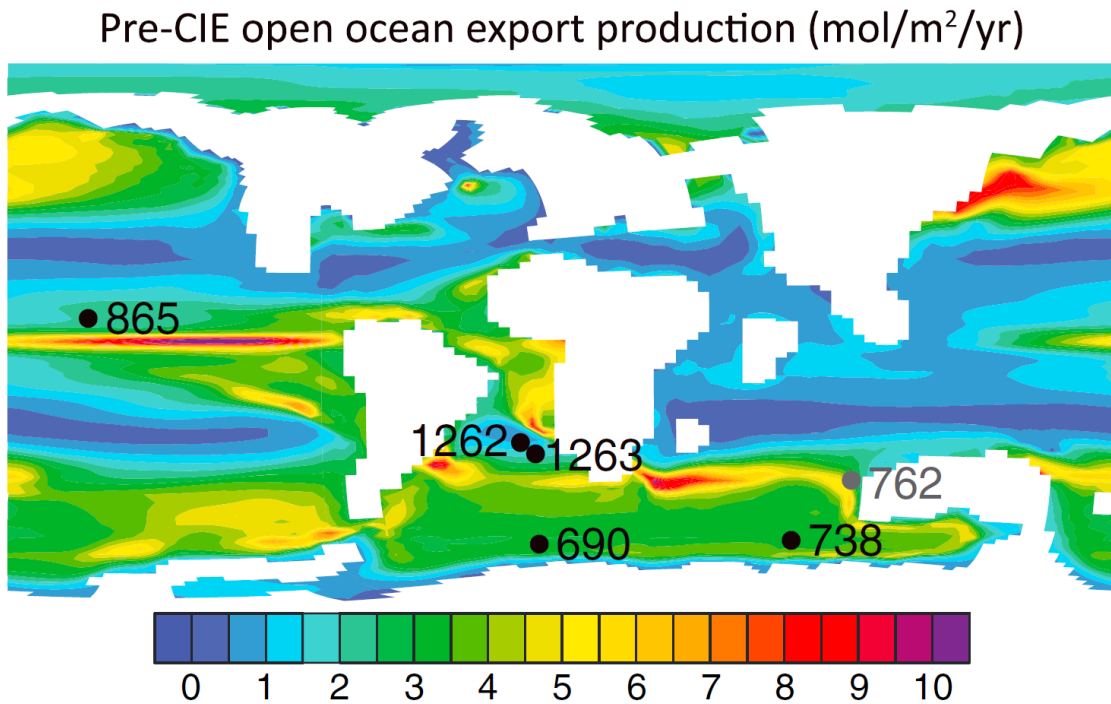


Figure 2. Studied sites plotted on a paleomap of the modeled export productivity during the late Paleocene (Winguth et al., 2012).

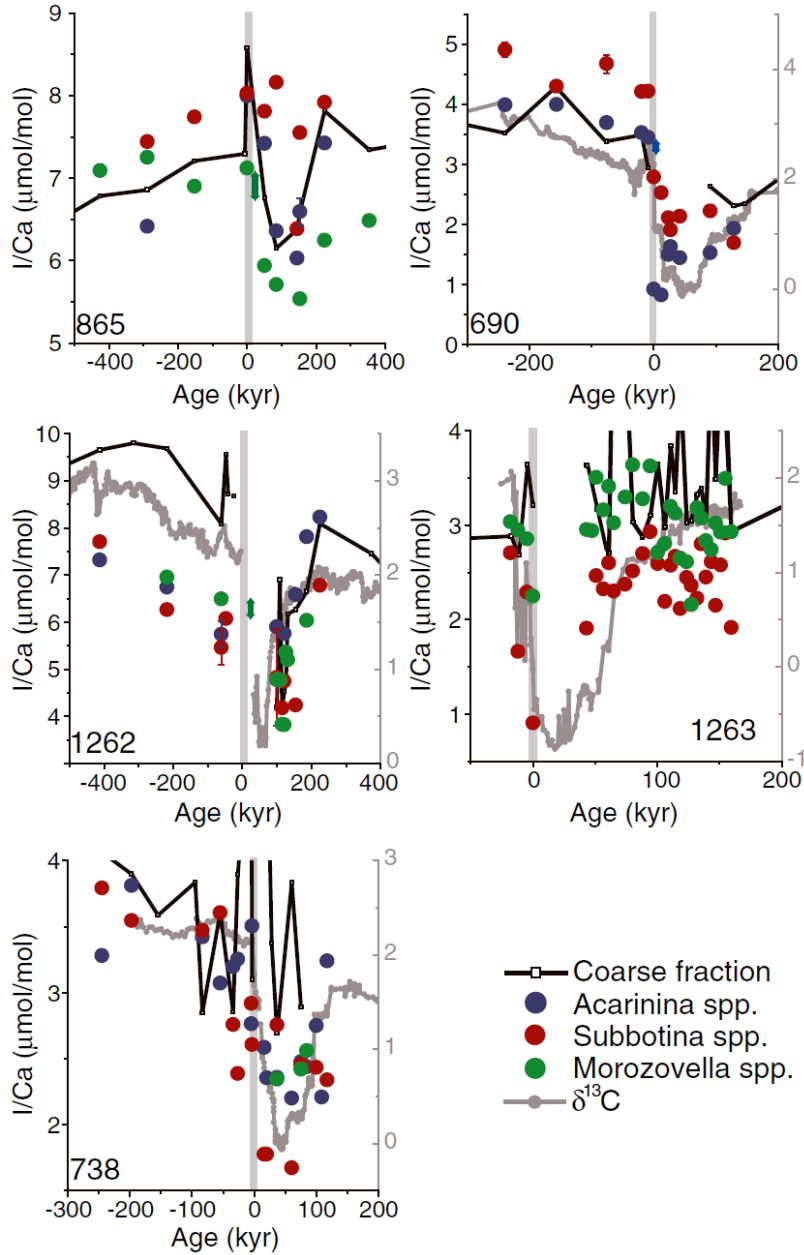


Figure 3. Coarse fraction and single genus I/Ca for open ocean sites. Error bars show standard deviations of repeated measurements on picked and cleaned shells. The colored double-headed arrows (green for Sites 865 and 1262 and blue for Site 690) next to the grey bar mark the potential I/Ca decrease caused by the warming-induced changes in the partition coefficient (Dunkley Jones et al., 2013). Bulk carbon isotope data for Sites 1262 and 1263 (Zachos et al., 2005), Site 690 (Bains et al., 1999), and Site 738 (Larrasoana et al., 2012).

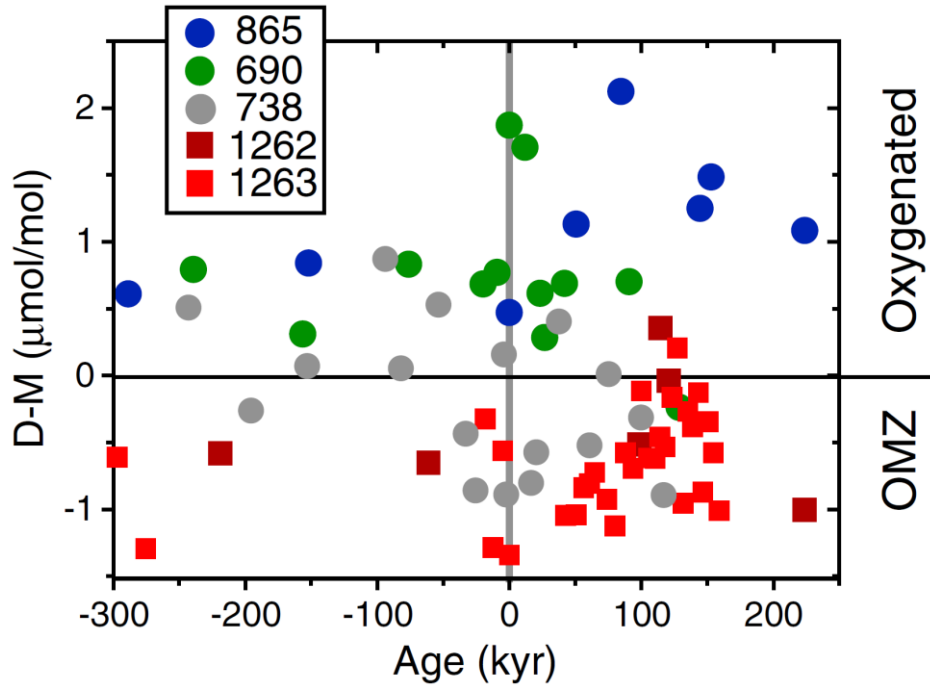


Figure 4. Differences in I/Ca between the deep (D) and mixed-layer (M) calcifiers for each site, indicating local iodate gradient and oxygenation.

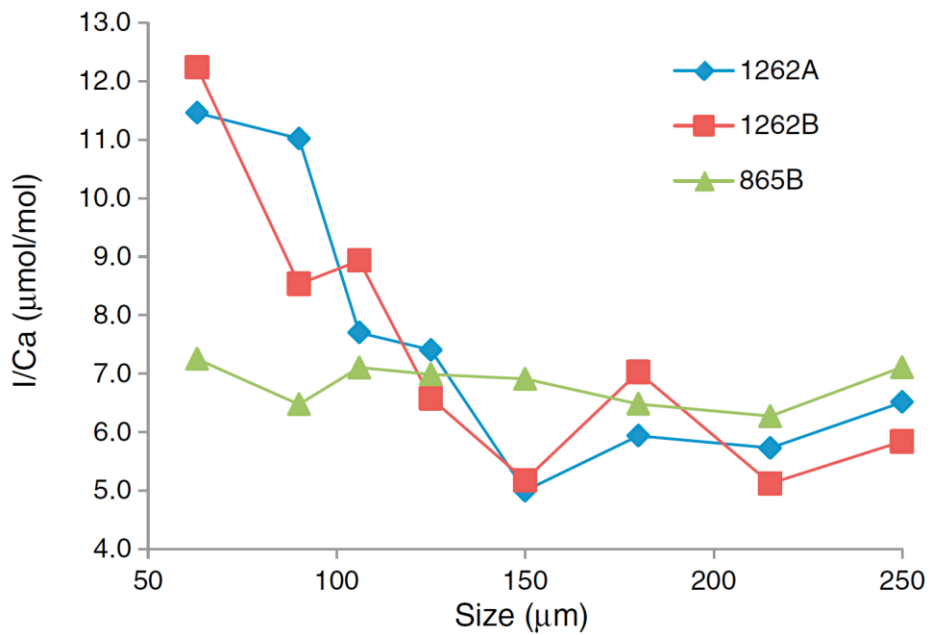


Figure 5. I/Ca values in different size fractions of bulk coarse fraction in samples from Sites 1262 and 865.

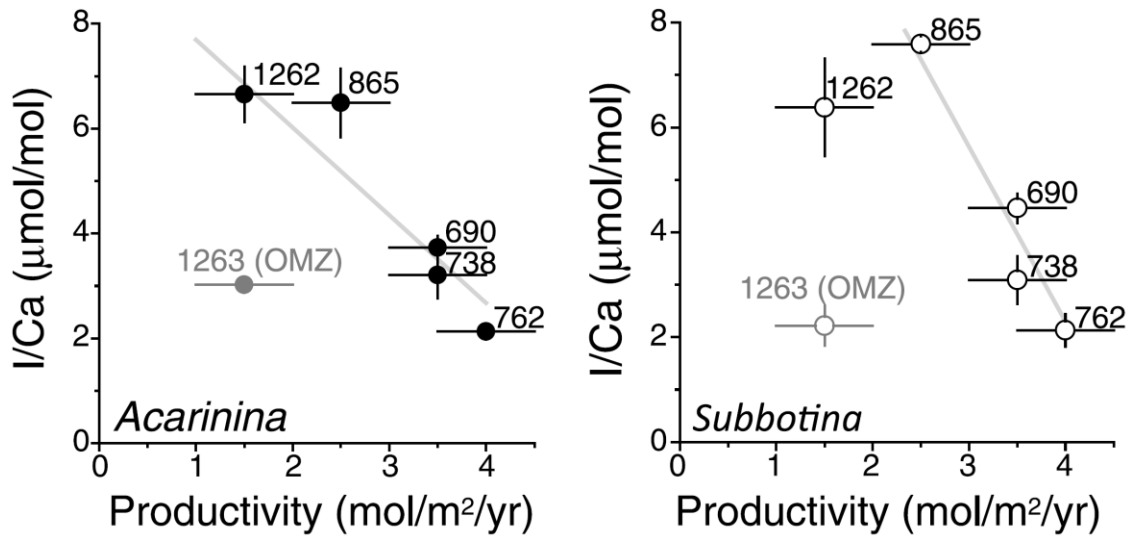


Figure 6. Average values and standard deviations of I/Ca in late Paleocene mixed-layer and deep-dwelling calcifiers, correlated with the modeled productivity in Winguth et al. (2012). *Morozovella* was used instead of *Acarinina* for Site 865 due to the lack of shells. Site 1263 falls off the trend and is related to a shallow OMZ.

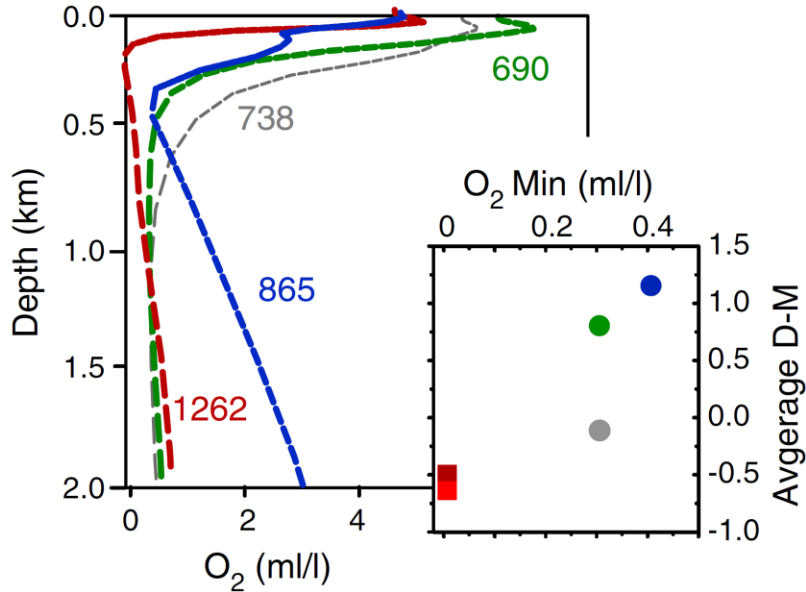


Figure 7. O₂ profiles simulated in CCSM3 model under 4xCO₂ conditions (Winguth et al., 2012). Insert compares the average D-M values for the studied interval (from -300 kyr to 250 kyr relative to the onset of the PETM) with the modeled minimum O₂ concentration at each site.

Biographical Data

Name of Author: Xiaoli Zhou

Place of Birth: Guangshui, Hubei, China

Date of Birth: December 18, 1989

Education:

Ph.D. in Earth Sciences, Syracuse University, 2016

B.S. in Geochemistry, University of Science and Technology of China, 2011

Honors and Awards:

GSA Travel Grant, 2015

Goldschmidt Best Poster Abstract Prize, 2015

Goldschmidt Student Assistance Grant, NSF and NASA, 2015

Stipend from Women in Science and Engineering-Future Professionals Program, SU, 2015

Graduate Student Publication Award, Department of Earth Sciences, SU, 2015

Marjorie Hooker Award for Outstanding Thesis Proposal, Department of Earth Sciences, SU, 2014

Publications:

Lu, Z., B. A. A. Hoogakker, C. Hillenbrand, **X. Zhou**, E. Thomas, K. M. Gutchess, W. Lu, L. Jones, and R. E. M. Rickaby, Oxygen depletion recorded in upper waters of the glacial Southern Ocean, accepted by *Nature Communications*.

Zhou, X., Z. Lu, R. E. M. Rickaby, E. W. Domack, J. S. Wellner, and H. A. Kennedy, 2015, Ikaite abundance controlled by porewater phosphorus level: potential links to dust and productivity, *Journal of Geology*, 123, 269-281, DOI:10.1086/681918.

Zhou, X., H. C. Jenkyns, J. D. Owens, C. K. Junium, X. Zheng, B. B. Sageman, D. S. Hardisty, T. W. Lyons, A. Ridgewell, and Z. Lu, 2015, Upper ocean oxygenation dynamics from I/Ca ratios during the Cenomanian–Turonian OAE 2, *Paleoceanography*, 10.1002/2014PA002741.

Zhou, X., E. Thomas, R. E. M. Rickaby, A. M. E. Winguth, and Z. Lu, 2014, I/Ca evidence for upper ocean deoxygenation during the Paleocene-Eocene Thermal Maximum (PETM), *Paleoceanography*, 29, 964-975.

- Lu, Z., S. T. Hummel, L. K. Lautz, G. D. Hoke, **X. Zhou**, J. Leone and D. I. Siegel, 2014, Iodine as a sensitive tracer for detecting influence of organic-rich shale in shallow groundwater, *Applied Geochemistry*, doi:10.1016/j.apgeochem.2014.10.019.
- Hardisty, D. S., Z. Lu, N. J. Planavsky, A. Bekker, **X. Zhou**, P. Philippot, and T. W. Lyons, 2014, An iodine record of Paleoproterozoic surface ocean oxygenation, *Geology*, *42*, 619-622.